PRECISION IN TRAFFIC MONITORING: HARNESSING PIEZOELECTRIC SENSORS FOR TIRE ANALYSIS AND VEHICLE CLASSIFICATION

Ву

Raheel Tariq

A THESIS

Submitted to
Michigan State University
in partial fulfillment of the requirements
for the degree of

Civil Engineering – Master of Science

2023

ABSTRACT

This research explored vehicular monitoring, emphasizing a unique approach incorporating piezoelectric sensor strands encased in a durable polymer. The aim was to use these sensors to pinpoint a vehicle's tire location and measure its width, factors critical for various traffic monitoring systems. A crucial task was determining the most suitable protective barrier for the sensors, considering environmental conditions and the strains from vehicle motion. Through comprehensive tests, the G-100 Ultra Impact Epoxy stood out for its consistent performance. Piezoelectric sensors, renowned for their ability to convert mechanical force into electrical signals, played a central role in this research. Their integration with the selected epoxy showcased their capability to capture the complex dynamics between vehicle tires and the road surface. Additionally, the research explored the compatibility of EPDM rubber with the sensors. Due to its durability, EPDM rubber served as both an effective shield and a base for the sensors, producing encouraging laboratory outcomes.

Field tests with a piezoelectric sensor-embedded EPDM strip validated the system's efficacy. When vehicles traversed the strip, the induced mechanical strains on the sensors generated voltage outputs that provided detailed tire information. A machine-learning model was developed to categorize trucks based on distinct signal patterns. The simulated behavior of the EPDM strip integrated with sensors yielded essential strain data. This data influenced the voltage outputs from the piezoelectric sensors, which helped ascertain the precise tire location, width, and the vehicle's classification. A standout observation was the system's enhanced sensitivity to the speed of load applications, pointing to its real-world deployment considerations. The derived results closely mirrored actual measurements, validating the system's accuracy.

This thesis is dedicated to my family, my fellow graduate students, and all my mentors who supported me throughout my journey.

ACKNOWLEDGEMENTS

I am deeply grateful to my advisors, Dr. Nizar Lajnef and Dr. Syed Waqar Haider, for their unwavering guidance and encouragement throughout the study. Dr. Lajnef and Dr. Haider have been fantastic mentors who taught me valuable lessons about the research process. They were always approachable and willing to help. This research would not have been possible without their valuable input. I thank them for the time they gave me throughout the study and while writing my thesis.

I extend my sincere appreciation to the committee members. Their teachings during my tenure have been instrumental, and I have consistently found their insights enlightening and inspiring.

Lastly, my heartfelt thanks go out to my family and friends, both within the academic circle and back home. Their unwavering support and motivation have been my pillars of strength. I am also thankful for the invaluable assistance of all those whose paths crossed mine during this pursuit.

TABLE OF CONTENTS

CHAPTER 1 INTRODUCTION	1
1.1 Problem Statement	1
1.2 Objectives	2
1.3 Outline of the Thesis	3
CHAPTER 2 LITERATURE REVIEW	4
2.1 Introduction	
2.2 Weigh-In-Motion System	
2.3 Evolution of WIM Systems	
2.4 Types of Weigh-In-Motion Systems	
2.5 Factors Affecting WIM Systems	
2.6 Cost Comparison of WIM Systems	
2.7 Piezoelectric Systems	
2.8 Machine Learning and Data Analysis	
2.9 Summary	
CHAPTER 3 DEVICE DEVELOPMENT AND LABORATORY TESTING	21
3.1 Epoxy Selection	
3.2 Prototype Sensor	
3.3 Temperature Chamber Test	
3.4 Summary	
CHAPTER 4 FIELD VALIDATION AND ALGORITHM MODELINGING	39
4.1 Field Validation	
4.2 Modeling the System	
4.3 Summary	
CHAPTER 5 CONCLUSIONS AND RECOMMENDATIONS	74
5.1 Conclusions	
5.2 Recommendations	
5.3 Recommendation for Future Work	
REFERENCES	78
APPENDIX	81

CHAPTER 1 INTRODUCTION

1.1 Problem Statement

In the rapidly advancing world of transportation and traffic management, the continuous monitoring of vehicular parameters is a cornerstone to ensure road transportation systems' safety, efficiency, and efficacy. Among these parameters, accurately determining tire position and width has emerged as a particularly pressing challenge, given its direct implications for vehicle classification, weight enforcement, and pavement analysis.

Traditionally, the tools and methods employed for vehicular monitoring have been plagued with accuracy, longevity, and resilience against the harsh conditions of roadways. The constant wear and tear from vehicular traffic, combined with the adverse impacts of environmental conditions such as temperature variations, rain, and snow, often result in significant degradation of monitoring equipment. The consequential data inaccuracies hinder traffic surveillance activities and lead to misinformed decisions in traffic management and infrastructure maintenance.

The utilization of sensors, specifically piezoelectric types, has emerged as a potential solution to this challenge. In context of high-speed vehicles, these sensors play pivotal role in vehicle detection and tire categorization [1]. Their reliability, stability, sensitivity, cost-effectiveness, and ease of installation have made them a preferred choice in WIM systems. The inherent property of piezoelectric sensors to convert mechanical forces into electrical signals offers a promising avenue for capturing the dynamic interactions between vehicles and the road. However, deploying these sensors directly on road surfaces without protective measures subjects them to environmental and mechanical challenges that have historically posed difficulties for conventional methods.

Main concern is the protection of these sensors. With the sensors' utility being contingent on their integrity and functionality, there is a dire need to identify materials that can protect them while not compromising their sensitivity. Preliminary investigations suggest that epoxy materials, particularly G-100 epoxy, exhibit promising durability and resilience. Yet, the selection isn't straightforward. These materials must endure the challenges roadways pose, from the immense pressure exerted by heavy vehicles to the cyclic freeze-thaw conditions in colder regions.

Furthermore, the actual deployment strategy for these sensors requires careful consideration. Their positioning relative to the road surface, integration with other materials like EPDM rubber, and the configuration of their array are all pivotal factors that determine the quality and accuracy of the data they capture. The initial findings suggest that sensors directly beneath the vehicular load offer the most accurate readings. This insight requires additional exploration and validation, particularly in real-world on-road scenarios.

In addition to the physical challenges, there's a dimension of data interpretation and analysis. While rich, the raw data from the sensors is meaningless without robust algorithms and models to decipher it. The emergence of machine learning and finite element modeling presents potential solutions, but their actual applicability in the context of piezoelectric sensor data from roads remains an open question.

In essence, while integrating piezoelectric sensors in traffic monitoring systems presents a promising path forward, it is laden with known and unforeseen challenges. Addressing them requires technical innovations and a holistic understanding of the vehicular-roadway interaction ecosystem. As the transportation landscape evolves, driven by technological advancements and increasing vehicular volumes, an urgent and unmet need exists to refine, validate, and implement a comprehensive vehicular monitoring system that stands the test of time and traffic.

This thesis addresses the multifaceted challenge of integrating piezoelectric sensors into traffic monitoring systems effectively and bridging the gap between technological advancements and practical implementation; the aim is to present a comprehensive vehicular monitoring solution equipped to evolve with the dynamic needs of the transportation industry.

1.2 Objectives

The objectives of this thesis are;

- Design a sensing system tailored for precisely detecting and categorizing wide-base tire
 (WBT) types. This system should be proficient in measuring a range of dynamic tire forces,
 ascertaining tire widths, classifying distinct vehicles, and tracking wheel deviations within
 lanes.
- Ensure the system can adeptly transform the mechanical forces exerted by traversing vehicles into electrical signals. Furthermore, there is a need for the development of software or firmware solutions that can distinguish vehicles based on their voltage response. The system should interpret these electrical signals to identify the vehicle type and tire dimensions.

• Expose the system to a wide range of environmental conditions during testing to ensure its long-term resilience and consistent performance is unaffected by external factors.

1.3 Outline of the Thesis

This thesis is organized into five chapters. Chapter 1 presents the crux of the problem and the core objectives the thesis aims to address. Chapter 2 offers a comprehensive literature review, illuminating the potential and practicalities of using piezoelectric sensors for vehicle tire width detection and classification. Chapter 3 provides a detailed account of the methodology, discussing the system's fabrication process and the various laboratory tests it underwent. Chapter 4 transitions to real-world scenarios, detailing the field validation of the system and the intricate modeling of the machine learning algorithm. Lastly, Chapter 5 summarizes the findings and provides overarching recommendations for optimally deploying piezoelectric sensors in vehicle data collection.

CHAPTER 2 LITERATURE REVIEW

2.1 Introduction

Weigh-in-Motion (WIM) systems have become a transportation and infrastructure management cornerstone. Essential for monitoring vehicular weight and movement, the heart of WIM technology is the piezoelectric sensor. These sensors transform mechanical pressure into electrical signals, revolutionizing vehicle movement and load data collection. Embedded strategically within the road surface, they capture and relay real-time information about passing vehicles' weight, speed, and axle configuration [2]. This data serves multiple purposes, from weight enforcement and toll collection to traffic management and research. This research aims to enhance system design, construction, and installation using piezoelectric sensors, striving to extend their operational lifespan and reduce user costs.

2.2 Weigh-In-Motion System

As per the American Society for Testing and Materials (ASTM) definition, a WIM system is a method for dynamically measuring tire forces from moving vehicles and estimating the resulting static tire loads [3]. This involves breaking down a vehicle's gross weight into discrete loads distributed across its individual axles or axle groups. When a vehicle crosses a WIM system, it captures a fraction of the total load, converting it into an electrical voltage output. This output is then processed using sophisticated algorithms and software to calculate the vehicle's overall weight precisely. A WIM system can continuously monitor and record various vital data, such as axle and vehicle weights, axle and vehicle count, classifications based on weight categories, and vehicle speeds, without causing any interruptions. The applications of WIM technology can be segmented into three primary domains:

- WIM technology plays a pivotal role in optimizing pavement design and transportation infrastructure management.
- WIM systems facilitate freight and trade planning and are instrumental in enforcing regulations related to vehicle weight and load distribution.
- They are also crucial for detecting overweight vehicles, ensuring road safety and infrastructure preservation.

ASTM E 1318-09 [3] classifies WIM systems into four distinct types based on their intended applications. This standard describes each type, specifies its intended accuracy level, and defines the associated user requirements. The variations characterizing these WIM system types include

differences in speed ranges, data recording capabilities, and alignment with specific user needs. Table 1 provides the classification and application information, while Table 2 elaborates on the functional performance requirements of these systems.

Table 1 WIM system classification and application [3] [4]

	Type I	Type II	Type III	Type IV
	16-130 km/hr	24-130 km/hr	16-130 km/hr	3-16 km/hr
Speed Range	(10-80 mph)	(15-80 mph)	(10-80 mph)	(2-10 mph)
	Traffic data	Traffic data	Weight	Weight
Application	Collection	Collection	Enforcement	Enforcement
Number of Lanes	Up to four	Up to four	Up to two	Up to two
Bending Plate	✓	✓	✓	✓
Piezoelectric Sensor	✓	✓		
Load cell	✓	✓	✓	✓
Wheel Load	✓	✓	✓	✓
Axle Load	✓	✓	✓	✓
Axle-Group Load	✓	✓	✓	✓
Gross Vehicle Weight	✓	√	✓	√
Speed	✓	✓	✓	✓
Axle Spacing	✓	✓	✓	√
Vehicle Class	✓	✓	✓	√
Site Identification Code	✓	√	✓	√
Lane and Direction of Travel	✓	✓	✓	✓
Date and Time of Passage	✓	√	✓	✓
Sequential Vehicle Record #	✓	√	✓	√
Wheelbase (front to rear				
axle)	✓	✓	✓	✓
Equivalent Single-Axle				
Load	✓	✓	✓	✓
Violation Code	√	√	√	√

Table 2 WIM requirements for functional performance [3]

	Tolerance for 95% Probability of Conformity				
	Type			Type IV	
Function	I	Type II	Type III	Value ≥ kg (lb)	±kg (lb)
Wheel Load	±25%	N/A	±20%	2300 (5000)	100 (300)
Axle Load	±20%	±30%	±15%	5400 (12000)	200 (500)
Axle group Load	±15%	±20%	±10%	11300 (25000),	500 (1200)
Gross Vehicle Weight	±10%	±15%	±6%	27200 (60000)	1100 (25000)
Speed	± 2 km/h (1 mph)				
Axle Spacing	± 0.15 m (0.5 ft)				

2.3 Evolution of WIM Systems

The development of WIM systems has seen significant progress, with sensors playing a leading role in their development. Unlike static weighing systems, WIM systems, while slightly less precise, significantly minimize traffic disruptions by weighing vehicles at highway speeds. This leads to minimal delays in the transportation network, making WIM systems a preferred choice for transportation infrastructure management [5] [6] [7]. Emerging in the mid-20th century, the quest for efficient vehicle weight measurement resulted in early WIM systems employing mechanical devices like strain gauges and load cells embedded in roadways [1]. While they provided foundational data, their accuracy and reliability were constrained [8]. The field underwent a revolution with the introduction of piezoelectric sensors. Their high sensitivity, durability, and accurate dynamic tire force measurements greatly enhanced WIM data precision.

As sensor technology matured, improvements in materials and design emerged. Strain gauge sensors improved for higher accuracy, and new technologies like capacitive and piezoresistive sensors expanded the options for WIM systems. These modern systems, fully integrated into the transportation infrastructure, support real-time data collection and automated weight enforcement. Their applications span from monitoring road and bridge conditions, assessing pavement designs, and enforcing highway weight limits. With vehicles moving faster than ever, high-speed WIM systems with advanced sensors and data processing techniques have been developed to cater to modern highway conditions.

In addition to weight measurement, WIM systems have expanded to classify vehicles based on their weight categories and to analyze traffic patterns [9], broadening the scope of WIM

technology in transportation planning and management. Advancements in sensor miniaturization and wireless communication have enabled the development of portable and mobile systems. These can be swiftly deployed for temporary data collection at various locations, providing critical insights into traffic and load dynamics. These systems incorporate sophisticated data processing algorithms and software, enabling real-time analysis, data storage, and remote monitoring. Furthermore, introducing international standards and regulations for WIM technology underscores its importance in transportation management and enforcement, ensuring consistency and precision in WIM systems globally.

Significant advancements in sensor technology, data processing, and integration into transportation infrastructure have characterized the evolution of Weigh-In-Motion systems. These developments have enhanced WIM systems' accuracy, reliability, and versatility, making them essential tools for modern transportation management and enforcement.

2.4 Types of Weigh-In-Motion Systems

Various types of WIM systems are employed worldwide. Some of the common one includes;

2.4.1 Load Cell-based WIM Systems

A Load Cell WIM system is a specialized technology used to measure the dynamic tire forces exerted by vehicles as they pass over the road surface [10]. It employs load cells and precision sensors designed to measure load accurately. These are typically embedded within the road or positioned beneath it at positions where vehicles traverse. When a vehicle passes over the sensors, the load cells detect the forces, including the vertical load and any lateral or horizontal forces, applied by the vehicle's tires. The deformation or strain in the load cells resulting from this load is converted into electrical signals, typically voltage changes. These signals are then processed to calculate parameters such as axle weights, individual tire loads, total vehicle weight, and vehicle classification based on weight categories. The precision for this type of sensor is within a margin of $\pm 6\%$ [11]. The Load Cell WIM system's classification under ASTM standards varies based on the site design, leading to categorizations like Type I, II, III, or IV [4]. A typical load cell system consists of three main components: a load cell, an inductive loop, and an axle sensor. The upstream inductive loop initiates the system, which serves as the trigger mechanism. The typical configuration of the load cell WIM system is shown in Figure 1 [12].

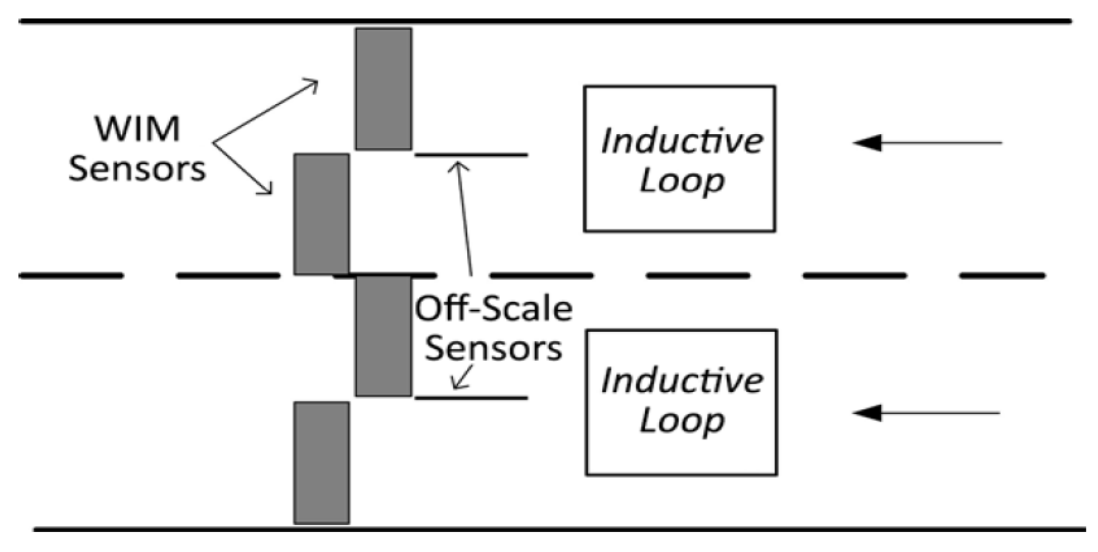


Figure 1 Configuration of load cell WIM system [12]

2.4.2 Bending Plate WIM Systems

This WIM system primarily utilizes specialized bending plate sensors installed within the road surface at specific locations where vehicles are expected to traverse [11]. As a vehicle moves over these sensors, its weight causes the thin, flexible plates to deflect, with the deflection being directly proportional to the load exerted by the vehicle's tires. Equipped with strain gauges affixed to their interior, these sensors detect deflections and convert them into electrical signals [13]. The system then processes these signals to ascertain the vehicle's weight, including its axle and wheel weights. The weight calculation is based on alterations in the resistance of the strain gauges as the vehicle passes over the plate [14].

This system typically incorporates one or two scales aligned perpendicularly to the direction of vehicle movement [12]. In its simplest form, a bending plate WIM system comprises a single scale accompanied by two inductive loops placed before and after the scale. An axle sensor is positioned downstream of the scale but before the second inductive loop to measure a vehicle's speed. In practical terms, the upstream inductive loop serves as the trigger for the system, initiating data collection as a vehicle approaches. In contrast, the downstream loop calculates the vehicle's speed and axle spacing. This setup and the data collection mechanism are illustrated in Figure 2 [12].

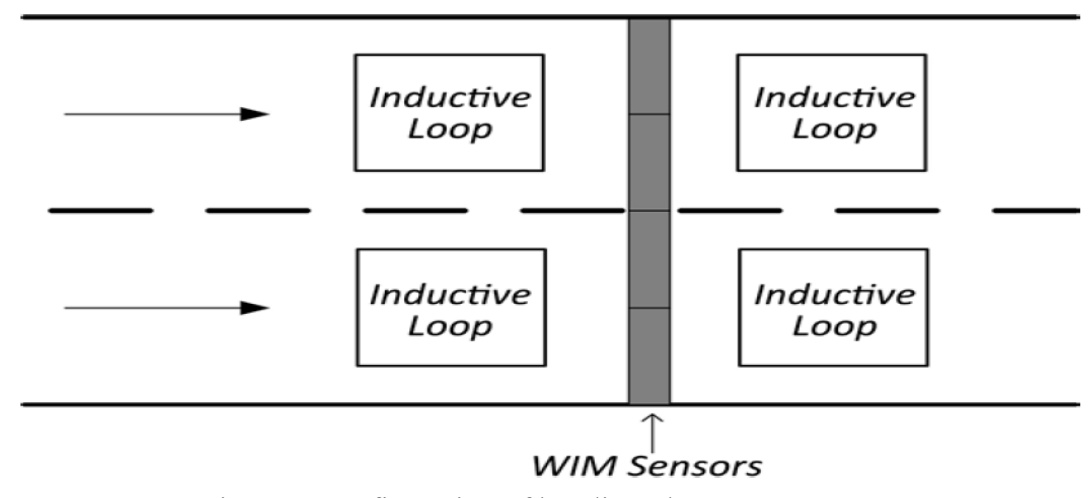


Figure 2 Configuration of bending plate WIM system [12]

2.4.3 Fiber Optics WIM Systems

This system uses fiber optic sensors to measure vehicles' dynamic tire forces and weight distribution as they traverse the road surface. Fiber optic cables are embedded within or alongside the roadway at specific locations to capture vehicle weight data [15]. The principle behind Fiber Optics WIM involves the modulation of light signals through the fiber optic cables due to the mechanical strain caused by the vehicle's tires [16]. When a vehicle passes over these sensors, the tire forces' strain alters the transmitted light's characteristics, resulting in changes in light intensity or wavelength. These variations are then detected and interpreted as weight data for different axles and vehicles [17]. Fiber Optics WIM systems are known for their high precision and durability, making them suitable for applications requiring accurate weight measurements, such as traffic monitoring, weight enforcement, and pavement analysis. The configuration of this system is shown in Figure 3 [18].

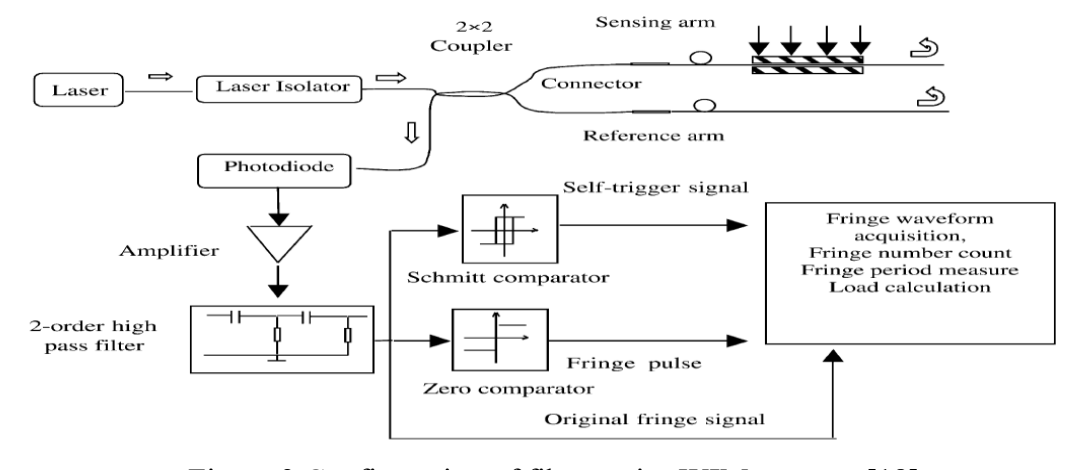


Figure 3 Configuration of fiber optics WIM systems [18]

2.4.4 Piezoelectric WIM Systems

A Piezoelectric WIM system is a specialized technology crafted to accurately assess a vehicle's weight and its dynamic tire forces as it moves across roadways or bridges. This system relies on piezoelectric sensors, which have become integral in understanding the relationship between moving vehicles and pavement deformation [19]. Typically, in-pavement WIM technologies utilize piezoceramic bars to measure the weight of passing vehicles [20]. Piezoelectric sensors, historically inspired by the discovery of piezoelectricity by Pierre and Jacques Curie in the late 19th century [21] [22], can produce electrical signals in response to mechanical pressure or deformation. As vehicle crosses over a sensor, the weight from its tires applies pressure on the piezoelectric elements, generating distinct electrical voltage signals. The characteristics of these signals, such as their amplitude and duration, are directly related to the forces and weight of the vehicle's tires. After thoroughly analyzing these electrical signals, the piezoelectric WIM system can derive critical data, such as axle weights and total vehicle weight, and sometimes even classify vehicles based on weight. The fundamental formula used by piezoelectric sensors is [10]:

$$U = k * \Delta P * F * 1 / L$$

Where in equation 1:

U: Output signal.

k: Sensibility factor.

 ΔP : Pressure variation applied to the sensor.

L: Length of the sensor.

1: Length where the pressure is applied.

Additionally, the factor F is given by:

$$F = (c / (c + m)) * ((e-t) / T)$$

Where in equation 2:

c and m: Constants.

e: Mathematical constant (approximately equal to 2.71828).

t: Time.

T: Another constant.

This system typically features at least one sensor and two inductive loops, as illustrated in Figure 4 [12]. These components can be embedded within the road or configured for portable use. The operational cycle of piezoelectric WIM systems is illustrated in Figure 5 [23].

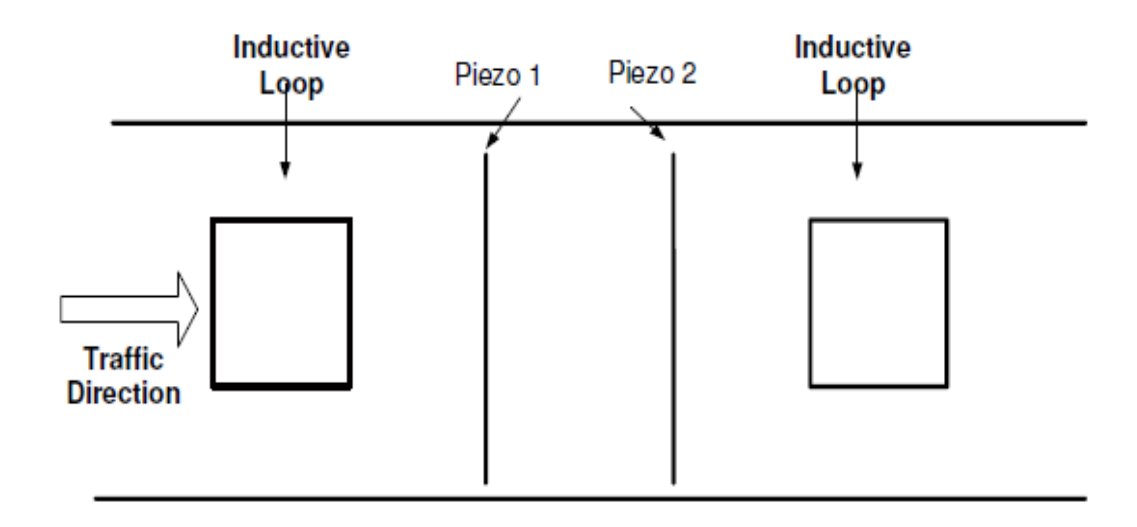


Figure 4 Configuration of piezoelectric WIM system [12]

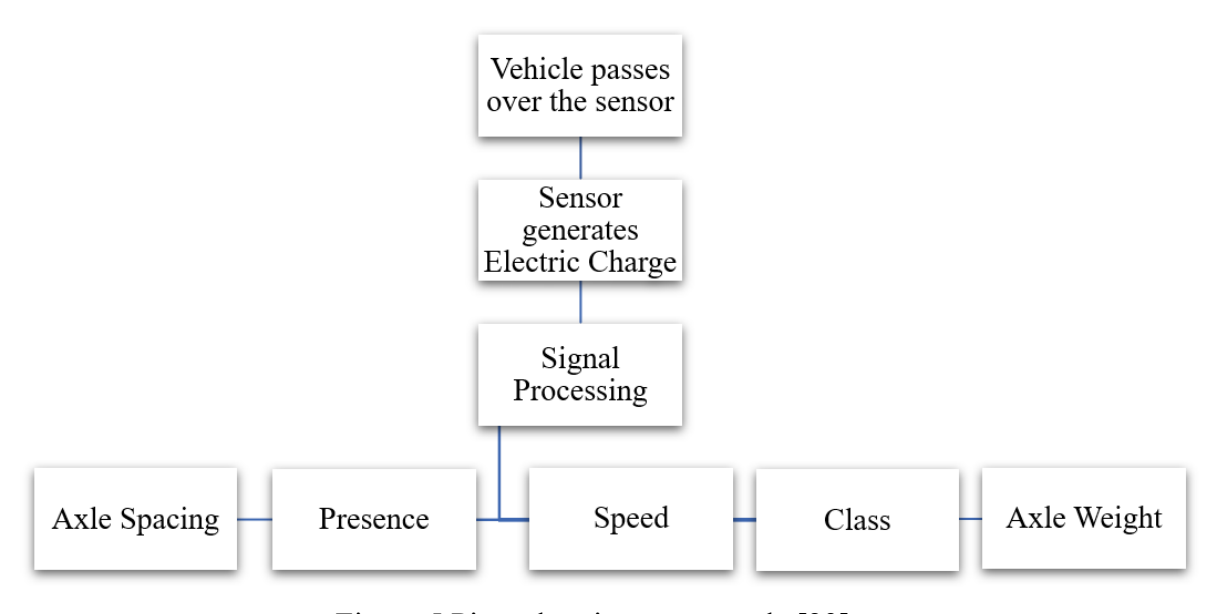


Figure 5 Piezoelectric system cycle [23]

2.4.4.1 Piezoelectric Sensor

Piezoelectric sensors transform mechanical pressure or deformation into electrical signals. The core principle underpinning these sensors is the piezoelectric effect [24], manifesting in certain materials like quartz, ceramics, and select polymers. When subjected to mechanical stress, these

materials' atomic and molecular structures shift, generating an electrical charge. The voltage produced is directly proportional to the applied mechanical force. In contrast, using an electrical voltage to these materials induces mechanical deformation—a phenomenon known as the reverse piezoelectric effect. Due to their high sensitivity, these sensors can register minute changes in mechanical force, making them apt for precision measurements. These characteristics make them invaluable in numerous applications across science, engineering, and various industries.

2.5 Factors Affecting WIM Systems

A multitude of factors can influence the quality and accuracy of WIM systems. Sensor calibration is paramount, as calibration inaccuracies can lead to recorded data errors. Environmental factors, such as temperature, moisture, and road conditions, also have a critical impact. Traffic speed is another critical factor, as WIM systems may be optimized for particular speed ranges, and deviations can lead to measurement inaccuracies. Accurate weight measurements rely on the exact positioning of sensors within the roadway, routine maintenance, and the use of appropriate data processing algorithms. Table 3 categorizes these factors into four groups [25].

Table 3 Factors affecting the wheel loads of moving vehicles [25]

Roadway Factors	Vehicle Factors	Environment Factors	Equipment Factors
Longitudinal Profile	Speed, Acceleration	Wind	Sensor Stiffness
Transverse Profile	Axle Configuration	Temperature	Sensor Oscillation
Grade	Body Type	Snow, Ice	Sensor Location
Cross Slope	Suspension System	Moisture	Sensor Sensitivity
			Signal
Curvature	Tires		Interpretation
Alignment	Load, Load Shift		
	Aerodynamic		
	Characteristics		
	Center of Gravity		

Obtaining the static weight of a vehicle involves applying an upward force, precisely matching the downward gravitational force acting on the motionless tires of the vehicle. This force is simultaneously measured using scales (force transducers) or a balance. In contrast, the in-motion weighing of a highway vehicle aims to estimate the static weight of the vehicle while the vehicle is in motion. This estimation is achieved by measuring the vertical component of dynamic (constantly changing) force applied to a smooth, level road surface by the vehicle's

tires. It's important to note that the vehicle's weight remains constant as it moves over the road, but the dynamic force exerted on the road surface by a rolling tire varies significantly. This force can range from more than double its static weight when encountering a bump, causing a substantial unbalanced force on the wheel mass, to zero when the tire momentarily separates from the road surface [26].

Dynamic loads can significantly influence the quality of WIM data. The force exerted on a pavement by a truck can vary swiftly due to multiple factors. These include road roughness, truck speed, suspension type, and tire pressure [27]. Such dynamic fluctuations in load introduce challenges and uncertainties when measuring and analyzing WIM data accurately.

Furthermore, as the temperature of the pavement increases, its stiffness decreases. The traditional "opposite and equal reaction" concept becomes less applicable. A portion of the energy, which would ideally rebound to support the system, gets absorbed by the more flexible pavement [28]. When higher temperatures result in lower stiffness, the tire load doesn't just press the pavement down vertically; it also causes lateral compression of the material. This sideways pressure diverts energy in multiple directions, deviating from the expected response. Notably, in polymer piezoelectric sensors, the amplitude rises with increasing temperature. In contrast, ceramic piezoelectric sensors display a drop in amplitude as pavement temperature ascends [29] [30].

Equipment factors also pose inherent challenges in weigh-in-motion systems. The interplay between sensitive electronic components and constantly changing environmental conditions can lead to unpredictable outcomes. Often, these issues give rise to systematic errors that, though partly inevitable, require mitigation. Conventionally, to calibrate WIM systems, trucks with a known weight are used. This is achieved by integrating them into the regular traffic flow or using dedicated trucks with a known weight, making repeated passes over the scale. Such calibration methods are designed to curtail errors arising from equipment variables.

2.6 Cost Comparison of WIM Systems

The economic assessment reveals notable differences in the initial investment and maintenance costs associated with different WIM systems, as detailed in Table 4 [4]. When comparing the expenses tied to Bending Plate, Load Cell, and Piezoelectric WIM systems, it's imperative to account for various factors. These include upfront installation costs, ongoing maintenance fees, and total lifecycle expenses [31].

Bending plate WIM systems typically present a cost-effective option for initial installation [13]. The components involved, including the bending plates and associated electronics, are often more affordable than those used in other WIM systems. Moreover, these systems tend to have relatively low maintenance costs since the bending plates are durable and require minimal upkeep. However, it's important to note that their accuracy may be slightly lower than load cell and piezoelectric systems, which could be considered for applications demanding high precision.

Load cell WIM systems typically involve a higher initial cost than bending plate systems. They require precision load cells, advanced electronics, and more robust infrastructure to support accurate weight measurements. While maintenance costs for load cell systems are higher due to the need for periodic calibration and load cell replacements, these can still be cost-effective over the system's lifecycle. Despite the higher upfront investment, their long-term performance and reliability often justify the initial expense, making them a cost-effective choice for precision-focused applications.

Estimated Initial Estimated Average No. **WIM System Performance** Cost/Lane **Cost Per Lane** Piezoelectric 1 Sensor $\pm 10\%$ \$9,500 \$4,224 **Bending Plate** 2 Scale \$18,900 \$4,990 $\pm 5\%$ **Double Bending** 3 \$35,700 \$7,709 Plate Scale $\pm (3-5) \%$ 4 Deep Pit Load Cell $\pm 3\%$ \$52,500 \$7,296

Table 4 Cost comparison of WIM systems [4]

Fiber optics WIM systems can have moderate to high sensor costs, depending on the complexity of the system and the length of fiber optic cables required. Installation costs may vary, with labor costs associated with laying and connecting the fiber optic cables and related hardware. Once installed, fiber optics systems are relatively low maintenance, which can be cost-effective in the long run.

The cost of piezoelectric WIM systems can vary depending on factors such as the type of piezoelectric sensors used and the complexity of the installation. High-quality piezoelectric sensors come at a higher price point, impacting the initial installation cost [32]. However, these systems are generally reliable and durable, requiring low maintenance. While calibration and occasional sensor replacement add to maintenance costs, piezoelectric systems' long-term

accuracy and sensitivity can make them cost-effective choices for applications demanding precision. Despite a moderate upfront cost, piezoelectric systems are valued for their excellent long-term performance and accuracy, rendering them suitable for critical weight measurements.

2.7 Piezoelectric Systems

2.7.1 Types of Piezoelectric Sensors

There are several types of piezoelectric sensors, with three commonly encountered variants being piezo-quartz, piezopolymer, and piezoceramic sensors [33]. Each of these sensor types possesses unique characteristics, along with its own sets of advantages and disadvantages.

2.7.1.1 Piezo-Quartz Sensors

Piezo-quartz sensors are based on synthetic quartz crystals that exhibit piezoelectric properties [34]. These sensors are susceptible and offer excellent stability and precision. Their characteristics include a wide operating temperature range and minimal drift over time. Piezo-quartz sensors are commonly used in high-accuracy applications, such as laboratory measurements, precision instruments, and timing devices like quartz watches. They are advantageous for their exceptional linearity, low noise, and reliable long-term performance. However, their main disadvantage is their relatively high cost compared to other piezoelectric sensor types [35].

2.7.1.2 Piezopolymer Sensors

Piezopolymer sensors employ polymeric materials with embedded piezoelectric elements. These sensors are lightweight, flexible, and cost-effective [36]. They have good sensitivity and are suitable for various applications, including medical devices, acoustic sensors, and industrial measurements. Piezopolymer sensors are advantageous for their ease of integration due to their flexibility and thin form factor. They can conform to curved surfaces and are relatively inexpensive to produce. However, they may exhibit higher hysteresis and lower temperature stability than piezo-quartz or piezoceramic sensors. Additionally, they are more susceptible to moisture and environmental conditions.

2.7.1.3 Piezoceramic Sensors

Piezoceramic sensors utilize ceramic materials with inherent piezoelectric properties. These sensors are robust, durable, and capable of withstanding harsh conditions. Piezoceramic sensors are advantageous for their high signal-to-noise ratio, wide operating temperature range, and resilience to environmental factors [35]. They are suitable for rugged environments where other

sensors may not perform reliably. However, piezoceramic sensors are relatively brittle and less flexible than piezopolymer [37]. Their sensitivity also decreases over time and exhibit nonlinear behavior under high loads.

2.7.2 Application of Piezoelectric Systems

Piezoelectric sensors play a pivotal role in WIM systems, contributing to various applications that extend beyond weight measurement. Some key applications and real-world implementations of piezoelectric sensors in WIM systems is as follows:

- Piezoelectric sensors are extensively used in WIM systems for vehicle detection by playing a
 critical role in monitoring traffic flow and congestion in urban areas. For example,
 piezoelectric sensors at intersections can detect vehicles' presence and trigger traffic lights to
 optimize signal timing, thus improving traffic flow and reducing congestion.
- Piezoelectric sensors can distinguish between different types of tires based on their characteristics and footprint. In highway weigh stations piezoelectric sensors categorize vehicles into various weight classes and tire types. This information is vital for enforcing weight regulations and meeting vehicle safety standards.
- Piezoelectric sensors are used for traffic data collection purposes. They gather data on
 vehicle counts, speeds, axle weight, and axle spacing, essential for traffic analysis and
 planning. Transportation agencies utilize piezoelectric WIM systems to collect real-time
 traffic data, allowing them to analyze traffic patterns, optimize road maintenance, and plan
 infrastructure improvements.
- In addition to transportation-related applications, piezoelectric sensors are also used for
 environmental monitoring. They can detect and monitor environmental factors such as
 seismic activity and vibrations. For example, piezoelectric sensors are utilized in
 seismometers to detect ground movements during earthquakes, providing valuable data for
 seismic research and early warning systems.

2.7.3 Design, Methodology, and Integration with Environment

While designing sensing systems incorporating piezoelectric sensors, a set of fundamental principles guides the process. Beginning with the careful selection of the appropriate type of piezoelectric sensor, such as piezo-quartz, piezopolymer, or piezoceramic, the specific application's requirements must be considered. This includes factors like sensitivity to detect minor changes in applied pressure, environmental conditions, and expected load range. The

placement of piezoelectric sensors within the roadway or structure is equally critical. It involves planning for sensor spacing, alignment, and the depth beneath the road surface. A robust data acquisition system is also essential for real-time data collection, storage, and processing. Furthermore, a reliable power supply system must be designed to ensure uninterrupted sensor operation. These design principles are essential for successfully integrating piezoelectric sensors into sensing systems while ensuring their precision, durability, and effectiveness in various applications.

Comprehensive testing and validation methodologies are necessary to ensure the accuracy and reliability of sensing systems utilizing piezoelectric sensors. The process begins with laboratory testing, providing controlled conditions to assess sensor performance. In this controlled environment, the sensors are subjected to various loads, speeds, and environmental factors to evaluate their accuracy and durability. Moving to field testing, the integrated sensor systems are tested in real-world conditions. Data collected from actual traffic is compared to reference measurements to validate the system's accuracy and reliability in practical applications. Regular calibration checks are a cornerstone of maintaining precision, ensuring the sensor system maintains its accuracy over time. Detailed data analysis is an integral part of the validation process, involving examination of collected data to assess the system's performance. Any discrepancies identified are addressed through fine-tuning and adjustments. Long-term monitoring is essential to evaluate durability and reliability.

Integrating environmental protections is also crucial for preserving the functionality and longevity of piezoelectric sensors within sensing systems. Protective enclosures or housings safeguard sensors from environmental elements, including moisture, dust, and temperature fluctuations. Sealing techniques for cable entry points and connections are employed to prevent moisture ingress, maintaining the integrity of the sensor system. Temperature fluctuations also have an impact on sensor performance. Vibration isolation techniques, such as incorporating rubber mounts or shock-absorbing materials, protect sensors from mechanical shock or vibrations. These measures collectively ensure that environmental challenges do not compromise piezoelectric sensor systems' accuracy, reliability, or durability, allowing them to excel in real-world applications while maintaining their precision and integrity.

2.7.4 Safeguarding the Piezoelectric Sensor

Piezoelectric sensors play a crucial role in various applications but are often exposed to harsh environmental conditions and wear. To ensure their longevity and reliability, protective measures like polymer encasement and rubber shielding are employed.

2.7.4.1 Rubber Shielding

One of the effective protective measures for piezoelectric sensors involves the application of rubber materials or covers to shield the sensor's surface. Rubber shielding serves as a resilient insulation layer, offering protection against mechanical shocks, vibrations, and various environmental factors. This shielding method is critical in enhancing the sensors' ability to withstand mechanical stress, particularly in high-traffic areas with heavy vehicles. It also provides a cushion against impacts and vibrations that could affect the sensor's accuracy and reliability. A comparative analysis of different rubber materials for sensor shielding further solidifies the importance of material selection. Silicone rubber, for example, exhibited superior resistance to temperature variations and environmental contaminants compared to other rubber compounds [38]. This emphasizes the significance of choosing the right shielding material to ensure optimal sensor protection.

2.7.4.2 Polymer Encasement

Polymer encasement offers a practical solution by enveloping these sensors in a protective layer made of polymers like epoxy resin [35]. This encasement is a robust barrier, shielding the sensors against moisture, dust, and potentially corrosive chemical contaminants. Beyond environmental protection, polymer encasement enhances mechanical resilience, reducing sensor wear and tear.

2.8 Machine Learning and Data Analysis

Machine learning and data analysis are indispensable tools in interpreting signals captured by piezoelectric sensors. These sensors generate intricate data patterns that can be challenging to decipher using conventional methods. Machine learning algorithms and data analysis techniques help extract meaningful insights from these signals across various applications, particularly in transportation and vehicle monitoring. By leveraging machine learning, it becomes possible to transform complex sensor data into actionable information, facilitating decisions and enhancing system performance.

Machine learning algorithms have emerged as a robust solution for vehicle classification based on signals acquired from piezoelectric sensors. In their work, Rajab et al. [9] introduced a vehicle classification technology that employs a single-element piezoelectric sensor positioned diagonally within a traffic lane. This technology utilizes the diagonal placement of piezoelectric strip sensors in conjunction with machine learning techniques to achieve precise and reliable vehicle classification. Testing conducted across multiple highway sites yielded up to 97% classification accuracy rates. By analyzing sensor data, these algorithms can differentiate between different vehicle types, such as cars, trucks, and motorcycles. The cluster of different vehicles can be found using machine learning [39]. The algorithm's ability to identify vehicle types based on load distribution patterns can prove instrumental in optimizing traffic management and enforcing weight regulations.

Accurate tire size estimation is paramount across numerous applications, including pavement design and load analysis. Machine learning models, trained on data derived from piezoelectric sensors, have demonstrated proficiency in predicting tire size by analyzing sensor signals. The model can establish correlations between specific signal patterns and known tire sizes, resulting in dependable estimations.

2.9 Summary

WIM systems have become crucial tools in transportation and infrastructure supervision. Integral for tracking and managing vehicle weights and routes across roads, bridges, and vital transport links, the center of WIM operations lies in piezoelectric sensors. These sensors uniquely transform mechanical forces into electronic signals, setting vehicle movement and load data collection standards. Positioned within roadways, they capture real-time details on transiting vehicles' weight, speed, and axle arrangement. Such data is multifunctional, aiding in weight regulation, tolling, traffic control, and academic research.

The ASTM characterizes WIM systems as dynamic tools to measure vehicular tire forces, further estimating their configuration. These systems segment a vehicle's total weight across individual axles or groups of axles. As a vehicle navigates a WIM setup, a weight fragment is captured and converted into an electronic voltage signal. Algorithms and dedicated software then process this data to estimate the vehicle's cumulative weight. The ASTM E 1318-09 distinguishes WIM systems into four categories according to their designated uses, elaborating on each type's descriptions, precision, and user stipulations.

With time, WIM technologies have undergone transformative advancements, mainly attributable to the role of sensors. Piezoelectric sensors, known for their heightened sensitivity, resilience, and precision in measuring dynamic tire pressures, pioneered changes in WIM designs. Subsequent developments included capacitive and piezoresistive sensors, augmenting WIM capacities. The scope of WIMs grew to involve weight-based vehicle categorization and traffic movement analysis. Temporary data gathering was made possible through mobile WIMs, while sophisticated algorithms facilitated instant data assessments, and storage. Global benchmarks and directives emerged to anchor uniformity and precision in WIM operations globally. The economic viability of WIM designs depends on aspects like upfront installation charges, upkeep costs, and comprehensive lifecycle expenditures.

Piezoelectric sensors manifest in diverse forms, including piezo-quartz, piezopolymers, and piezoceramics, each offering specific attributes and uses. Recognized for their heightened sensitivity and sturdiness, these sensors are adaptable to various applications. Protective methods like rubberized covers and polymer casings are employed to enhance their durability, particularly in challenging settings or under intense mechanical pressure. Machine learning and data analysis are essential to deciphering intricate sensor outputs and gleaning actionable information, especially in vehicle classification and tire dimension assessment. Central to an array of systems, piezoelectric sensors facilitate precise vehicle classification and have vast applications in the transport sector. Their continual evolution promises further refinements, ultimately contributing to the establishment of more secure and efficient transportation networks.

CHAPTER 3 DEVICE DEVELOPMENT AND LABORATORY TESTING

The development of the system involves integrating piezoelectric sensor strands encased in a protective polymer material along with the rubber strip. This polymer shielding and the rubber strip ensure the sensors are safeguarded from the impact of traffic loads and environmental conditions. Each lane will be equipped with these piezoelectric sensors, which will be installed securely using a chair [35] to hold them in place during installation. The system relies on piezoelectric sensors to detect changes in voltage resulting from the pressure applied by the tires on an axle. By measuring the change in voltage, the system can infer the amount of pressure applied to the sensors, thereby estimating the tire width, presence, and classification of the vehicle.

3.1 Epoxy Selection

Three distinct types of epoxies, as outlined in Table 5 and shown in Figure 6, were chosen for testing to determine the most suitable epoxy for the protection of piezoelectric sensors. The objective was to identify an epoxy that could effectively withstand the impact of weather conditions and the wear and tear resulting from continuous exposure to wheel loads.

Table 5 Epoxies

S/No.	Ероху
1	G-100 Ultra High Impact Epoxy
2	3 Part Epoxy Patch
3	Max MCR Epoxy





Figure 6 3 Part Epoxy and G-100 Ultra Impact Epoxy

3D printer was employed to fabricate a 1-inch cube mold to facilitate the testing of various epoxies. The epoxies were thoroughly blended and poured into the cubes to prepare the samples

for subsequent analysis and evaluation. Figure 7 displays the cubical samples of epoxies that were specifically prepared to test and calculate the elastic modulus. Following the molding process, the epoxies were carefully removed from the molds and allowed to stabilize at room temperature, ensuring a uniform and homogeneous mixture was attained prior to subsequent analysis.

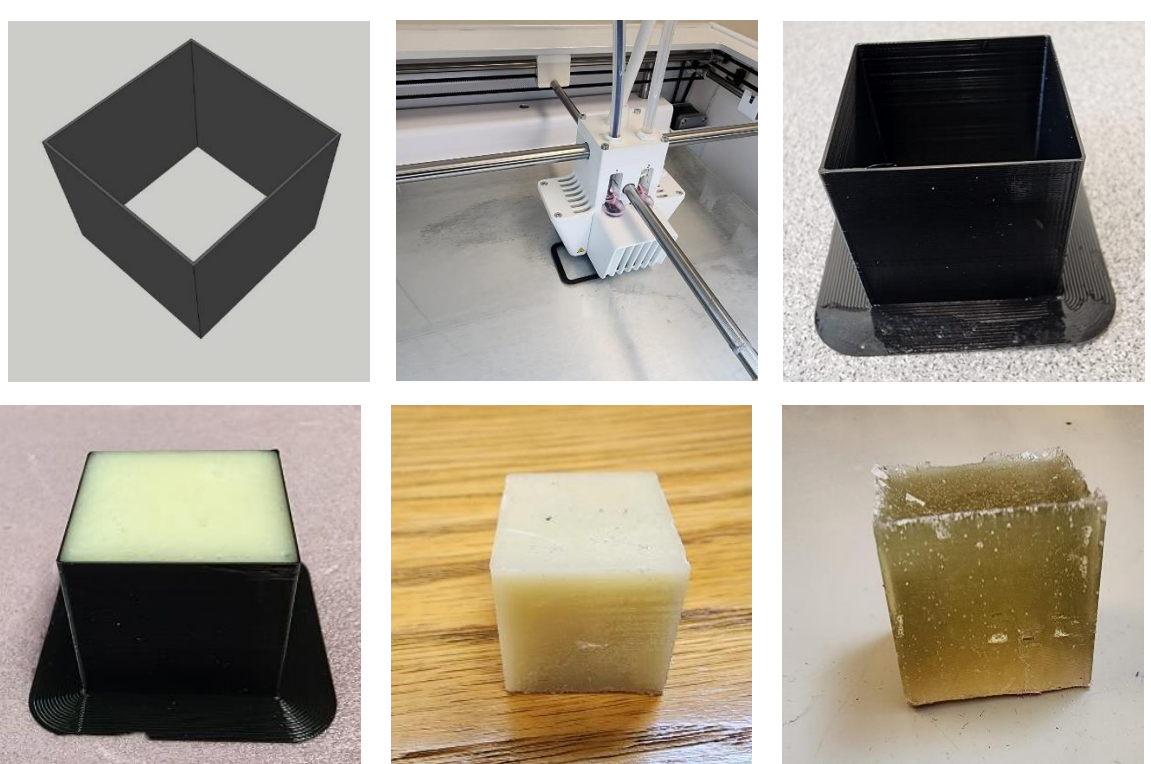


Figure 7 Epoxy samples for testing

3.1.1 Room Temperature

Fatigue testing was carried out to assess the fatigue performance of each epoxy material under room temperature conditions. Their reactions during these tests were monitored and documented. For the testing, an MTS machine, as shown in Figure 8, was employed. This machine applies controlled cyclic loading to materials and components, ensuring precision and repeatability. Each epoxy sample underwent 2 million cycles at a constant displacement. Analysis of the data from these tests offered insights into the epoxies' durability, structural integrity, and resilience to cyclic loading. These findings were pivotal in determining the epoxies' appropriateness for specific applications.

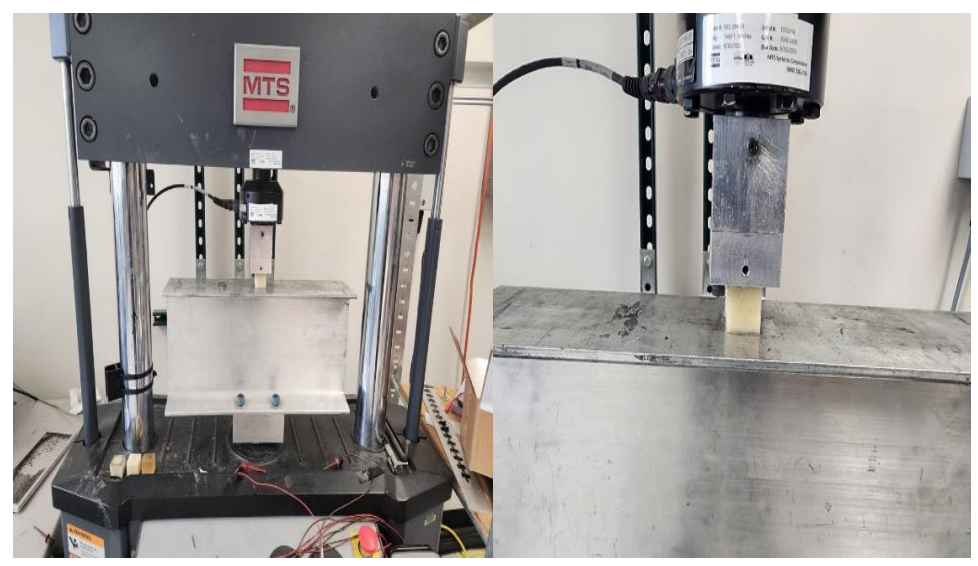


Figure 8 Fatigue testing of epoxies using MTS

The fatigue testing results for the G-100 Ultra Impact Epoxy demonstrated a consistent response throughout the applied cyclic loading at room temperature, as depicted in Figure 9, indicating uniform behavior and suggesting that the overall sustainability of the epoxy remained unchanged. The epoxy exhibited a stable and consistent performance throughout the duration of the testing, suggesting its ability to withstand repeated loading without significant degradation or failure. It implies that epoxy can sustain its mechanical properties and structural integrity even when subjected to prolonged cyclic loading, making it a promising choice for applications where fatigue resistance is crucial.

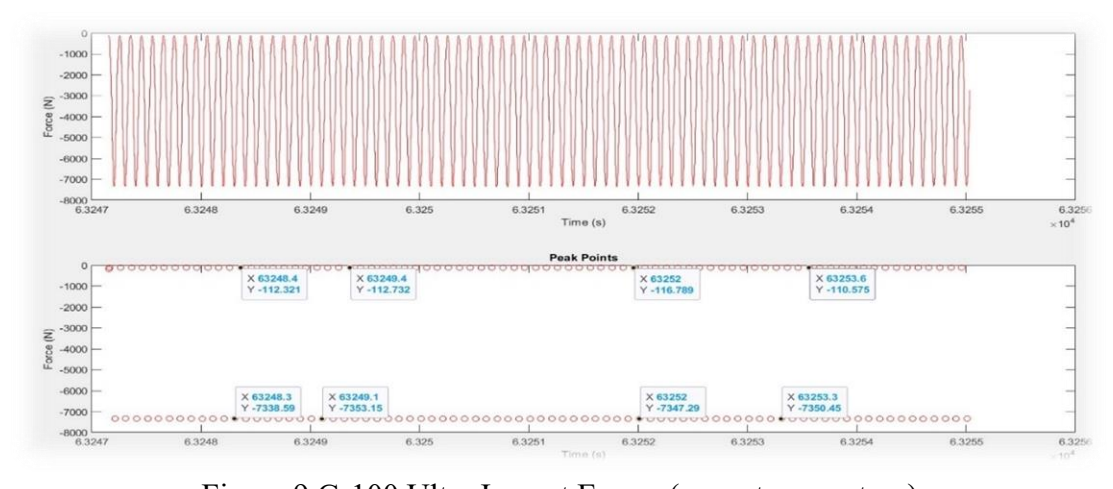


Figure 9 G-100 Ultra Impact Epoxy (room temperature)

Likewise, the 3 Part Epoxy Patch demonstrated a steady behavior during fatigue loading at room temperature, as shown in Figure 10. This behavior indicated that the epoxy patch preserved

its structural properties and endured consistently over the applied cyclic loading, indicating its reliability and uniform performance.

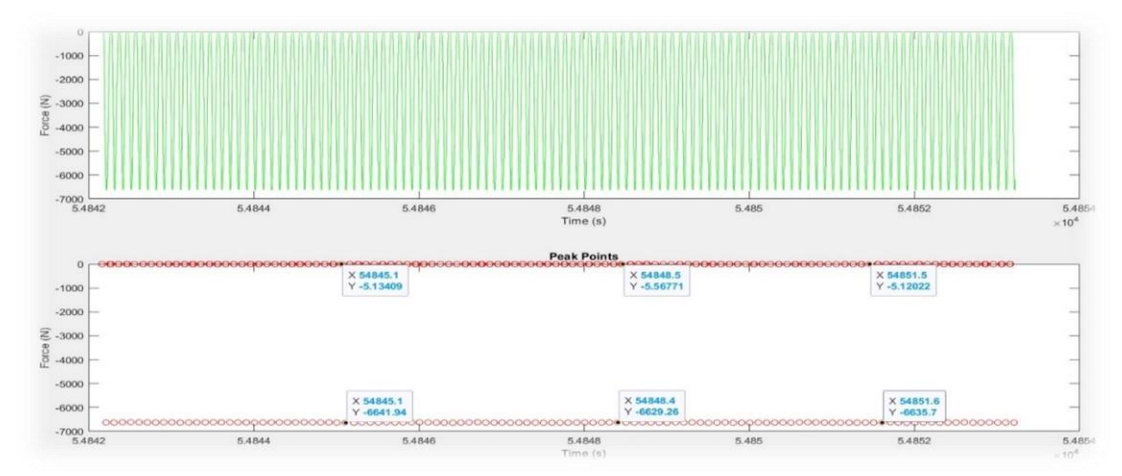


Figure 10 3 Part Epoxy Patch (room temperature)

In contrast to the G-100 Ultra Impact Epoxy and the 3 Part Epoxy Patch, the Max MCR Epoxy showed inconsistent behavior under fatigue loading at room temperature, as illustrated in Figure 11. This fluctuating response indicates that the Max MCR Epoxy had some degree of elasticity and adaptability throughout the testing cycles.

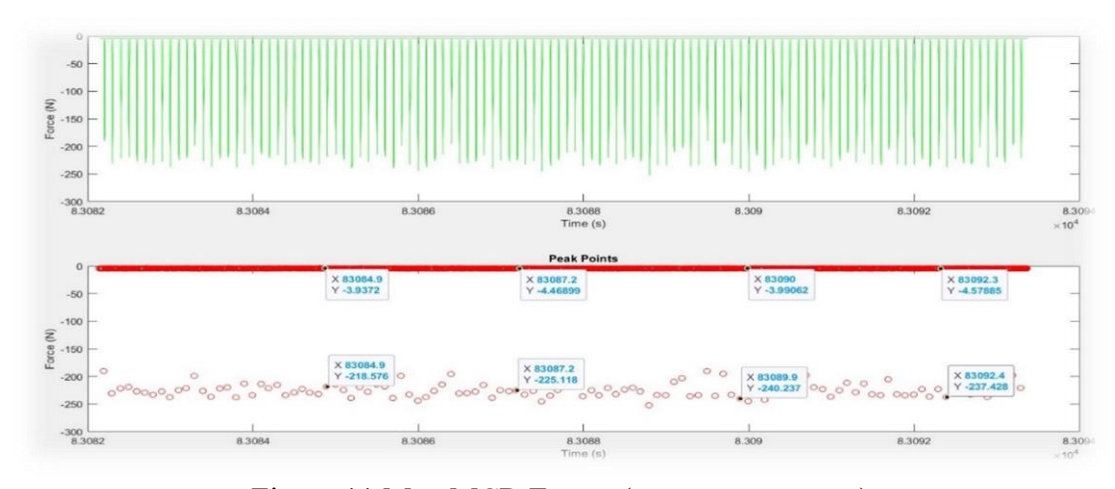


Figure 11 Max MCR Epoxy (room temperature)

3.1.2 Outdoor Environment

After the preliminary fatigue testing, the epoxies underwent a subsequent test to evaluate their behavior and capability to endure continuous pressure outdoors. To simulate real-world conditions and challenges that these epoxies might encounter, they were methodically placed outdoors for 14 days. This deliberate exposure was designed to subject the epoxies to varying atmospheric conditions, including temperature fluctuations, moisture, and other environmental

factors that could influence their structural and mechanical properties. Following this outdoor exposure period, reintroduction to fatigue testing was executed, applying a consistent displacement to each epoxy sample. The central objective of this phase of testing was multifaceted. Firstly, it aimed to discern the epoxies' ability to maintain consistent performance across another 2 million cycles, especially after being subjected to real-world environmental stressors. Secondly, the test intended to uncover any nuanced changes in their performance metrics, resilience levels, or overall capacity to withstand and sustain the pressures of repeated loading. It ensured that any deviations, anomalies, or shifts in epoxy behavior due to environmental factors were adequately captured and analyzed.

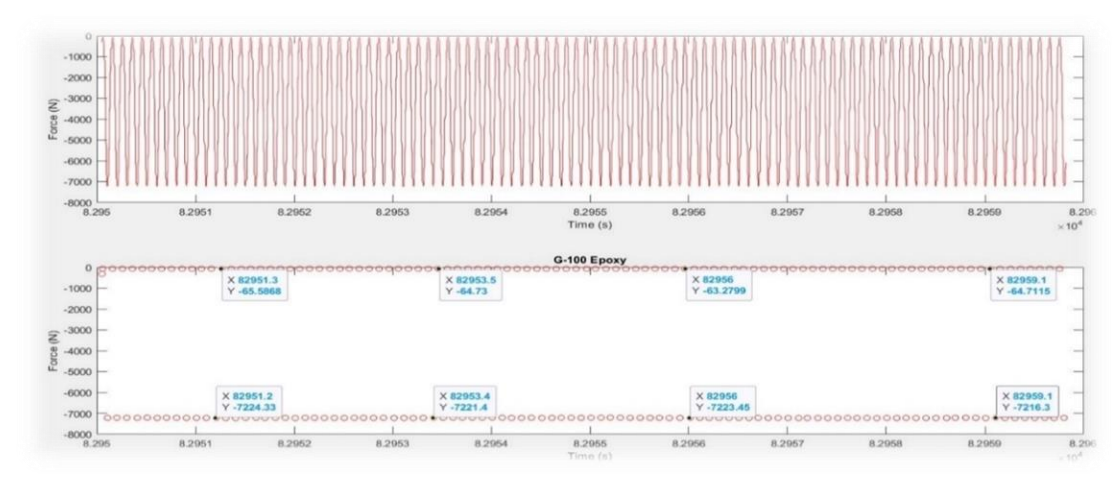


Figure 12 G 100 Ultra Impact Epoxy (outdoor environment)

As per Figure 12, the G-100 Ultra Impact Epoxy responded consistently to the loading cycle, even after a 14-day outdoor exposure. The consistent behavior depicted in Figure 12 underscores the epoxy's durability and reliability in indoor and outdoor settings. This data also highlights the epoxy's robust fatigue resistance and capacity to preserve its structural integrity and mechanical properties despite prolonged cyclic loading and environmental challenges. The G-100 Ultra Impact Epoxy's steadfast response, especially after outdoor exposure, suggests its aptness for applications demanding enduring performance under cyclic loads.

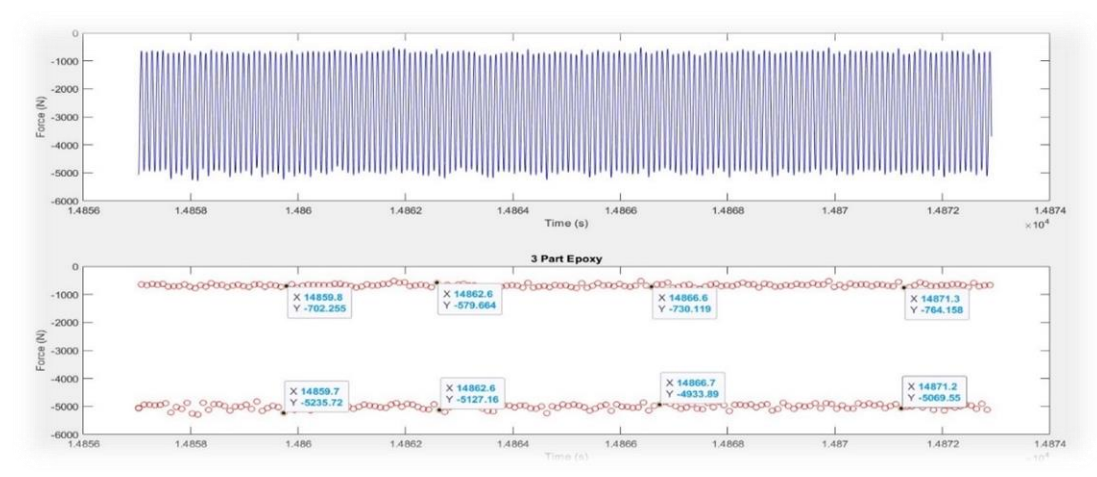


Figure 13 3 Part Epoxy Patch (outdoor environment)

Based on Figure 13, the 3 Part Epoxy Patch displayed an inconsistent response to the loading cycle after a 14-day exposure to the outdoor conditions. The figure reveals a declining trend in the epoxy's ability to bear the load. This suggests potential degradation of the 3 Part Epoxy Patch. Such decline in load-bearing capacity implies possible compromises in the epoxy's fatigue resistance and overall durability.

Figure 14 reveals that the Max MCR Epoxy also demonstrated an inconsistent response to fatigue loading, with its strength diminishing over time following a 14-day exposure to the outdoor environment, suggesting that epoxy may have undergone some form of degradation due to environmental factors, impacting its fatigue resistance and overall performance.

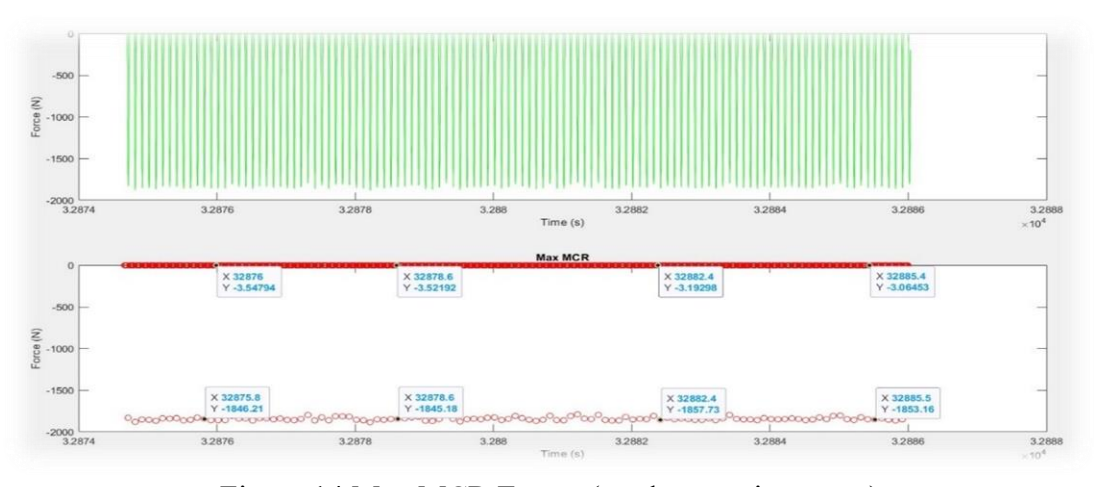


Figure 14 Max MCR Epoxy (outdoor environment)

The primary objective of utilizing epoxy in this setting is to shield piezoelectric sensors from environmental elements, fatigue wear, and the friction generated by vehicular tires. Figure 15 presents the response of the examined epoxies under cyclic loading, with the red curve

representing the G-100 Ultra Impact Epoxy, the green curve for the 3 Part Epoxy Patch, and the blue curve signifying the Max MCR Epoxy.

The G-100 epoxy showcased the most stable behavior of the three epoxies tested, registering a mere variation of under 4% throughout the cyclic loading examination. Conversely, the responses of the other epoxies displayed a pronounced decline, especially after exposure to outdoor conditions. The G-100 epoxy's consistent performance at room and outdoor temperatures under cyclic loading conditions positions it as a prime candidate for this application. Its negligible deviation in response suggests its proficiency in safeguarding piezoelectric sensors and ensuring their continued operation over prolonged usage durations.

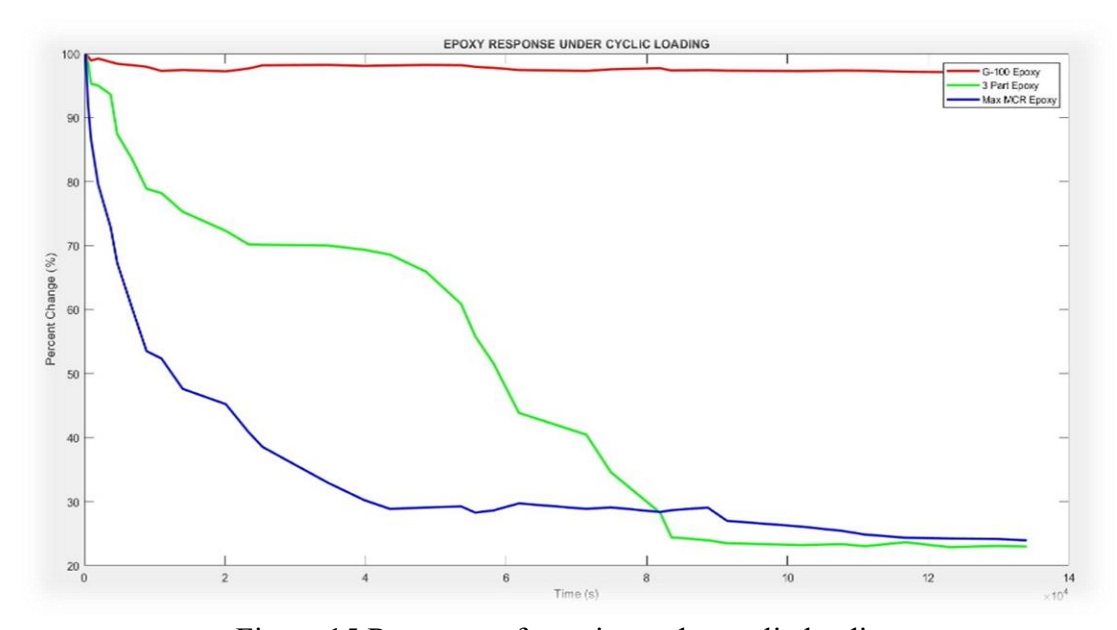


Figure 15 Response of epoxies under cyclic loading

3.1.3 Piezoelectric sensors embedded in G-100 Ultra Impact Epoxy

Among the trio of epoxies analyzed, the G-100 epoxy emerged as the preferred choice. Three distinct samples were crafted using the G-100 epoxy to delve deeper into its performance. Each of these samples incorporated a set of three piezoelectric sensors, equidistant from each other, with a spacing of 1 cm. This arrangement ensured that the sensors spanned the entire breadth of the sample, from one edge to the opposite one. The physical dimensions of these samples were specified as 8.6 cm length, 7.6 cm width, and 0.8 cm thickness. This configuration is shown in Figure 16.



Figure 16 Piezoelectric sensor embedded within G 100 epoxy

Two distinct scenarios involving vehicle tires passing over the G-100 Ultra Impact Epoxy embedded with piezoelectric sensors were examined. In the initial scenario, labeled as Case 1 and illustrated in Figure 17, the experiment's design allowed the samples to experience compressive loads targeted precisely at the middle of the piezoelectric sensor strip, spanning the entire width of the sensor, effectively simulating a situation where a vehicle's tire directly traverses and entirely envelops the sensor.

Conversely, in the subsequent scenario, designated as Case 2 and also visualized in Figure 17, the experimental approach subjected the samples to compressive loads that engaged only a specific segment of the sensor's width. This setup replicated the real-world situation in which a vehicle's tire grazes or partially covers the sensor rather than fully overlapping it.

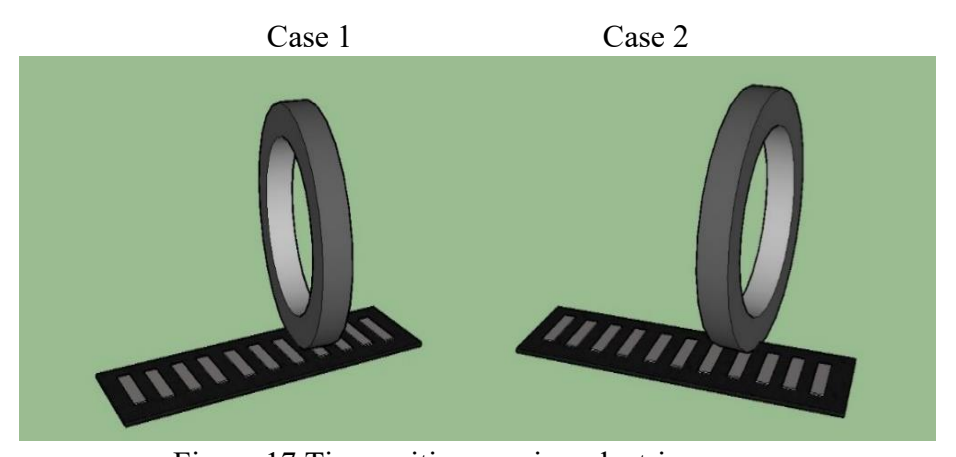


Figure 17 Tire position on piezoelectric sensors

To evaluate the samples' performance under different conditions, they were exposed to loading with varying amplitudes from 1 to 1.5 kilonewtons (KN) and at frequencies ranging from 1 to 3 Hertz (Hz). These tests were conducted using an MTS machine, as depicted in Figure 18. Within this setup, the load applied had a sinusoidal pattern and underwent 1000 cycles at both 1 Hz and 3 Hz frequencies. The pressure exerted on the samples was spread across a contact area

of 1.13 cm². As a result, the samples experienced a total applied pressure of approximately 1.21 ksi.

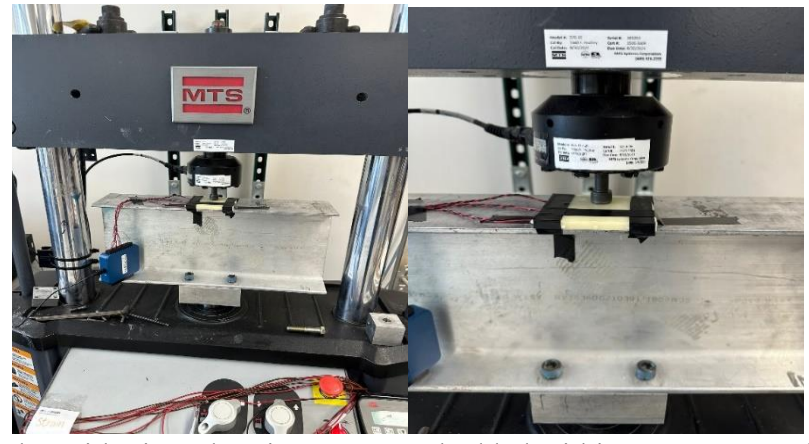


Figure 18 Samples with piezoelectric sensors embedded within G-100 epoxy loaded on MTS

During the initial cycle, the sample was positioned on the MTS machine so that the load was applied exclusively to the right-most piezoelectric sensor, aligning with case 1 as previously described. The results from this setup are shown in Figure 19. The piezoelectric sensor directly beneath the applied load registered a peak output of roughly 10V. In contrast, the other two sensors recorded diminished outputs of about 3V and 0.5V, respectively, based on their proximity to the load application point. When compared to the right sensor, the measured voltage outputs revealed a decline of about 70% and 95% for the middle and left sensors. This data suggests substantial voltage reduction of around 70% at a distance of 1 cm from the tire's edge.

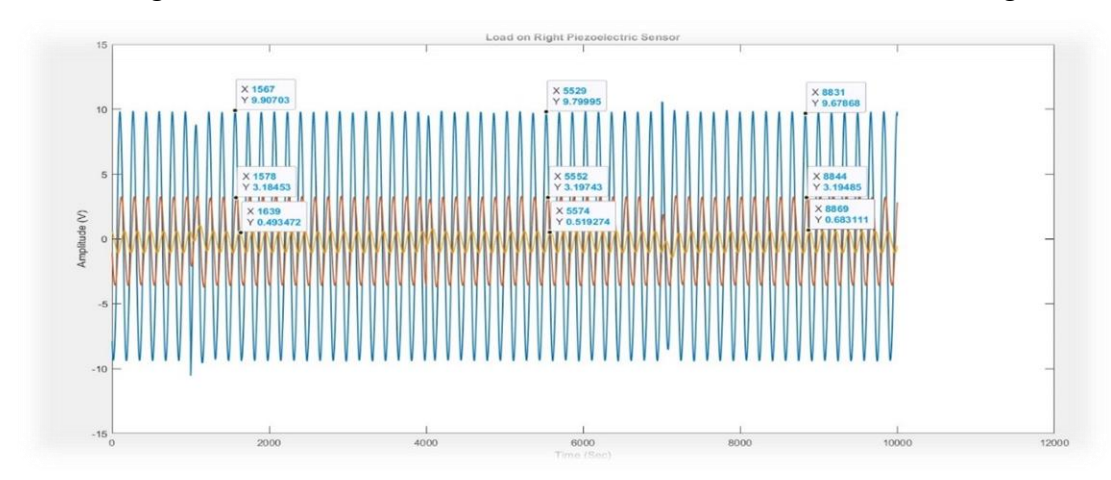


Figure 19 Load on right piezoelectric sensor

In the subsequent cycle, the load was positioned over the center of the leftmost sensor, in alignment with case 1. The results acquired from this test mirrored the prior experiment, as illustrated in Figure 20. The piezoelectric sensor directly under the load showed a peak output of

about 10V. In contrast, the other two sensors exhibited roughly 5V and 1V outputs, respectively. These measurements reflect a decrease in output by about 50% and 90% relative to the output of the leftmost sensor. The congruence in the responses between this test and the preceding one reinforces the observation that the placement of the load on the sensors significantly influences their outputs.

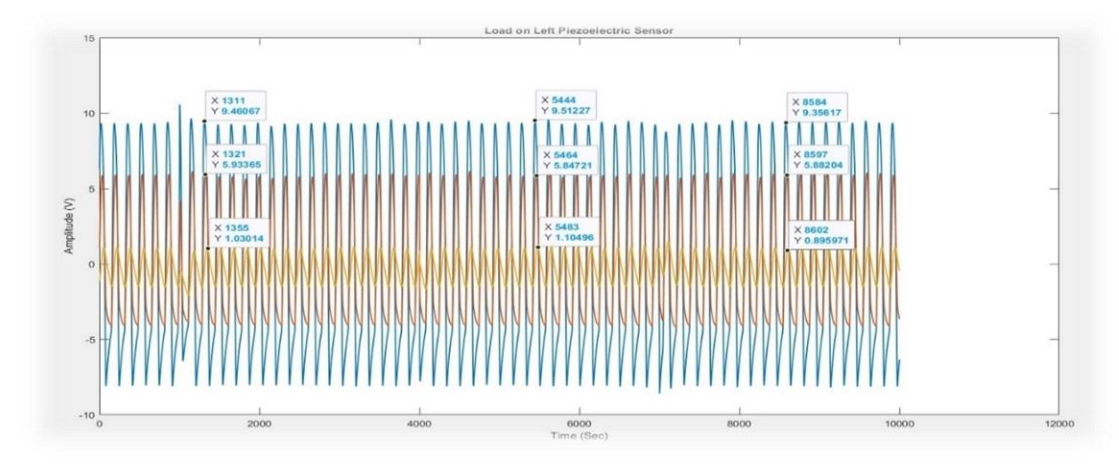


Figure 20 Load on left piezoelectric sensor

During the third testing cycle, load was applied directly over this middle sensor, aligning with the parameters set in case 1. As presented in Figure 21, the empirical results from this focused test proved insightful. The piezoelectric sensor, situated right beneath the applied load, responded with a peak output of around 8V. Conversely, the other two sensors, which were equidistant from the central load-bearing point, mirrored each other's performance, registering outputs of approximately 2.5V. Parsing these results, the output of the middle sensor was markedly superior when compared with the readings from its neighboring sensors, which demonstrated a significantly diminished voltage generation capacity.

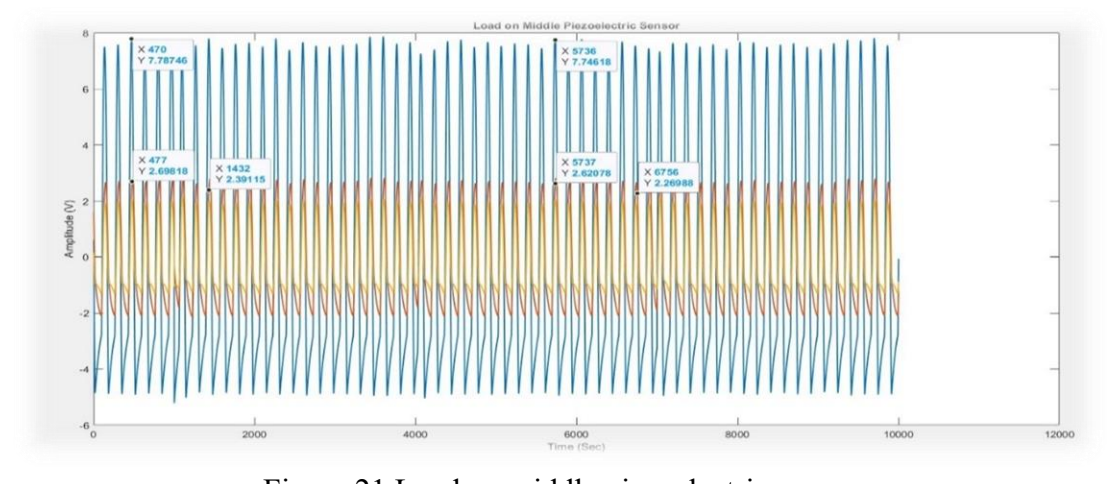


Figure 21 Load on middle piezoelectric sensor

In the next testing cycle, the load was applied at the center of two piezoelectric sensors, covering only a portion of both sensor strips, representing case 2. The response obtained from this configuration is depicted in Figure 22. The sensors between which the load was applied exhibited identical outputs of approximately 6V. On the other hand, the sensor on which no direct load was applied displayed an output of roughly 1V. These findings indicate that when a tire passes directly over two or more sensors, the outputs of these sensors will be the same and will have the highest magnitude compared to the rest of the piezoelectric sensors. This characteristic can be utilized to determine the position and size of the tire accurately. This information makes it possible to precisely locate the tire's position and determine its dimensions based on the uniform and higher outputs observed in the sensors that directly interacted with the load.

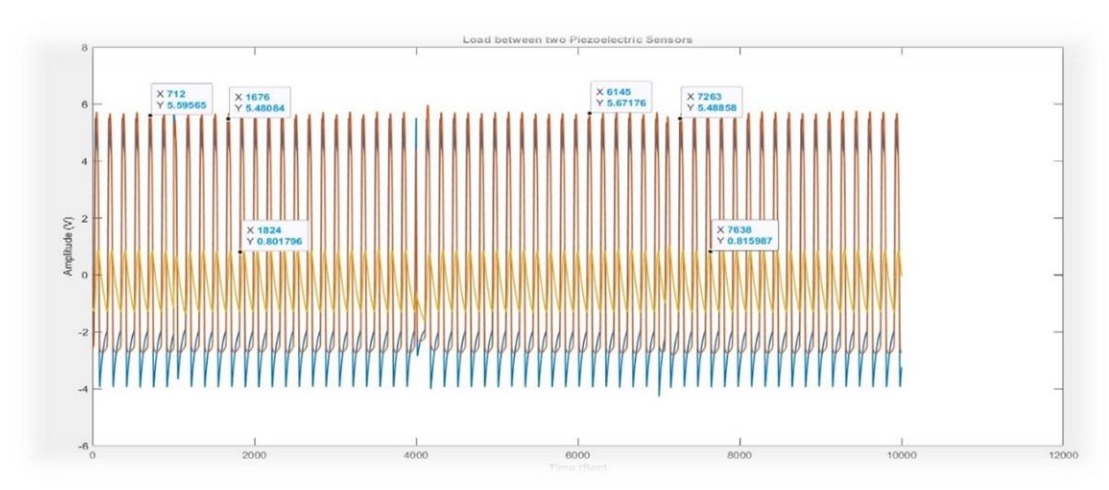


Figure 22 Load on left & middle piezoelectric sensor

3.2 Prototype Sensor

EPDM (Ethylene Propylene Diene Terpolymer) is a commonly utilized material for traffic count cables due to its properties [41]. It is known for its durability, fatigue resistance, and ability to withstand harsh weather conditions. In this research, samples of EPDM rubber were procured from McMaster-Carr to assess their suitability for use in conjunction with piezoelectric sensors. To conduct the feasibility testing, the EPDM rubber samples were cut with dimensions of 36 inches length, 6 inches width, and 0.5 inches thickness. The strip's width was kept at 6 inches to fully encompass the tire's movement impact and to facilitate a lower frequency, thereby extending the tire's contact duration with the strip. Piezoelectric sensors were installed on the rubber samples' surface, as depicted in Figure 23. The subsequent step involved subjecting the samples to compressive loading to observe and measure their response. By examining the

response of the EPDM rubber samples with the installed piezoelectric sensors, the study aimed to evaluate the performance and feasibility of this material in conjunction with the sensors.



Figure 23 EPDM strip with piezoelectric sensors

The primary function of EPDM rubber is to serve as a protective shield for these sensors from environmental elements and potential wear from traffic loads [35]. During the laboratory tests, samples were created by attaching seven piezoelectric sensors to the EPDM rubber strip, a process visually represented in Figure 24. This arrangement facilitates the assessment of sensor performance in a controlled environment. The piezoelectric sensors were combined with the G-100 Ultra Impact Epoxy on the EPDM strip for field tests. This epoxy offers an added layer of protection, further fortifying the sensors against potential external damage. The EPDM rubber also functions as an assembly base for the sensors, forming strips that span a roadway's width. This setup allows for strategically placing sensors on roadways, enabling data acquisition from diverse points concurrently. In essence, the EPDM rubber strip furnishes a protective foundation for the piezoelectric sensors, enhancing their durability against environmental influences and the strain of vehicular traffic.

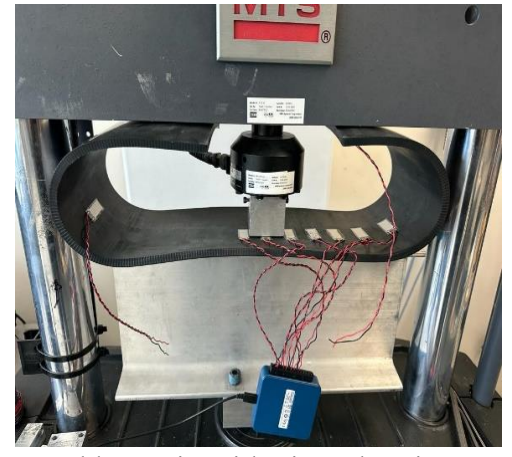


Figure 24 EPDM rubber strip with piezoelectric sensors under MTS

Two distinct load-application heads, with 1.13 cm² and 25 cm², were utilized to apply pressure on the sensors. The resulting outputs from the sensors were then observed and

documented, as illustrated in Figure 25. An NI (National Instruments) card facilitated recording the sensors' output signals.

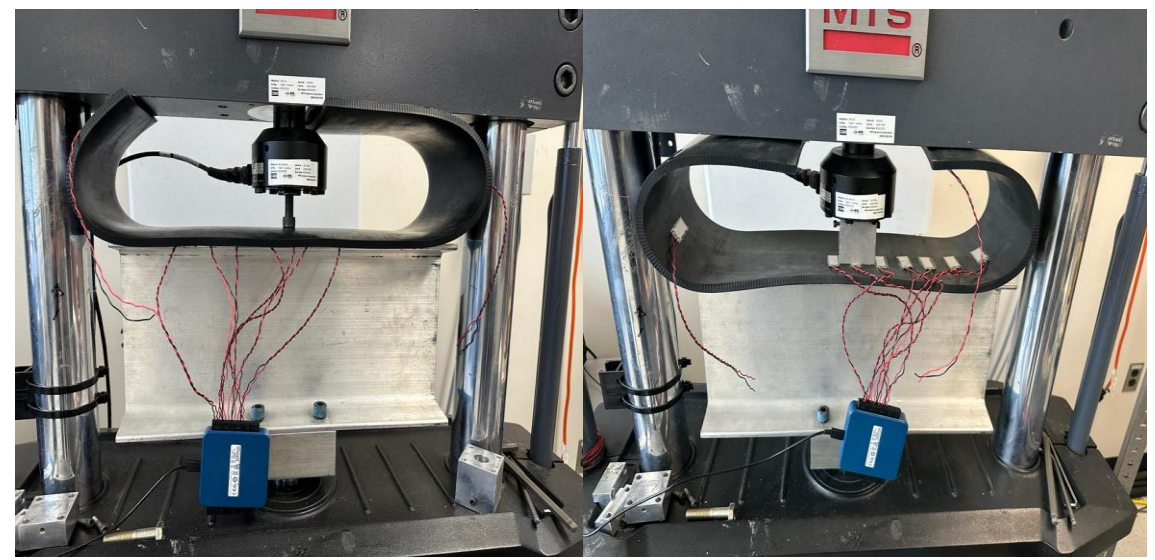


Figure 25 Load heads of 1.13 cm² and 25 cm²

In the initial cycle, a load was applied using a 1.13 cm² head specifically onto a single piezoelectric sensor. The response of the sensor, along with adjacent sensors, is shown in Figure 26. Observing the figure, it becomes apparent that the sensor directly subjected to the load exhibited a notable voltage output. Furthermore, the two neighboring sensors displayed an output of approximately 70%. Conversely, the remaining sensors showed negligible output since the force was not effectively transmitted through the EPDM strip.

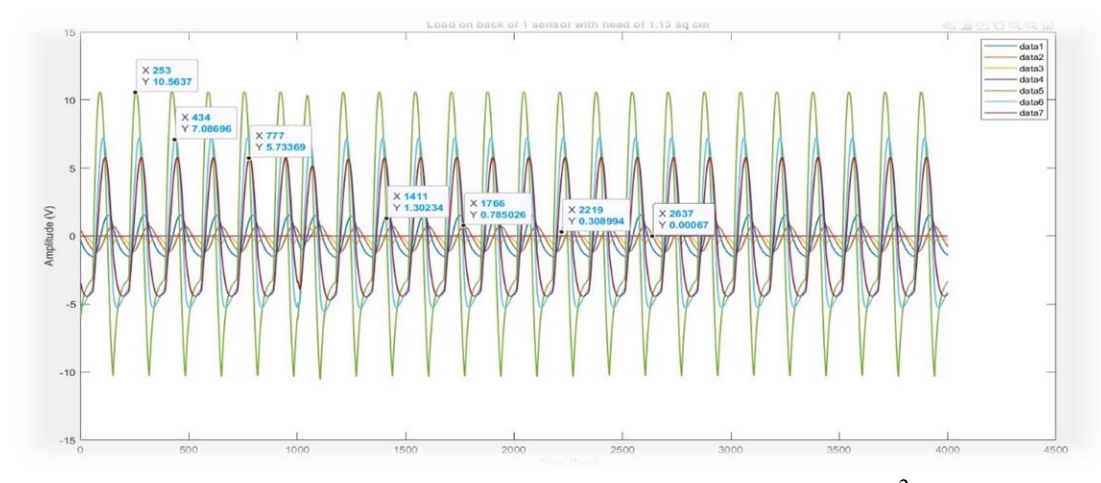


Figure 26 Load on one sensor with a head of 1.13 cm²

The load was applied between the two sensors using the same 1.13 cm² head in the next cycle. The voltage response of the sensors was measured and is depicted in Figure 27. In this case, both sensors exhibited approximately equal output. Additionally, the third adjacent sensor

displayed an output of roughly 50%. However, the remaining sensors indicated negligible output since the force was not effectively transmitted to them through the EPDM strip.

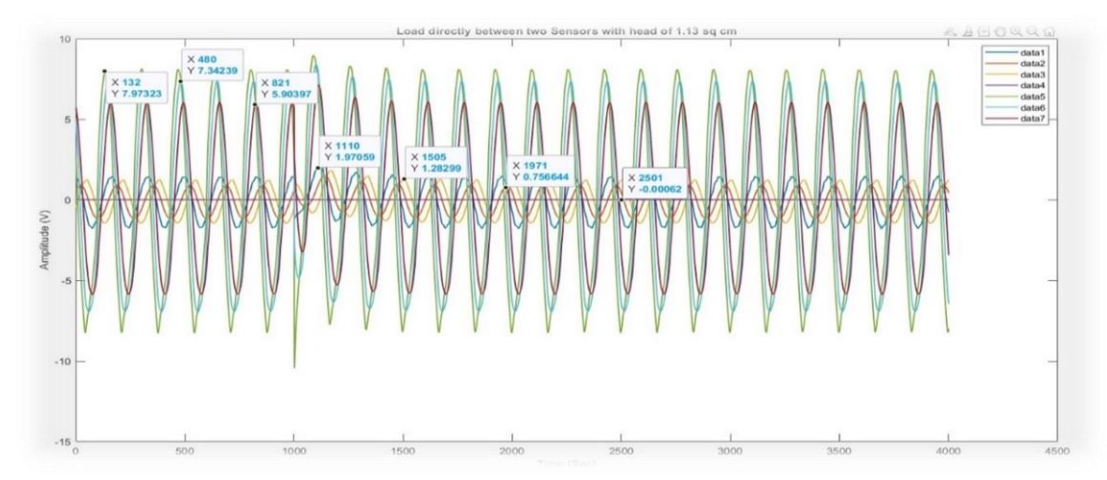


Figure 27 Load between two sensors with a head of 1.13 cm²

In the next cycle, the 25 cm² load head was used on three sensors from the left corner covering the middle sensors and half of the sensors on either side, and their response was recorded. As shown in Figure 28, the output of the middle sensor was the maximum, whereas the sensors on either side had approximately 65% of the voltage output as compared to the middle sensor. The rest of the sensors had negligible output as the force was not directly applied on these sensors.

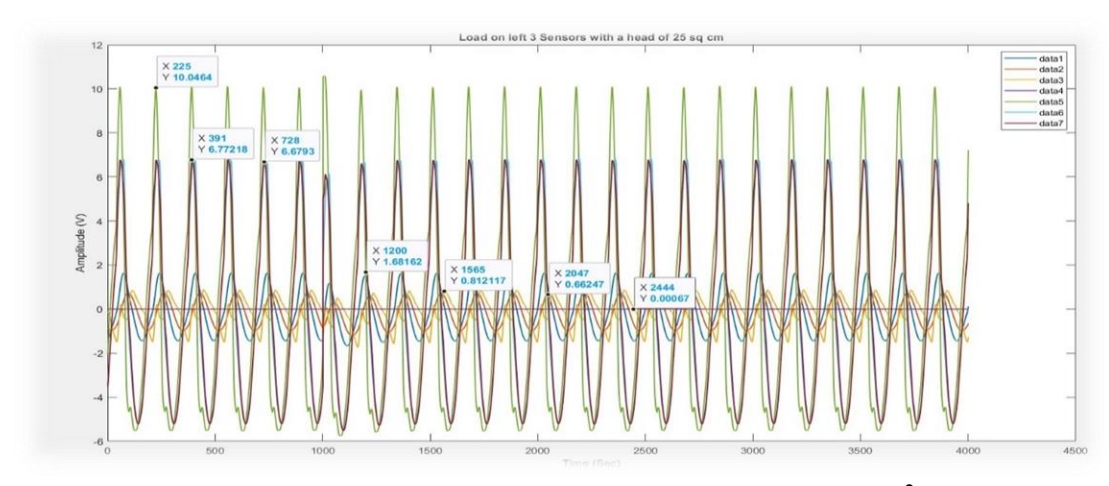


Figure 28 Load on left 3 sensors with a head of 25 cm²

To attenuate the amplitude of the sensor outputs, $1M\Omega$ resistors were integrated into all the sensors, and their subsequent responses were documented, as depicted in Figure 29. The sensors directly subjected to the load demonstrated the highest output, while the outputs from the remaining sensors were minimal.

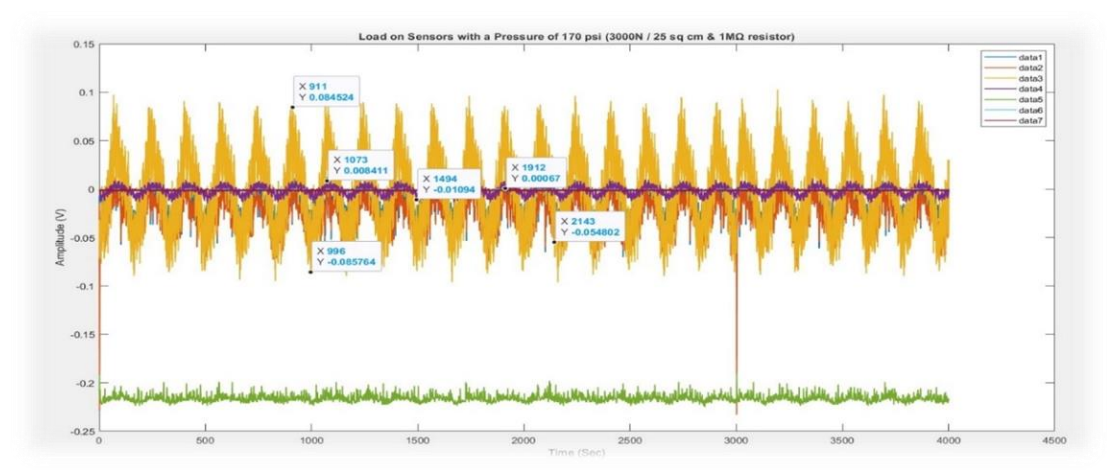


Figure 29 Load on sensors with head of 25 cm² (1M Ω resistor)

3.3 Temperature Chamber Test

In order to investigate the impact of temperature variations on the performance and durability of piezoelectric sensors integrated within epoxy material, the samples were subjected to a temperature chamber test. To assess these effects, the samples were subjected to freeze-thaw cycle tests following the guidelines outlined in the ASTM C666 standard [40]. This standard is typically employed for evaluating the influence of freezing and thawing on concrete specimens. Still, it was adapted to study epoxy samples in this particular context.

The samples underwent a repetitive cycle involving temperature changes during the freeze-thaw test. The cycle consisted of lowering the temperature from 4°C (39.2°F) to -18°C (-0.4°F), followed by raising it back to 4°C (39.2°F). The transition between these temperatures took approximately 1 hour each, and the specimens were maintained at each extreme temperature for 1 hour before transitioning again. This cycle was repeated 8 times, resulting in a testing duration of 4 hours per complete cycle, as presented in Table 6 and Figure 31. The overall setup is shown in Figure 30.



Figure 30 Freeze-Thaw cycles test setting

Table 6 Time duration of 1 Freeze-Thaw cycle

Temperature	Time (Hr)	Remarks
25°C	0	Room temperature
4°C	1	Lowering temperature from room temperature to thaw temperature
-18°C	2	Lowering temperature from thaw temperature to freezing temperature
-18°C	3	Samples kept for 1 hour
4°C	4	Increasing temperature from freeze temperature to thaw temperature
4°C	5	Samples kept for 1 hour
		Cycle restart

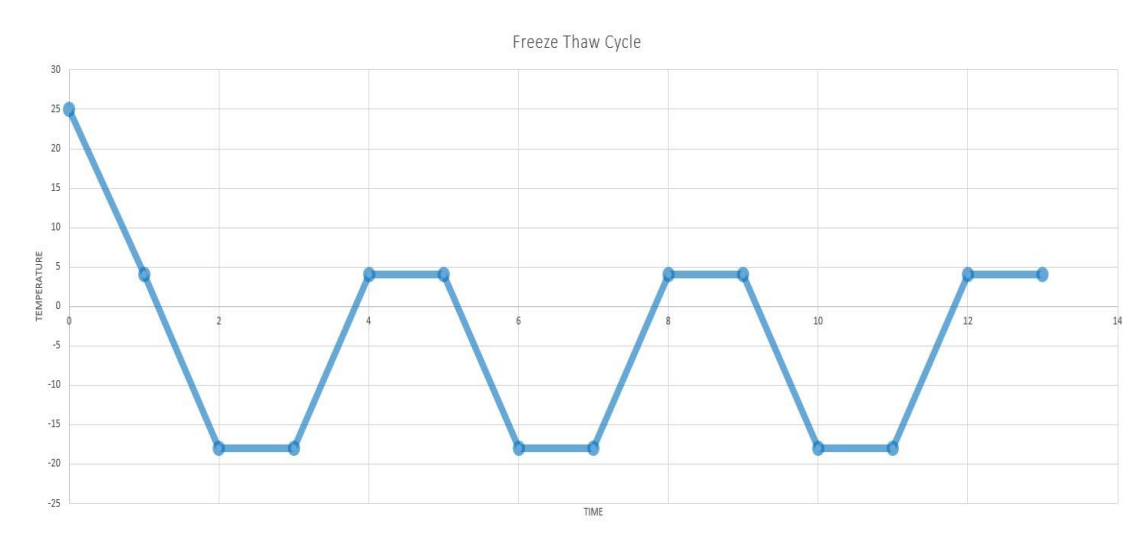


Figure 31 Freeze-thaw cycles

The sample underwent 10,000 cycles at these specific temperatures, applying a constant displacement of 0.8 mm to generate roughly 7000N force. G-100 Ultra Impact epoxy demonstrated a consistent response when subjected to continuous fatigue loading at both 4°C (39.2°F) and -18°C (-0.4°F), as illustrated in Figures 32 and 33 respectively. These figures indicate that the epoxy exhibited uniform behavior and sustained its overall durability at these temperatures, indicating that the response of the epoxy remained largely unaltered when compared to the same number of cycles conducted at normal room temperature.

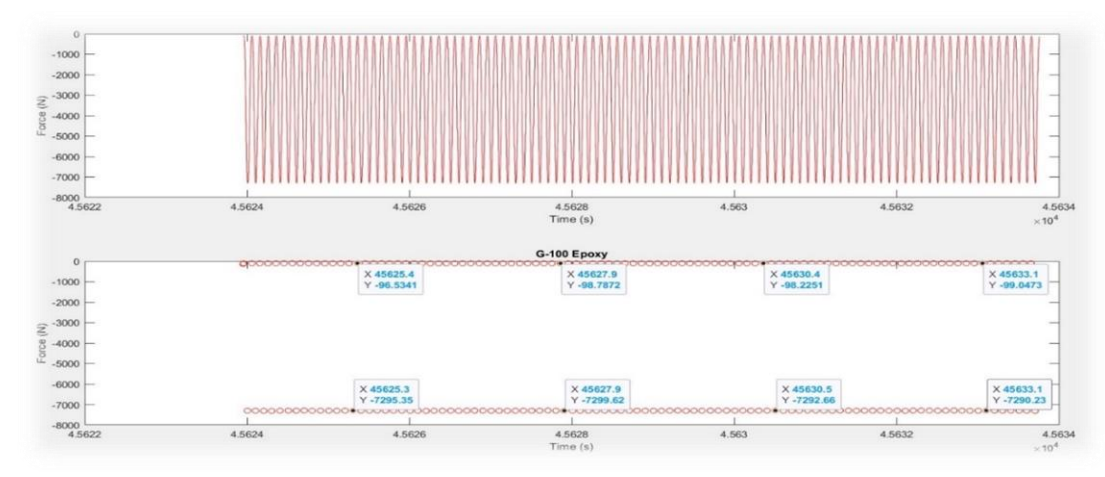


Figure 32 G-100 Ultra Impact Epoxy at 4°C (39.2°F)

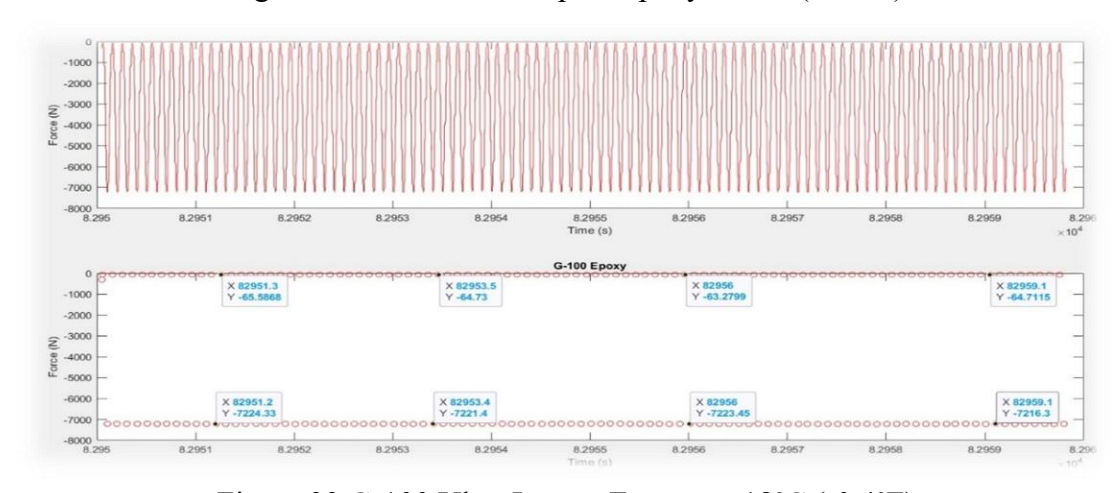


Figure 33 G-100 Ultra Impact Epoxy at -18°C (-0.4°F)

3.4 Summary

This chapter describes the employment of piezoelectric sensor strands housed in a protective polymer to monitor voltage fluctuations due to tire pressure, offering a method for assessing a vehicle's tire position and width. Central to this research was identifying an optimal epoxy to shield these sensors from environmental elements and vehicular traffic stress. Three distinct epoxies were evaluated: G-100 Ultra Impact Epoxy, 3 Part Epoxy Patch, and Max MCR Epoxy. Preliminary fatigue evaluations at ambient temperature yielded consistent outcomes for G-100 and the 3 Part Epoxy Patch. However, Max MCR presented more variable results. After two weeks of exposure to outdoor conditions, the 3 Part Epoxy Patch and Max MCR Epoxy demonstrated diminished efficiency, hinting at potential degradation. Among the contenders, G-100 epoxy emerged as the most dependable and robust, earmarking it as the preferred choice for this use case.

Subsequent tests incorporated the G-100 Ultra Impact Epoxy due to its consistent performance during cyclic loading changes. In these tests, three samples integrated with piezoelectric sensors underwent evaluation under conditions simulating tire load. In instances of direct load application, the sensor situated directly beneath the load registered the maximum voltage output, whereas neighboring sensors displayed marked voltage reductions. For partial load scenarios, sensors located directly under the tire yielded equivalent high outputs, underscoring their potential utility in accurately gauging tire dimensions and positioning. Moreover, EPDM rubber underwent compatibility tests with piezoelectric sensors. This rubber acts as a shield against environmental wear and tear, as well as traffic-induced fatigue. In controlled lab conditions, a rubber strip with seven piezoelectric sensors was subjected to various load tests, revealing that the sensors' voltage outputs were contingent on the distribution of the applied force and their proximity to the point of load application. Including $1M\Omega$ resistors effectively reduced the amplitude of the sensor output, facilitating the measurement of more substantial loads. Furthermore, the resilience of the epoxy was affirmed through freeze-thaw cycle evaluations. The epoxy's behavior consistently mirrored its ambient temperature performance across fluctuating temperatures and stress levels.

CHAPTER 4 FIELD VALIDATION AND ALGORITHM MODELINGING

4.1 Field Validation

The system discussed in Chapter 3 was adapted for field validation. The experimental setup consisted of constructing a strip comprising 16 piezoelectric sensors placed on an EPDM rubber pad, as depicted in Figure 34. This active strip housed the 16 piezoelectric sensors and had a total length of 1.2 feet. Each individual piezoelectric sensor had a width of 1.6 cm, and the spacing between adjacent sensors was maintained at 0.7 cm. To capture the output voltage signals generated by the sensors, two NI cards were utilized. These cards were responsible for acquiring and processing the data from the piezoelectric sensors during the experiment. Furthermore, an additional EPDM rubber strip was placed over the sensors to protect them from potential friction caused by tire loads and the pavement. This protective layer minimized any possible damage or interference that could affect the accuracy of the measurements. Figure 35 provides a comprehensive overview of the entire test setup, illustrating the arrangement and configuration of the various components in the experiment.



Figure 34 EPDM rubber strip with 16 piezoelectric sensors



Figure 35 Setup for the field test

The designed experiment laid out an EPDM strip with integrated piezoelectric sensors on the roadway. Tests were performed using two distinct vehicle types, each driven at five predetermined speeds: 10 mph, 15 mph, 20 mph, 30 mph, and 40 mph. To detail the contact region between the vehicle tires and the sensor-laden strip, the width of the tire's imprint was assessed. The SUV's contact width was approximately 15.1 cm, while the sedan exhibited a slightly narrower contact width of roughly 13.4 cm. These determinations provide insight into the extent of direct interaction between the tires of the tested vehicles and the embedded sensors on the EPDM strip. Additionally, the wheelbase for the SUV was registered at 3.4 m, whereas the sedan had a shorter wheelbase of 2.8 m. A visual representation of the entire testing arrangement can be seen in Figure 36.



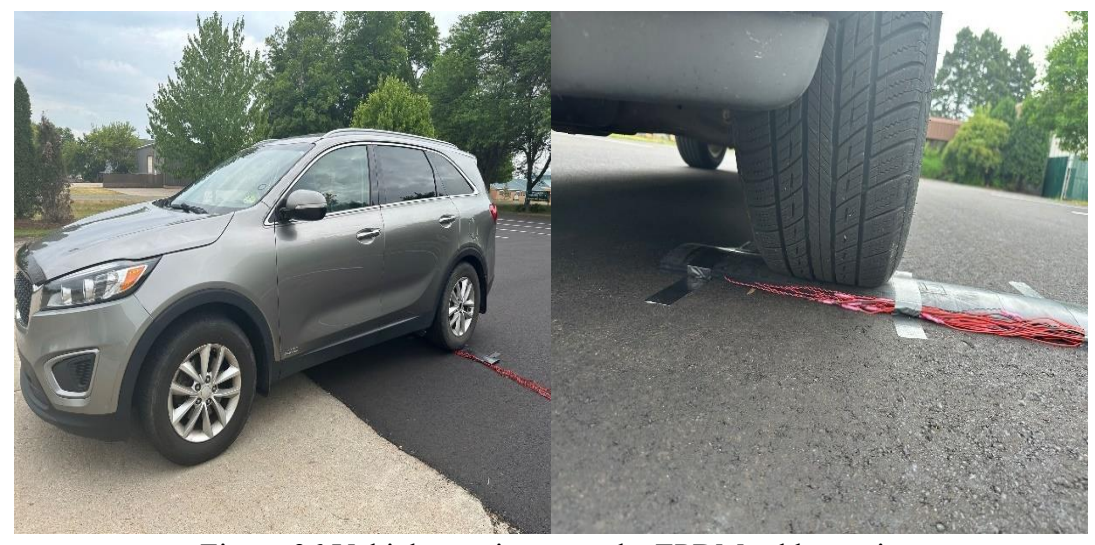


Figure 36 Vehicle passing over the EPDM rubber strip



During the test, as the vehicle's tires passed over the sensors, the voltage was increased in the sensors' output. This voltage increase can be attributed to the piezoelectric effect, producing a measurable voltage response. The overall results for all the passes of the SUV and sedan at various speeds over the rubber strip are attached as Appendix A.

4.1.1 Testing with SUV

In the initial test, an SUV was used to pass over the strip. The vehicle speed varied between 10mph to 40mph. Multiple passes and measurements were conducted. As the tire of the vehicle passed over the strip, a surge in the voltage output of the sensors was observed.

SUV at 15 MPH

As the vehicle passed over the rubber strip, the initial set of eight piezoelectric sensors exhibited substantial responses of approximately 10V, 9.8V, and 9V in sensors 1, 2, and 3, respectively. Conversely, the remaining sensors in this set displayed a limited response, as illustrated in Figure 37. Additionally, the final set of eight piezoelectric sensors' response was recorded when the vehicle's tire traversed over the first set of eight sensors. However, it is noteworthy that the observed response in this set reached a maximum of only 40%, as depicted in Figure 38. This response observed in the final set of eight sensors can be attributed to the dynamic forces of thrust and jerk exerted by the vehicle's tire on the EPDM rubber strip, given that the strip was not embedded within the pavement structure.

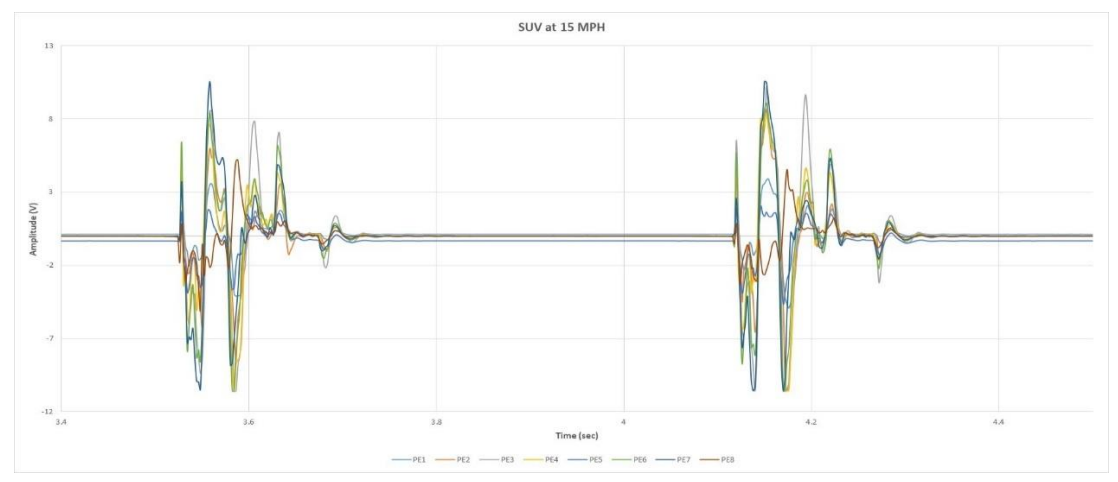


Figure 37 Voltage response of first 8 piezoelectric sensors for SUV (15 mph)

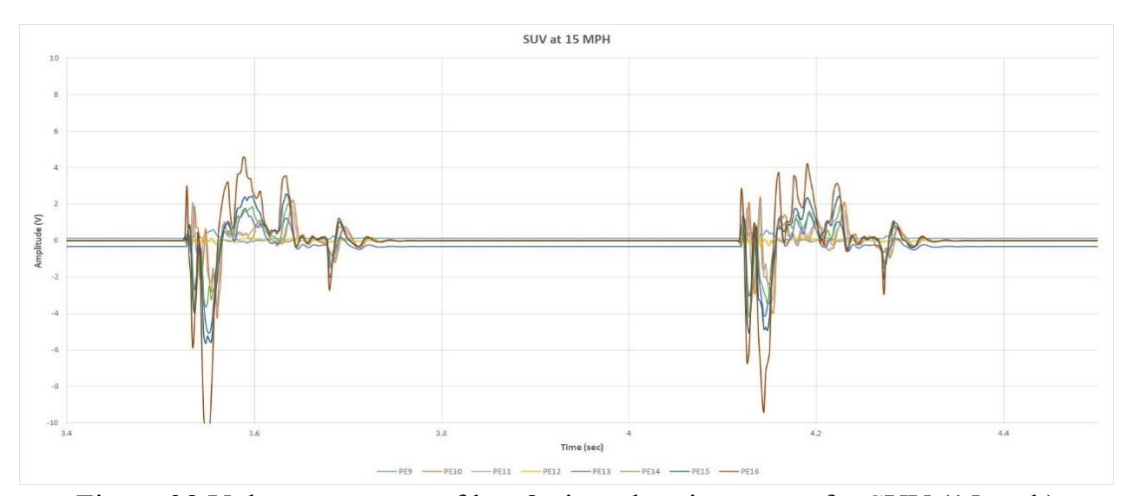


Figure 38 Voltage response of last 8 piezoelectric sensors for SUV (15 mph)

From Figure 37, it was determined that the time between the subsequent tires passing over the EPDM strip was 0.5 seconds. By utilizing the known speed of the vehicle, the wheelbase of the vehicle was calculated as: wheelbase = $6.71 \text{ m/s} \times 0.5 \text{s} = 3.36 \text{ m}$.

The tire width was estimated by selectively considering the sensors that exhibited an output voltage exceeding 5V, as shown in Figure 39. By using the preset distances between these sensors, the tire width for SUV was calculated as 7 Piezoelectric sensors = $7 \times 1.6 \text{ cm} = 11.2 \text{ cm}$; spacing between sensors = $6 \times 0.7 \text{ cm} = 4.2 \text{ cm}$; So, the tire width was estimated at 15.4 cm (1.99% error).

Table 7 summarizes the calculated tire width for four passes of the SUV at each speed. At higher speeds, the tire width calculation had an error of approximately 13% due to the spacing between the sensors, which resulted in not having complete contact between the sensors and the tire. At higher speeds, as the vehicle tire moved over the rubber strip, the overall width of the tire

was unable to completely cover the piezoelectric sensors due to the spacing between the subsequent sensors, thereby generating an error. However, the overall mean error for all the passes was 2.5%.

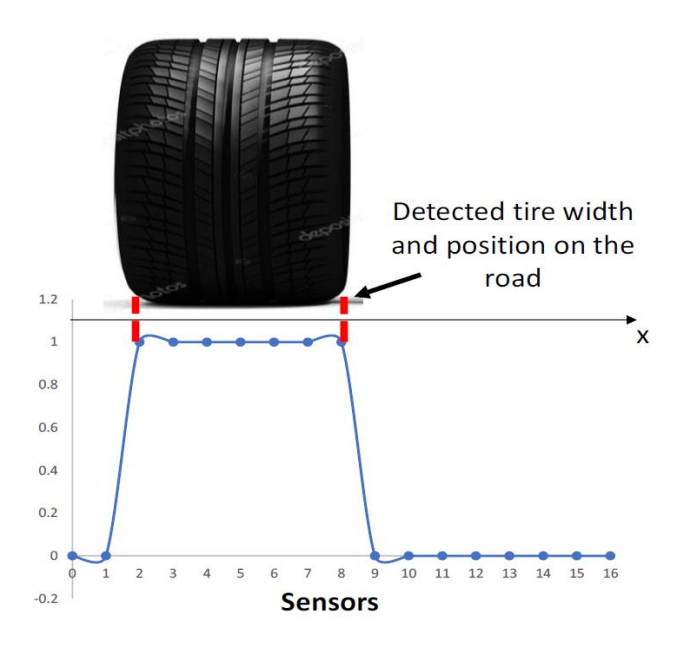


Figure 39 Sensor output at tire contact for SUV (15 mph)

Table 7 Summary of tire width of SUV

Speed (mph)	Measured Tire Width (cm)	Calculated Tire Width (cm)	Error (%)
10	15.1	15.4	1.99
	15.1	15.4	1.99
	15.1	15.4	1.99
	15.1	15.4	1.99
15	15.1	15.4	1.99
	15.1	15.4	1.99
	15.1	15.4	1.99
	15.1	15.4	1.99
20	15.1	15.4	1.99
	15.1	15.4	1.99
	15.1	13.1	-13.25
	15.1	15.4	1.99

Table 7 (cont'd)

40	15.1	15.4	1.99
	15.1	13.1	-13.25
	15.1	13.1	-13.25
	15.1	13.1	-13.25
I	Mean		2.5%
	1.6%		
	Standard Error 95% Confidence Into	1.6% 0.56% to 5.72%	

Table 8 presents a summary of the calculated wheelbase for the four passes of the SUV conducted at each speed. The analysis indicates a mean error of 1.06% for all the passes at four different speeds in the calculated wheelbase from the measured wheelbase of the SUV.

Table 8 Summary of the wheelbase of the SUV

Speed (mph)	Measured Wheelbase (m)	Calculated Wheelbase (m)	Error (%)
	3.4	3.36	-1.18
10	3.4	3.32	-2.35
10	3.4	3.39	-0.29
	3.4	3.34	-1.76
	3.4	3.36	-1.18
15	3.4	3.41	0.29
13	3.4	3.38	-0.59
	3.4	3.39	-0.29
	3.4	3.39	-0.29
20	3.4	3.42	0.59
20	3.4	3.46	1.76
	3.4	3.38	-0.59

Table 8 (cont'd)

	95% Confidence Interval			
Standard Error			0.5%	
<u> </u>	Mean		1.06%	
	3.4	3.55	4.41	
40	3.4	3.51	3.24	
40	3.4	3.54	4.12	
	3.4	3.57	5.00	
	3.4	3.51	3.24	
30	3.4	3.5	2.94	
30	3.4	3.46	1.76	
	3.4	3.48	2.35	

4.1.2 Testing with Sedan

Similar to the SUV tests, multiple speeds and passes were performed. As the sedan tire passed the rubber strip housing piezoelectric sensors, a similar surge in voltage output as observed for the SUV occurs due to the pressure from the vehicle tires onto the piezoelectric sensors.

Sedan at 15 MPH

As the sedan passed over the rubber strip at 15 mph, the second set of eight piezoelectric sensors exhibited substantial responses of approximately 8V in sensors 10, 11, and 12. Conversely, the remaining sensors in this set displayed a limited response, as illustrated in Figure 40. The response of the first set of eight piezoelectric sensors was also recorded when the vehicle's tire traversed over the sensors 10, 11, and 12. However, the observed response was negligible, as depicted in Figure 41.

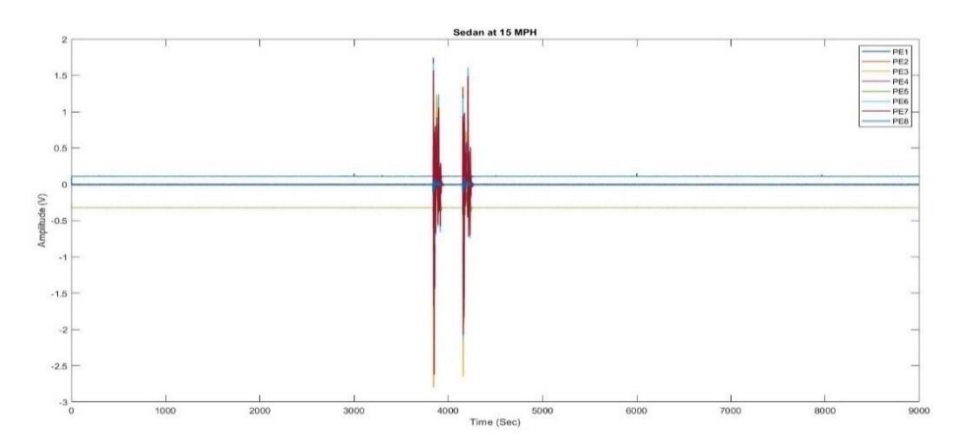


Figure 40 Voltage response of last 8 piezoelectric sensors for sedan (15 mph)

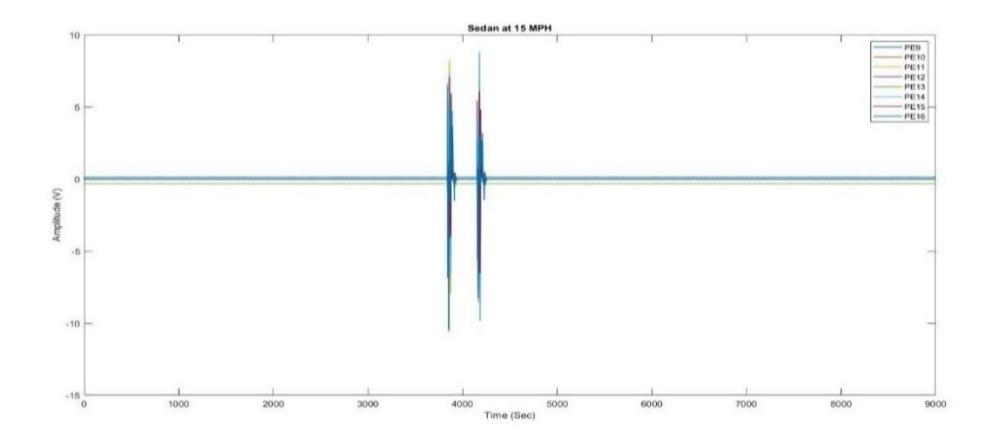


Figure 41 Voltage response of last 8 piezoelectric sensors for sedan (15 mph)

Also, in this test, the width and position of the tire were estimated from the sensors' responses. As shown in Figure 42, using the size and the preset distances between the sensors, the tire width was calculated as 13.1 cm, while the actual tire width was 13.4 cm. The calculated results from the four passes of the sedan at each speed limit are summarized in Table 9. The mean error in the calculated tire width for sedan was close to 5% from the actual tire width.

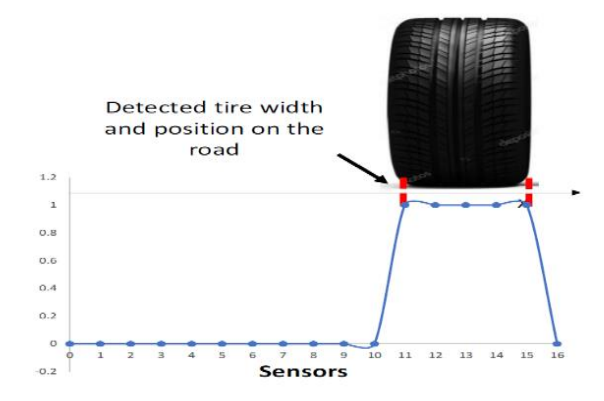


Figure 42 Sensor output at tire contact for sedan (15 mph)

Table 9 Summary of tire width of sedan

Speed (mph)	Measured Tire Width (cm)	Calculated Tire Width (cm)	Error (%)
10	13.4	13.1	-2.24
	13.4	13.1	-2.24
	13.4	13.1	-2.24
	13.4	13.1	-2.24
15	13.4	13.1	-2.24
	13.4	13.1	-2.24
	13.4	13.1	-2.24
	13.4	13.1	-2.24
20	13.4	13.1	-2.24
	13.4	15.4	14.93
	13.4	15.4	14.93
	13.4	13.1	-2.24
30	13.4	15.4	14.93
	13.4	13.1	-2.24
	13.4	15.4	14.93
	13.4	15.4	14.93
40	13.4	15.4	14.93
	13.4	15.4	14.93
	13.4	15.4	14.93
	13.4	13.1	-2.24
	Mean		4.74%
	Standard Error		1.91%
	95% Confidence Interva	al	1% to 8%

Table 10 summarizes the calculated wheelbase for the four passes of the sedan conducted at each speed. The analysis indicates a mean error of 2.63% in the computed wheelbases for all the passes from the measured wheelbase of the sedan.

Table 10 Summary of the wheelbase of the sedan

Speed (mph)	Measured Wheelbase (m)	Calculated Wheelbase (m)	Error (m)
	2.8	2.72	-2.86
10	2.8	2.74	-2.14
10	2.8	2.69	-3.93
	2.8	2.73	-2.50
	2.8	2.75	-1.79
15	2.8	2.76	-1.43
13	2.8	2.74	-2.14
ļ	2.8	2.75	-1.79
	2.8	2.86	2.14
20	2.8	2.89	3.21
20	2.8	2.83	1.07
ļ	2.8	2.88	2.86
	2.8	2.95	5.36
30	2.8	2.92	4.29
30	2.8	2.97	6.07
Ī	2.8	3	7.14
	2.8	3.04	8.57
40	2.8	3.1	10.71
1 0	2.8	3.09	10.36
	2.8	3.06	9.29
I	Mean		2.63%
	Standard Error		1.09%
	95% Confidence Int	erval	0.5% to 4.76%

4.2 Modeling the System

The primary objective of the model study was to develop and train an algorithm capable of interpreting the signals obtained from the piezoelectric sensors embedded in the pavement. Using a machine learning model, the algorithm aimed to identify truck passing events within the time response signal and subsequently classifying them based on their type and spacing. A finite

element model was developed to simulate the behavior of the rectangular strip and the road. The model encompassed the dimensions of the rectangular strip, the material properties, and the boundary conditions of the road. The first step involved creating the geometry of the rectangular strip within the software. This entailed defining the length, width, and thickness of the strip. The material properties, such as elasticity, poisons ratio, and stiffness, were assigned to the respective components. Next, boundary conditions were specified to represent the interaction between the strip and the road. These boundary conditions included constraints or fixed supports at the bottom face of the rubber to mimic the actual conditions of the strip's installation on the road. 77 piezoelectric sensors were modeled and fixed to the top face of the rubber strip in an edge-toedge configuration along the length of the rubber strip. After setting the model, varying loads and speeds that the rectangular strip would encounter were input into the simulation. The finite element software then performed the necessary calculations to simulate the response of the rectangular strip with piezoelectric sensors under the specified loads and speeds. The analysis output included various results, such as strain distribution and voltage output, which provided insights into the strip's behavior and piezoelectric sensors' behavior. By utilizing the finite element model and incorporating the appropriate loads and speeds, the analysis aimed to understand and predict the behavior of the rectangular strip along with the piezoelectric sensors in response to real-world conditions, facilitating the evaluation of its performance and design optimization.

4.2.1 Finite Element Modeling

A finite element model was developed based on the insights gleaned from the field test to investigate the impact of differently loaded trucks operating at various speeds on the sensors. This involved designing an EPDM rubber strip with specific dimensions, measuring 36 inches in length, 6 inches in width, and 0.375 inches in thickness. The material properties of the rubber were also set with the young's modulus as 3 MPa, poisons ratio as 0.495, and mass density as 0.87 g/cm³. Figure 43 shows the overall geometry of the rubber strip.

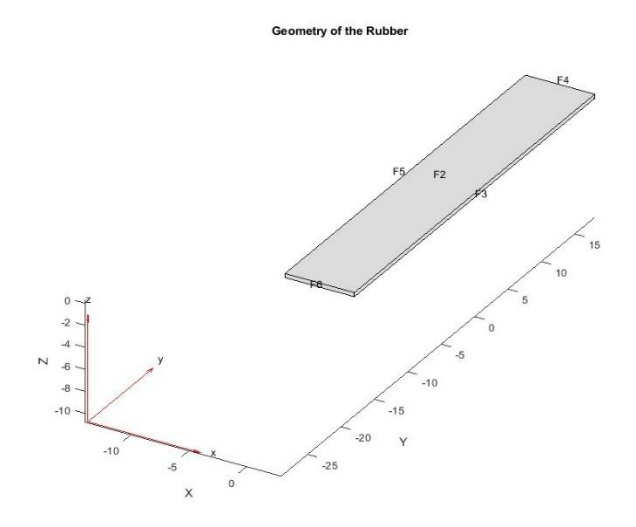


Figure 43 EPDM strip geometry

In the finite element model, the bottom face of the EPDM strip (F1 in Figure 43) was secured and fixed at all nodes, ensuring stability and immobility to the ground. Along the top face of the EPDM strip (F2 in Figure 43), 77 piezoelectric sensors were positioned in an edge-to-edge configuration along the length of the rubber strip in the y-direction. The meshing of this setup is depicted in Figure 44.

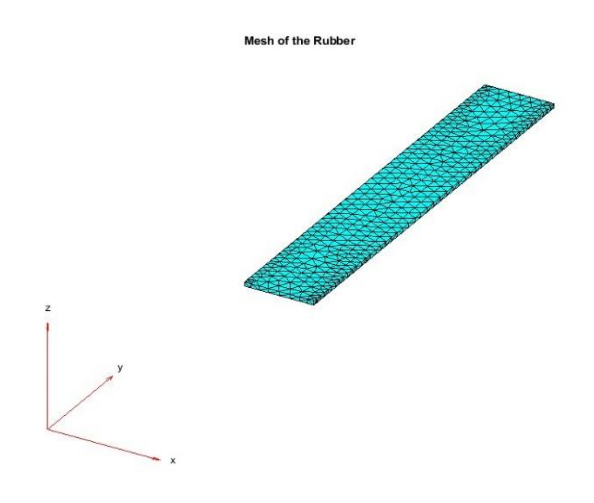


Figure 44 Mesh of the setup

4.2.2 FEM Analysis of Single Wheel

Single tire from the truck configuration was modeled and passed over the EPDM rubber strip. The speed at which the tire traversed the strip was varied, ranging from 45 mph to 70 mph. A dynamic load of 6 kips was applied to simulate real-world conditions. This wheel load was designed to mimic real-time conditions, and the contact area between the tire and the rubber strip

was maintained at 6x6 inches. Figure 45 shows the arrangement and configuration of the model components. Figure 46 presents the model analysis results, specifically focusing on the strain distribution. Figure 47 displays the longitudinal strain experienced by both the rubber and sensors as the front tire was driven over the rubber strip at 60 mph. These strain values offer valuable insights into the behavior of the rubber strip under specific test conditions.

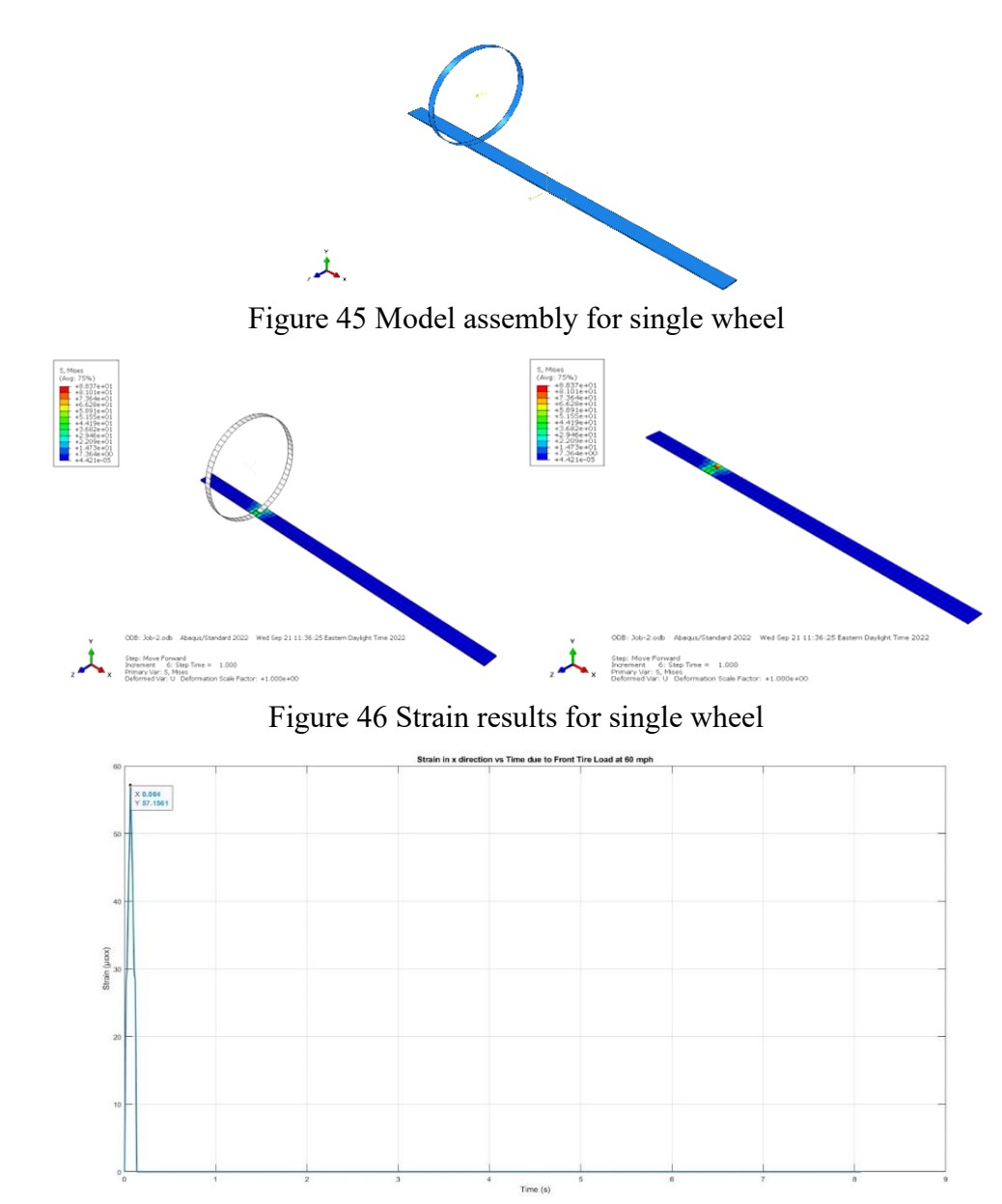


Figure 47 Strain for the front tire

As the tire contacts the strip, the strains accumulate and reach their peak values of 57.15 $\mu\epsilon$ when the tire is fully positioned on the strip. As the tire gradually departs from the rubber contact

area, these strains gradually diminish, ultimately returning to zero. This pattern reflects the dynamic response of the materials involved as the tire interacts with the rubber strip.

For the truck's rear tire, a dynamic load was applied, amounting to 4.25 kips and the contact area between the tire and the rubber strip was maintained at 6x6 inches. Figure 48 displays the strain values obtained when the rear tire was driven over the rubber strip at 60 mph. As the tire contacts the strip, the strains accumulate and reach their peak values of 40.16 µɛ when the tire is fully positioned on the strip. Subsequently, as the tire gradually departs from the rubber contact area, these strains diminish, ultimately returning to zero.

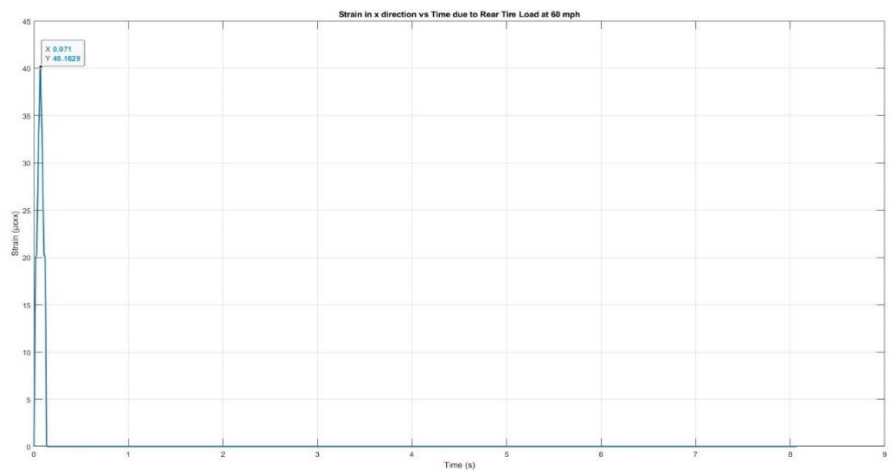


Figure 48 Strain for the rear tire

To validate the accuracy of the calculated strains, an ABAQUS model was designed to simulate the motion of a tire rolling over the rubber strip, as shown in Figure 51. The strain values computed for the rear tires in the ABAQUS model were calculated as 46.1 μ E, which was approximately the same as those presented in Figure 49.

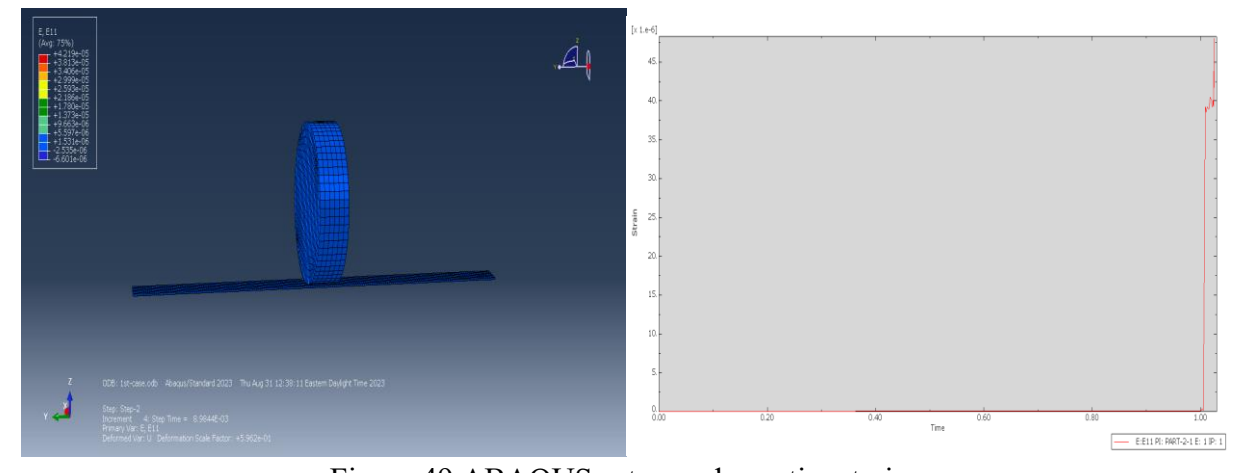


Figure 49 ABAQUS setup and rear tire strains

4.2.3 FEM Analysis of Complete Truck

Following the computation of strains for individual wheels moving over the rubber strip, the strain analysis was extended to encompass the entire truck as it passed over the strip. In this configuration, the dynamic load applied to the front tire was set at 6 kips, while the loads for the remaining tires on each axle were set at 4.25 kips. The truck was set to travel at speed of 60 mph. The wheelbase measurements between the axles were set as follows:

- Between axle 1 and axle 2: 3.05 meters
- Between axle 2 and axle 3: 1.22 meters
- Between axle 3 and axle 4: 8.54 meters
- Between axle 4 and axle 5: 1.22 meters

The model assembly for the complete truck is shown in Figure 50, whereas the model results for strain are shown in Figure 51. Figure 52 illustrates the longitudinal strains observed when the entire truck passed over the rubber strip. The strain caused by the front and each subsequent tire was calculated as $56.9 \mu\epsilon$, $53.2 \mu\epsilon$, $51 \mu\epsilon$, $46.7 \mu\epsilon$, and $46.1 \mu\epsilon$, respectively.

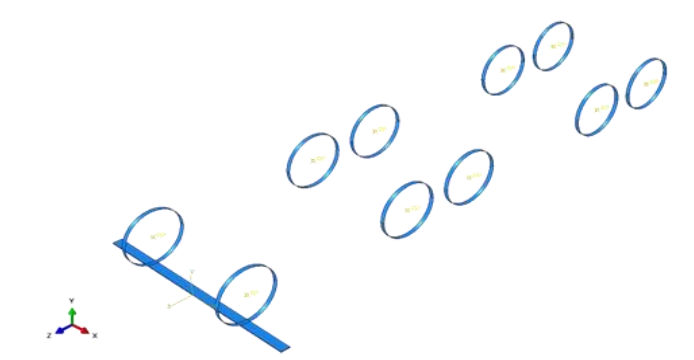


Figure 50 Model assembly for complete truck

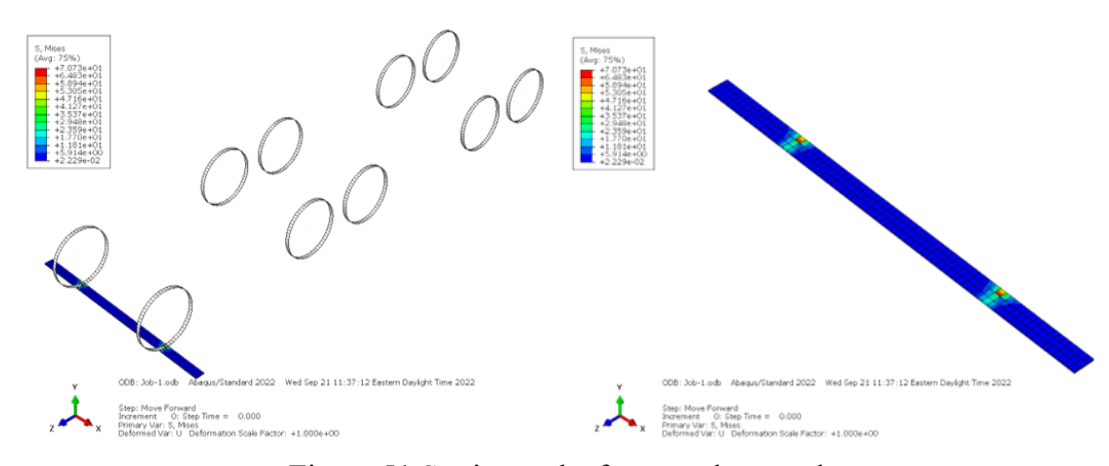


Figure 51 Strain results for complete truck

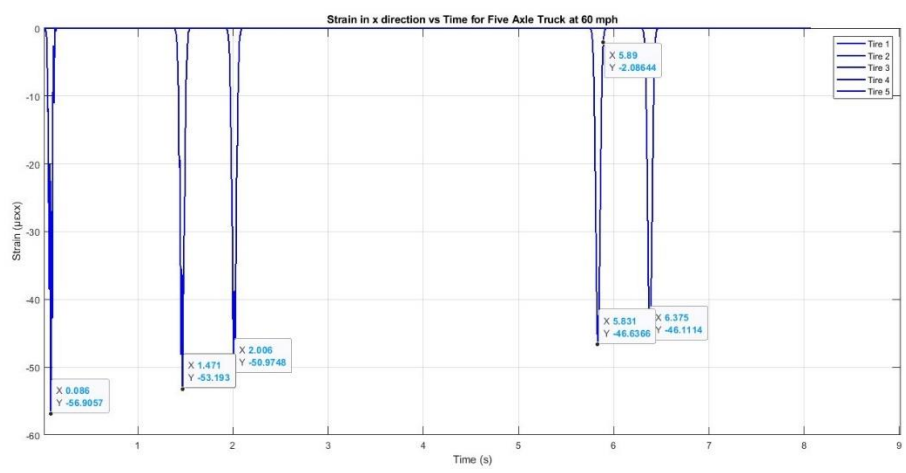


Figure 52 Strains for complete truck

The analysis extended to calculating voltage output generated by the piezoelectric sensors in response to the complete truck passing over them. Figure 53 represents the voltage output resulting from the strains induced by each truck tire as it passed over the sensors. This data provides insights into the electrical responses of the sensors to the dynamic loading of the entire vehicle. As the front tire generated more strain than the other tires, the voltage output for the front tire was also higher than the rest of the tires.

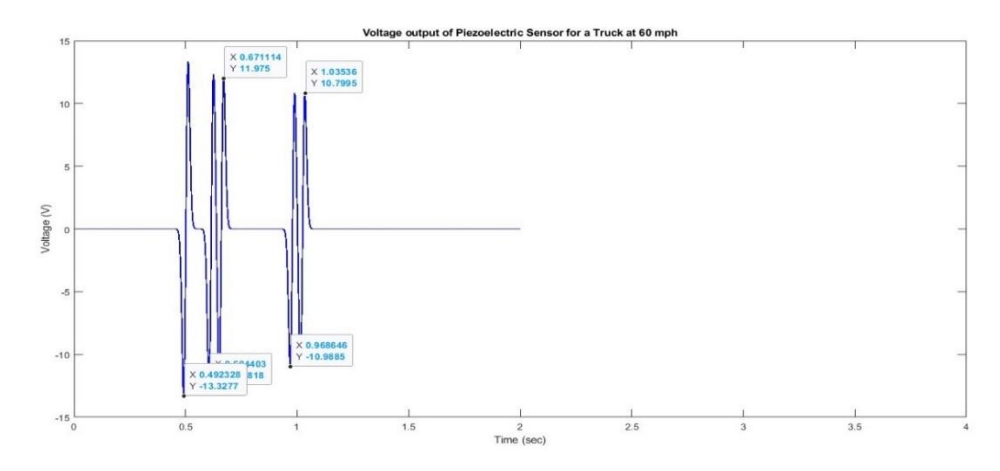


Figure 53 Voltage output for the complete truck

4.2.4 FEM Analysis for 10 Trucks

To introduce variability into the analysis, a set of 10 trucks was generated. The speed of each truck was randomly selected from a range of 45 mph to 70 mph while maintaining consistent wheelbases across all trucks. The load applied to the front tire was set at a constant 6 kips; the loads on the rear tires were randomly assigned values ranging from 3.5 kips to 5 kips. The contact area between the tires and the rubber strip remained uniform at 6 x 6 inches for most

trucks. However, within this set of 10 trucks, 10% were designated as "Wide Base Trucks," for which the contact area was enlarged to 10 x 6 inches, and the loads on the rear tires were randomly distributed within the range of 7 kips to 10 kips. This differentiation in contact area and load for the wide base trucks introduced additional complexity to the analysis, reflecting real-world variability in truck configurations and loading conditions. The distance between each truck ranged from 5 meters to 10 meters. The complete configuration of the trucks is shown in Table 11.

Table 11 Truck data

	Axle	Axle	Axle	Axle	Axle		Contact		Distance to
Truck	Loads 1	Loads 2	Loads 3	Loads 4	Loads 5	Speed	Length	Contact	Next Truck
Number	(kips)	(kips)	(kips)	(kips)	(kips)	(mph)	(in)	Width (in)	(m)
1	6	4.87	4.87	4.87	4.87	64	6	6	7.73
2	6	4.94	4.94	4.94	4.94	61	6	6	9.79
3	6	7.11	7.11	7.11	7.11	66	10	6	9.82
4	6	4.90	4.90	4.90	4.90	61	6	6	5.79
5	6	4.64	4.64	4.64	4.64	63	6	6	9.85
6	6	4.09	4.09	4.09	4.09	61	6	6	9.79
7	6	3.76	3.76	3.76	3.76	62	6	6	7.43
8	6	3.55	3.55	3.55	3.55	51	6	6	9.00
9	6	3.57	3.57	3.57	3.57	47	6	6	5.71
10	6	4.74	4.74	4.74	4.74	62	6	6	7.11

The simulation involved the movement of the trucks over the rubber strip. Additionally, the trucks were assigned different paths along the length of the rubber strip to emulate real-world conditions. Figure 54 and Table 12 present the strain results obtained for these trucks. This data offers insights into the dynamic strain patterns experienced by the rubber strip and sensors as multiple trucks traverse the strip. These results are crucial for understanding the impact of varying truck configurations and movements on the system's performance. The strain values for most of the trucks remained the same; however, the strain generated by the wide-base trucks was higher.

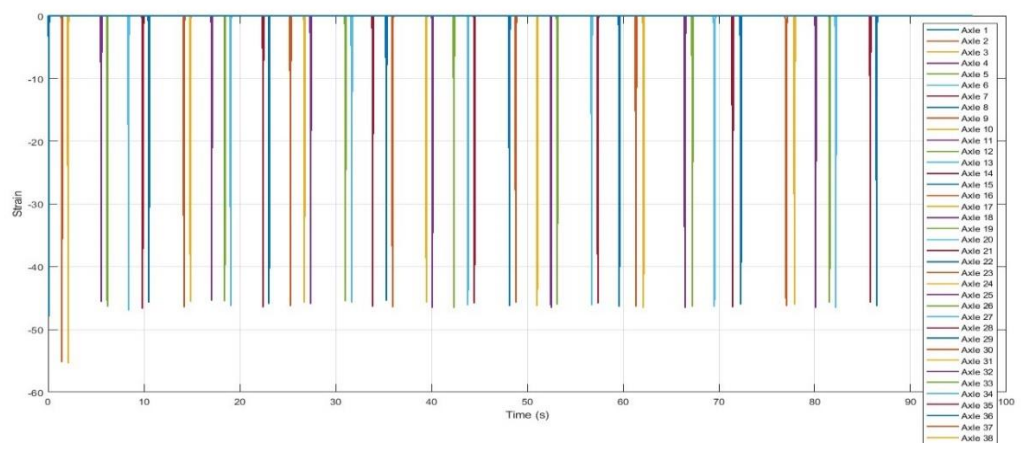


Figure 54 Strain values for 10 trucks

Table 12 Strain values for 10 trucks

Truck	Speed	Axle1	Axle2	Axle3	Axle4	Axle5	Distance to
Number	(mph)	(με)	(με)	(με)	(με)	(με)	Next Truck (m)
1	64	57.5	55.2	55.4	45.5	46.3	7.73
2	61	56.4	46.6	45.7	46.4	45.5	9.79
3	66	59.8	63.6	64.7	65.0	64.3	9.82
4	61	55.4	45.7	45.9	45.5	45.7	5.79
5	63	55.6	45.3	46.4	45.7	46.5	9.85
6	61	55.8	46.1	45.7	46.2	45.7	9.79
7	62	55.4	46.5	46.0	46.1	45.8	7.43
8	51	55.6	46.3	46.5	46.5	46.4	9.00
9	47	55.6	46.4	46.0	46.3	46.0	5.71
10	62	55.8	45.7	46.5	45.7	46.2	7.11

The strain values obtained were subsequently used to analyze the piezoelectric sensors' voltage response, modeled on the rubber strip's upper surface. The voltage response was found to be at its highest value for the sensors directly engaged with the tires of the passing trucks. Additionally, limited responses were observed for sensors located near the tire path. The output voltage remained zero for sensors not subjected to direct tire contact. Figures 55 to 62 provide an overall visualization of the voltage responses generated by the 77 piezoelectric sensors for ten truck passes over different paths along the length of the rubber strip. These responses show the

dynamic interaction between the sensors and the passing trucks, reflecting the system's sensitivity to tire placement and contact variations.

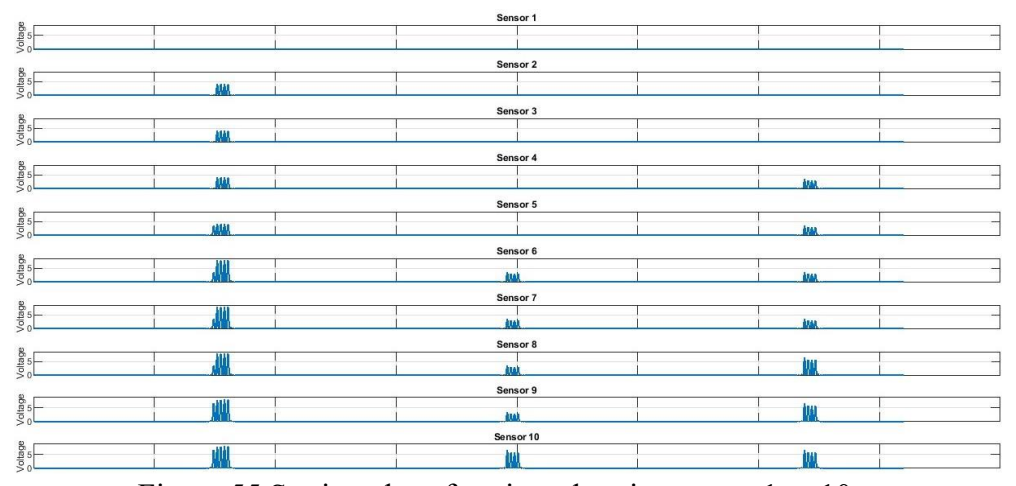


Figure 55 Strain values for piezoelectric sensors 1 to 10

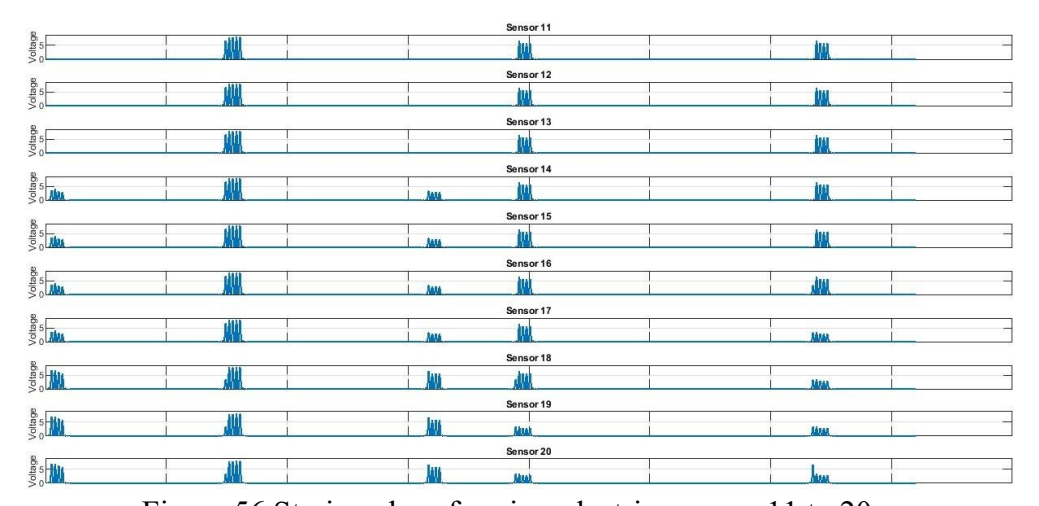


Figure 56 Strain values for piezoelectric sensors 11 to 20

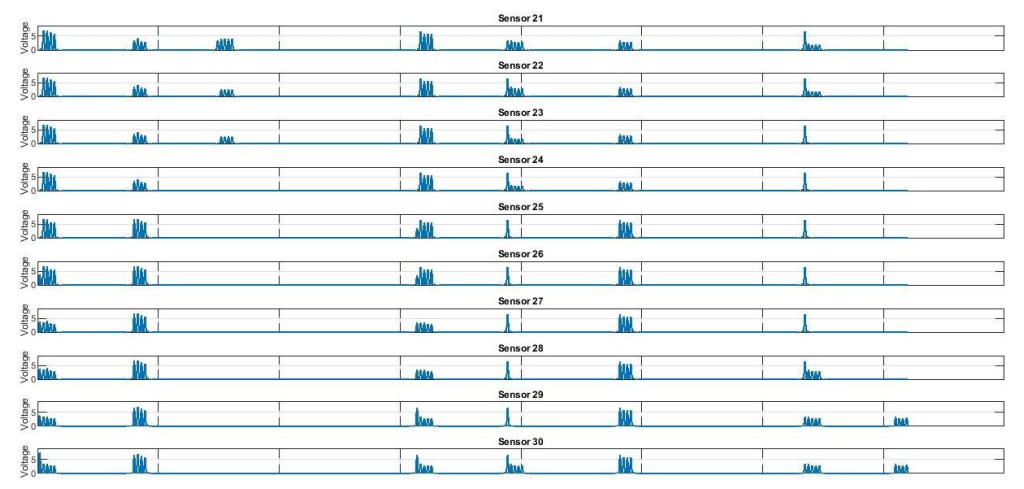


Figure 57 Strain values for piezoelectric sensors 21 to 30

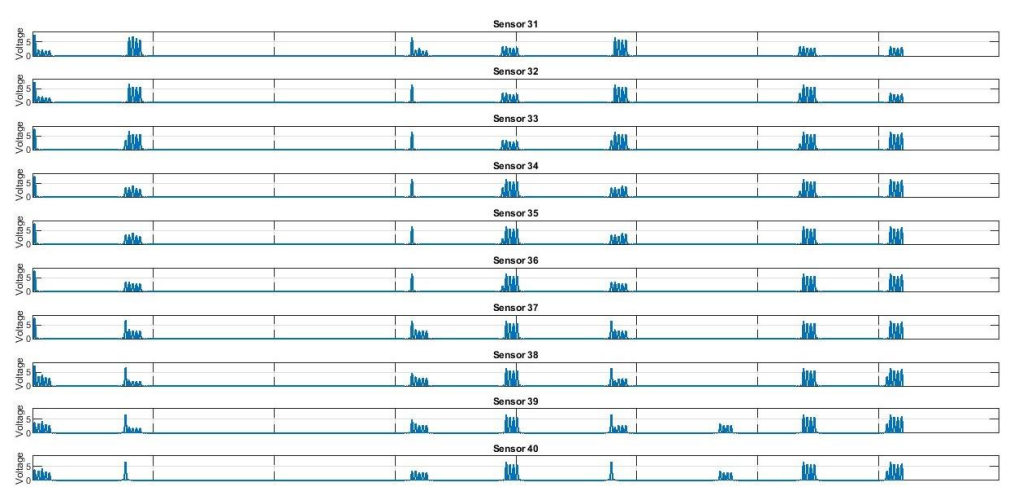


Figure 58 Strain values for piezoelectric sensors 31 to 40

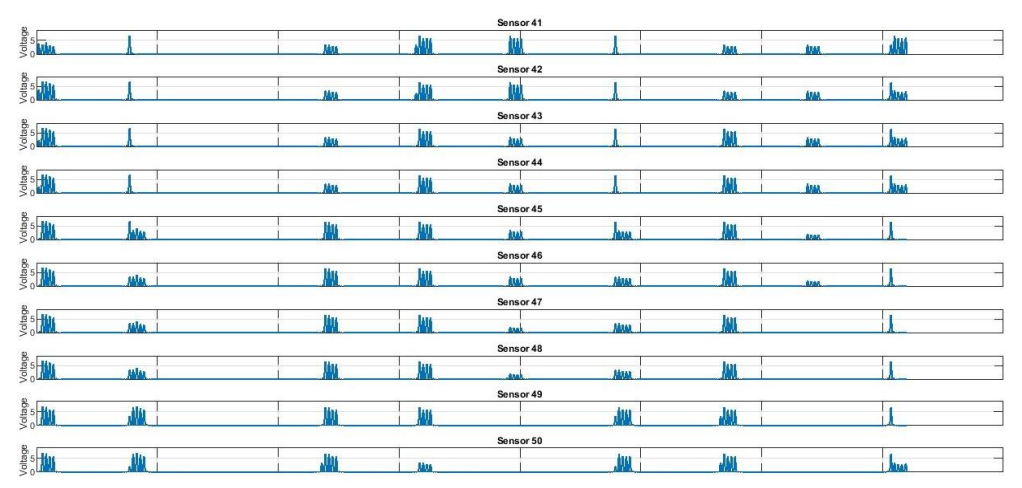


Figure 59 Strain values for piezoelectric sensors 41 to 50

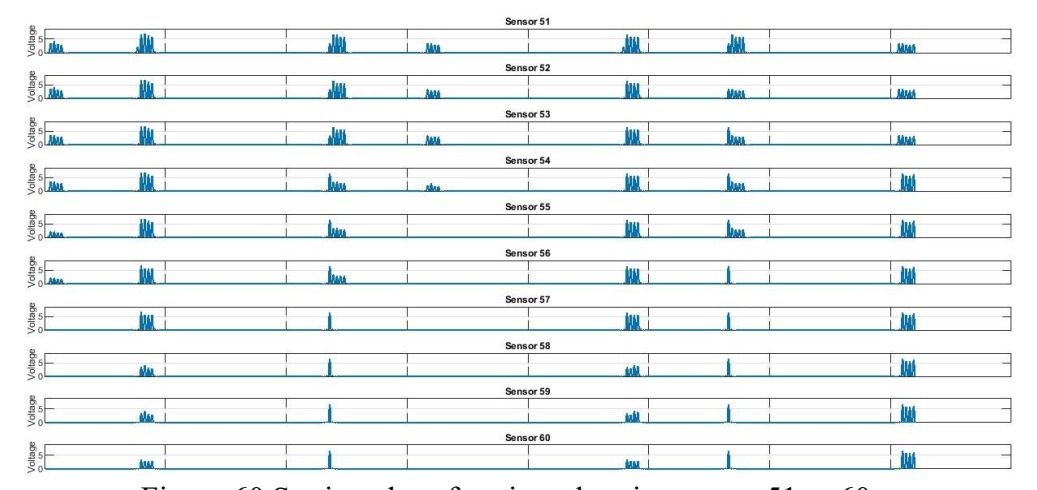


Figure 60 Strain values for piezoelectric sensors 51 to 60

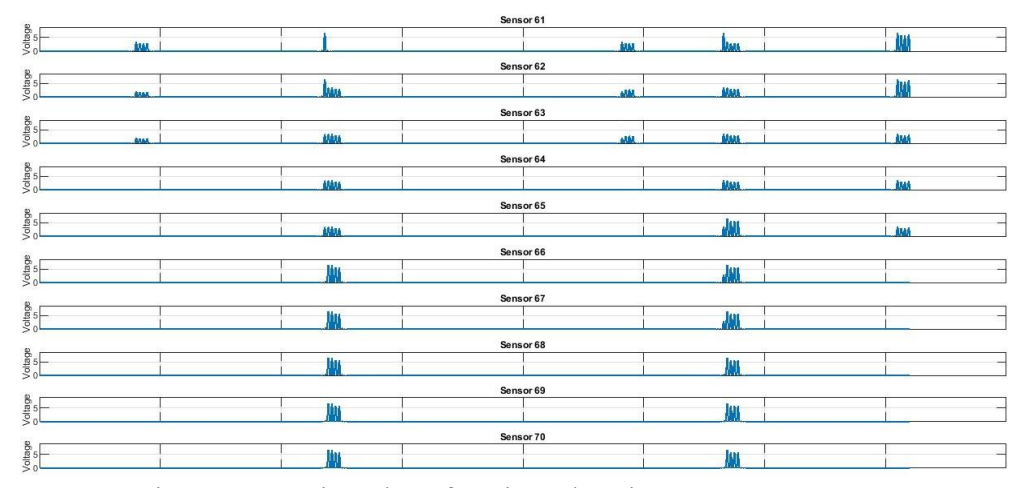


Figure 61 Strain values for piezoelectric sensors 61 to 70

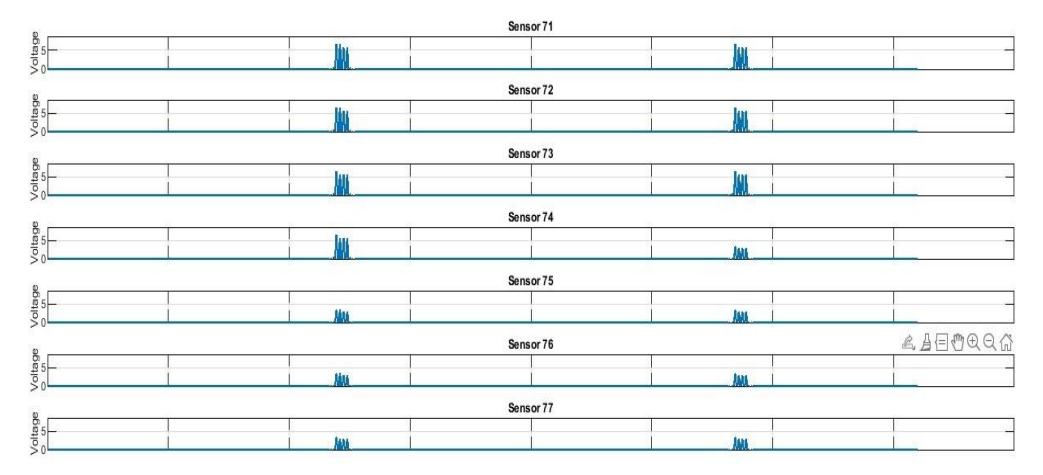


Figure 62 Strain values for piezoelectric sensors 71 to 77

The voltage responses were analyzed with the primary objective of employing them to train an algorithm to distinguish and categorize trucks from random traffic loads. Furthermore, the sensor data was also utilized to estimate the tire width. This estimation was achieved by considering the responses of sensors that exhibit the highest voltage levels when in direct contact with the truck's tires. The tire width is determined by multiplying the number of sensors demonstrating maximum response under direct tire contact by the width of each individual sensor.

In order to achieve the above-mentioned objective, only those sensors for which the voltage response was more than the threshold value of 5V were considered, as the rest of the nearby sensors showed reduced output voltage which was due to the dynamic forces of thrust of the moving vehicle tires. The number of sensors indicating voltages more than 5V under each tire is then multiplied by the width of the sensor to get the tire width. The model also analyzes the

number of tires passing over the rubber strip to categorize the number of axles each truck has and then classify the trucks. The overall results obtained from the voltage response of the sensors are summarized in Table 13. The mean error in the estimation of the tire width was approximately 1%.

Table 13 Truck classification

m 1	m·	I 4 ID *** (6	Tire Width	T. 1 T.	Actual Tire	Error
Truck	Tire 1	Lateral Position (Sensors) 30 31 32 33 34 35 36 37 38	(Inch)	Truck Type	Width (Inch)	(%)
	1	18 19 20 21 22 23 24 25 26 42 43 44 45				
	2	46 47 48 49 50				
		18 19 20 21 22 23 24 25 26 42 43 44 45				
1	3	46 47 48 49 50	5.94	Class 9 Truck	6	1
1		18 19 20 21 22 23 24 25 26 42 43 44 45	3.51	Class y Track	Ü	1
	4	46 47 48 49 50				
		18 19 20 21 22 23 24 25 26 42 43 44 45				
	5	46 47 48 49 50				
	1	37 38 39 40 41 42 43 44 45				
		25 26 27 28 29 30 31 32 33 49 50 51 52				
	2	53 54 55 56 57				
		25 26 27 28 29 30 31 32 33 49 50 51 52				
2	3	53 54 55 56 57	5.94	Class 9 Truck	6	1
		25 26 27 28 29 30 31 32 33 49 50 51 52				
	4	53 54 55 56 57				
	_	25 26 27 28 29 30 31 32 33 49 50 51 52				
	5	53 54 55 56 57			_	
	1	9 10 11 12 13 14 15 16 17	5.94		6	1
	_	6 7 8 9 10 11 12 13 14 15 16 17 18 19				
2 20 6 7 8 9 10 11 12	6 7 8 9 10 11 12 13 14 15 16 17 18 19					
3	3	20		Super Single		
3		6 7 8 9 10 11 12 13 14 15 16 17 18 19	9.9	Truck	10	1
	4	20				
		6 7 8 9 10 11 12 13 14 15 16 17 18 19				
	5	20				
	1	54 55 56 57 58 59 60 61 62				
		45 46 47 48 49 50 51 52 53 66 67 68 69				
	2	70 71 72 73 74				
		45 46 47 48 49 50 51 52 53 66 67 68 69				
4	3	70 71 72 73 74	5.94	Class 9 Truck	6	1
		45 46 47 48 49 50 51 52 53 66 67 68 69				
	4	70 71 72 73 74				
	_	45 46 47 48 49 50 51 52 53 66 67 68 69				
	5	70 71 72 73 74				
	1	29 30 31 32 33 34 35 36 37				
		18 19 20 21 22 23 24 25 26 41 42 43 44	5.04	C1 0.TD 1		1
5	2	45 46 47 48 49	5.94	Class 9 Truck	6	1
	2	18 19 20 21 22 23 24 25 26 41 42 43 44				
	3	45 46 47 48 49				

Table 13 (cont'd)

		Table 13 (cont	<u>u)</u>			
		18 19 20 21 22 23 24 25 26 41 42 43 44				
	4	45 46 47 48 49				
		18 19 20 21 22 23 24 25 26 41 42 43 44				
	5	45 46 47 48 49				
	1	22 23 24 25 26 27 28 29 30				
		10 11 12 13 14 15 16 17 18 34 35 36 37				
	2	38 39 40 41 42				
		10 11 12 13 14 15 16 17 18 34 35 36 37				
6	3	38 39 40 41 42	5.94	Class 9 Truck	6	1
		10 11 12 13 14 15 16 17 18 34 35 36 37			-	
	4	38 39 40 41 42				
		10 11 12 13 14 15 16 17 18 34 35 36 37				
	5	38 39 40 41 42				
	1	37 38 39 40 41 42 43 44 45				
	-	25 26 27 28 29 30 31 32 33 49 50 51 52				
	2	53 54 55 56 57				
		25 26 27 28 29 30 31 32 33 49 50 51 52				
7	3	53 54 55 56 57	5.94	Class 9 Truck	6	1
,		25 26 27 28 29 30 31 32 33 49 50 51 52	3.74	Class / Truck	O	1
	4	53 54 55 56 57				
		25 26 27 28 29 30 31 32 33 49 50 51 52				
	5	53 54 55 56 57				
	1	53 54 55 56 57 58 59 60 61				
	1	43 44 45 46 47 48 49 50 51 65 66 67 68				
	2	69 70 71 72 73				
		43 44 45 46 47 48 49 50 51 65 66 67 68				
8	3	69 70 71 72 73	5.94	Class 9 Truck	6	1
0		43 44 45 46 47 48 49 50 51 65 66 67 68	3.74	Class / Truck	O	1
	4	69 70 71 72 73				
		43 44 45 46 47 48 49 50 51 65 66 67 68				
	5	69 70 71 72 73				
	1	20 21 22 23 24 25 26 27 28				
	1	8 9 10 11 12 13 14 15 16 32 33 34 35				
	2	36 37 38 39 40				
		8 9 10 11 12 13 14 15 16 32 33 34 35				
9	3	36 37 38 39 40	5.94	Class 9 Truck	6	1
		8 9 10 11 12 13 14 15 16 32 33 34 35	2.7	Janes y Truck		1
	4	36 37 38 39 40				
	Ė	8 9 10 11 12 13 14 15 16 32 33 34 35				
	5	36 37 38 39 40				
	1	42 43 44 45 46 47 48 49 50				
		33 34 35 36 37 38 39 40 41 54 55 56 57				
	2	58 59 60 61 62				
		33 34 35 36 37 38 39 40 41 54 55 56 57				
10	3	58 59 60 61 62	5.94	Class 9 Truck	6	1
		33 34 35 36 37 38 39 40 41 54 55 56 57	3.71	Ciaso y Truck		
	4	58 59 60 61 62				
	<u> </u>	33 34 35 36 37 38 39 40 41 54 55 56 57				
	5	58 59 60 61 62				
<u> </u>		1	1	<u> </u>		ı

4.2.5 FEM Analysis for 1000 Trucks

To conduct a more comprehensive evaluation of the model's performance, a sample size comprising 1000 trucks was generated. Within this sample, 10% of the trucks were designated as "Wide Base Trucks," while the remaining 90% were designated as "Class 9 trucks with 6" tire width." The distribution of this sample size is visually presented in Figure 63, representing the relative proportions of Wide Base Trucks and Class 9 trucks within the dataset. This expanded dataset served as a foundation for assessing and refining the model's classification capabilities, enhancing its overall accuracy and effectiveness in real-world applications.

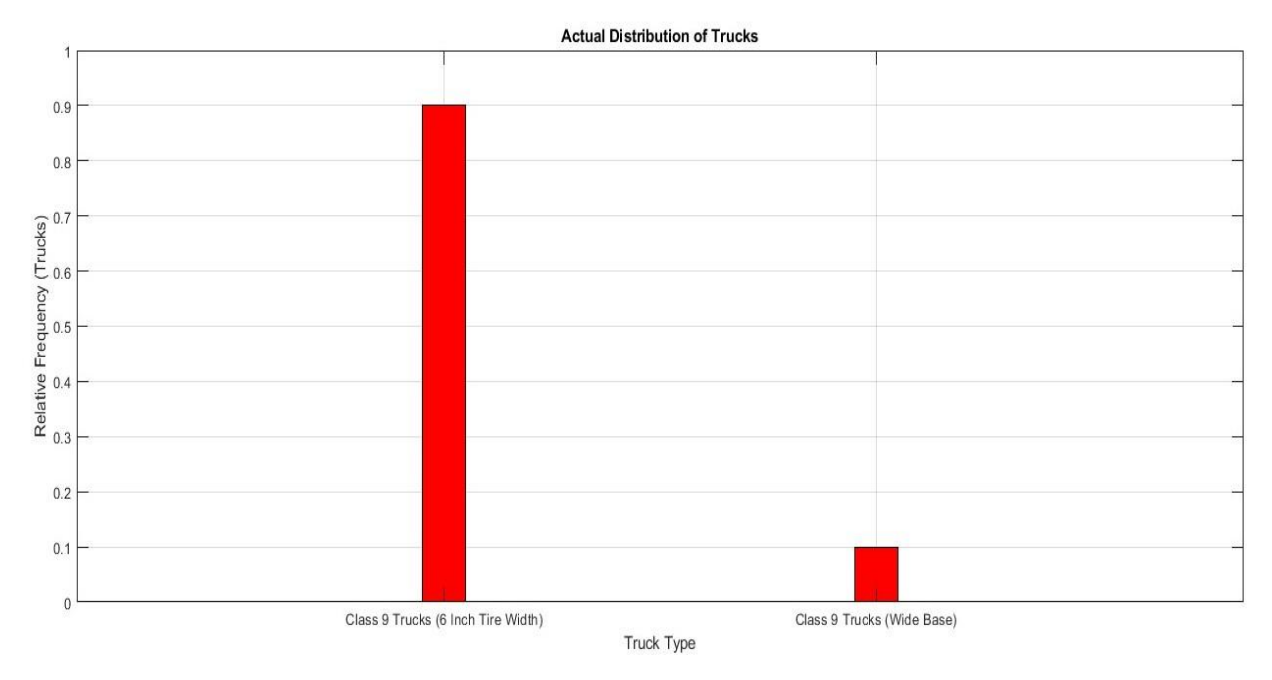


Figure 63 Distribution of 1000 trucks

To simulate the real-world conditions, the speeds of the 1000 trucks within the sample were randomized between 45 and 70 mph. This randomized assignment of speeds was instrumental in creating a diverse and representative dataset, capturing the variability in vehicular speeds encountered in practical scenarios. The distribution of these speeds among the trucks is visualized in Figure 64. Within this graphical representation, the x-axis delineates the range of speeds in miles per hour, offering a comprehensive spectrum of the span of speeds. The y-axis serves as an indicator of the relative frequency of trucks traveling at each of these speeds. This graphical depiction provides a clear and informative portrayal of the distribution of speeds across the sample, facilitating an examination of the model's performance under diverse speed conditions.

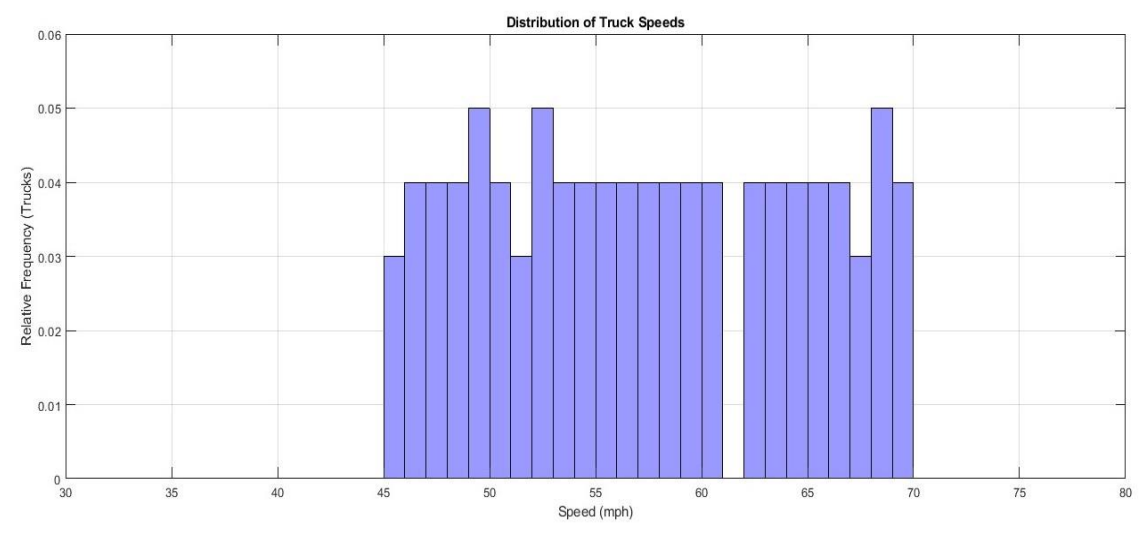


Figure 64 Distribution of truck speed

For majority of trucks, a uniform tire width specification was applied. The width of both the front tire and all the tires within the dual tandem configuration was consistently set at 6 inches. In contrast, for Wide Base Trucks, a distinct tire width configuration was implemented. In this category, the width of the front tire was standardized at 6 inches, while the subsequent tires were set at a broader width of 10 inches. The collective distribution of these tire widths across the sample of 1000 trucks is graphically presented in Figure 65. Within this graphical representation, the x-axis encapsulates the spectrum of tire widths, distinguishing between the 6-inch and 10-inch widths and on the y-axis, the relative frequencies. This graphical depiction conveys the distribution of tire widths within the sample, revealing a substantial prevalence of 92% of the tires with a width of 6 inches. Concurrently, 8% of the tires were categorized as wide-based, possessing a width of 10 inches.

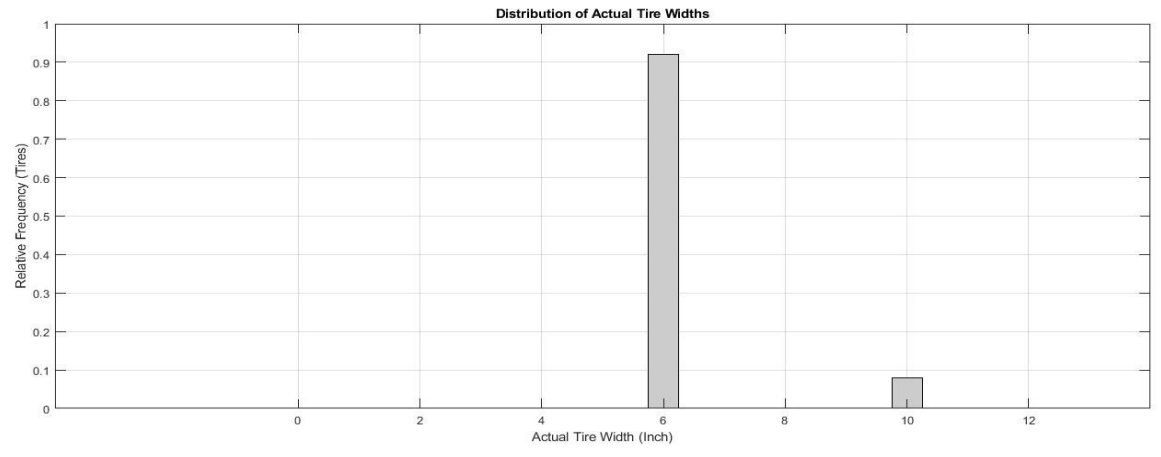


Figure 65 Actual tire width distribution

The trucks were then moved across an EPDM rubber strip, previously modeled with an array of 77 sensors. During this phase, the trucks were assigned random paths along the length of the rubber strip, simulating real-world scenarios. This lateral deviation was measured from the edge of the rubber strip to precisely gauge how far each truck deviated from its anticipated path. Figure 66 visually represents the observed wheel wander for the trucks as they traversed the rubber strip, relative to the designated paths. This offers insights into the dynamic behavior of trucks during their transit over the sensor-equipped rubber strip enabling a thorough assessment of their alignment with the designated paths of the vehicles.

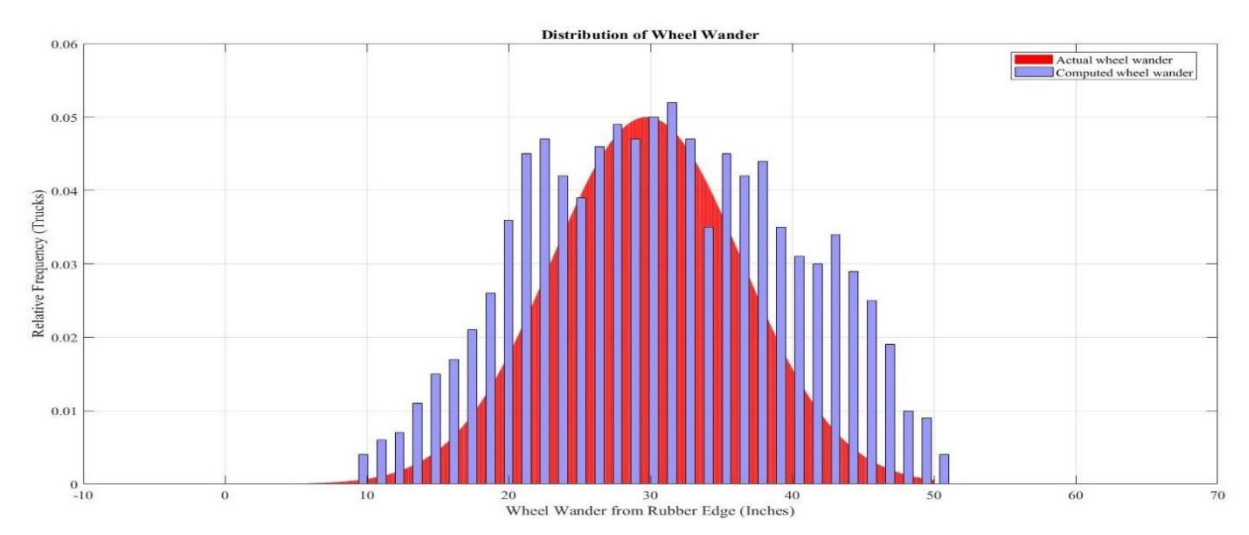


Figure 66 Distribution of assigned and computed wheel wander

In the case of most trucks having all tires width of 6 inches, the load applied to the front tire was maintained at 6 kips. In contrast, the loads on the rear tires were randomized, encompassing values that ranged from 3.5 kips to 5 kips. The contact area between these tires and the EPDM rubber strip was uniformly established at 6x6 inches, ensuring standardized conditions for these trucks. Conversely, for Wide Base Trucks, the contact area between the tires of Wide Base Trucks and the rubber strip was enlarged to 10x6 inches. Furthermore, the loads applied to the rear tires of these trucks were randomly distributed with a range spanning from 7 kips to 10 kips. Moreover, the distance between each truck varied, ranging from 5 to 10 meters. This variation in inter-truck distance contributed to emulating real-world traffic scenarios where vehicles are not uniformly spaced along the road.

As the trucks traversed the EPDM rubber strip, their movements generated strains within the material. These strains were subsequently translated into voltage responses through the piezoelectric effects of the sensors. The computational model adeptly calculated the width of

each tire based on these voltage responses. The outcomes of these calculations are illustrated in Figure 67, which provides a distribution of the computed tire widths.

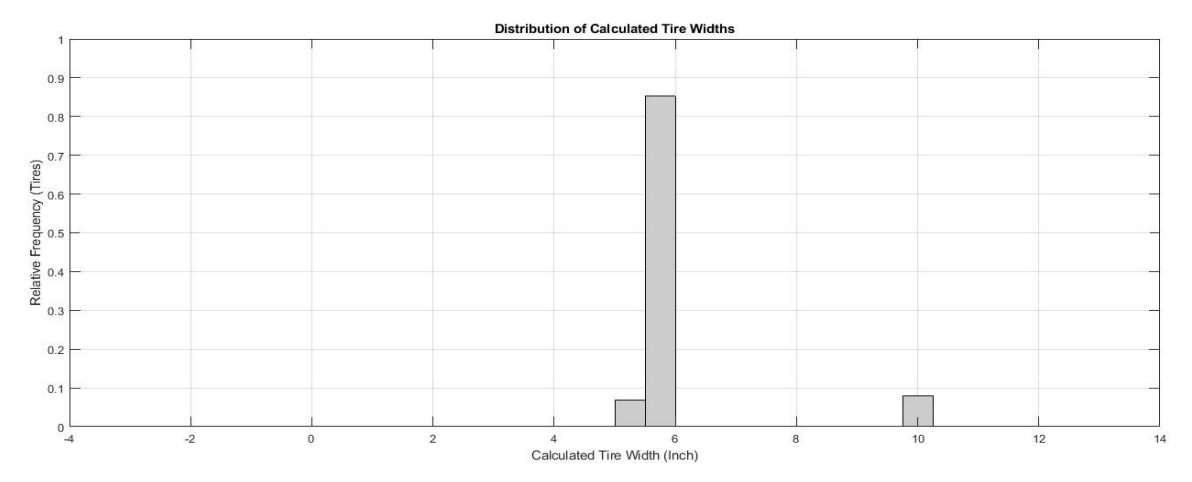


Figure 67 Computed tire width distribution

The results of the model's calculations are closely aligned with the actual tire widths within the dataset. Specifically, 85.2% of the tire widths were accurately calculated as approximately 5.94 inches, demonstrating high precision in the model's predictions. Additionally, 6.8% of the tire widths were estimated to be close to 5.2 inches, showcasing a relatively small margin of error in these calculations. Furthermore, 8% of the tire widths were calculated as 9.9 inches, providing additional evidence of the model's capacity to approximate tire dimensions correctly. This close correspondence between the calculated and actual tire widths affirms the effectiveness of the model in accurately estimating vehicular parameters.

Figure 68 illustrates the relationship between the distribution of tire width and the speed of the trucks that was assigned, and Figure 69 presents the distribution of computed tire widths with the trucks' operating speeds. The figure highlights specific speed ranges and their corresponding distributions of tire widths, each denoted by distinct color bars. The figures present an overview of how the accuracy of tire width calculations correlates with varying truck speeds, shedding light on the model's performance under different velocity conditions. This includes as follows:

• The blue bar signifies a speed range of 45-54 mph. Within this speed range, 50% of the total tires possess a width of 6 inches, indicating a prevalent tire configuration for trucks. Additionally, 3.4% of the tires in this category exhibit a width of 10 inches, indicating a minority of wider tires. In the computed tire widths in this range, 50% of the trucks had their tire widths accurately estimated close to 6 inches, reflecting a high degree of precision in the model's predictions. Moreover, for 3.4% of the trucks in this category, the calculated tire

- widths closely approximated 10 inches, depicting the model's versatility in accommodating a range of tire dimensions.
- The black bar corresponds to a speed range of 55-65 mph. In this range, 36.2% of the total tires maintain a width of 6 inches and 2.8% of the tires in this category possess a width of 10 inches, indicating a smaller presence of wider tires. In the computed tire widths in this range, 34% of the trucks had their tire widths accurately calculated close to 6 inches and 2.8% of the trucks in this range had their tire widths accurately estimated at close to 10 inches. However, 2.2% of the truck's calculated tire widths deviated slightly, measuring 5.28 inches, marginally lower than the actual 6-inch width.
- The red bar represents the speed range of 66-75 mph. Within this category, 5.8% of the total tires had a width of 6 inches and 1.8% of the tires were characterized by a width of 10 inches. For trucks traveling at speeds within this range, 2% of the trucks had their tire widths accurately calculated close to 6 inches, while 1.8% had their tire widths accurately estimated close to 10 inches. However, 3.8% of the tire widths were calculated as 5.28 inches, slightly lower than the 6-inch width.

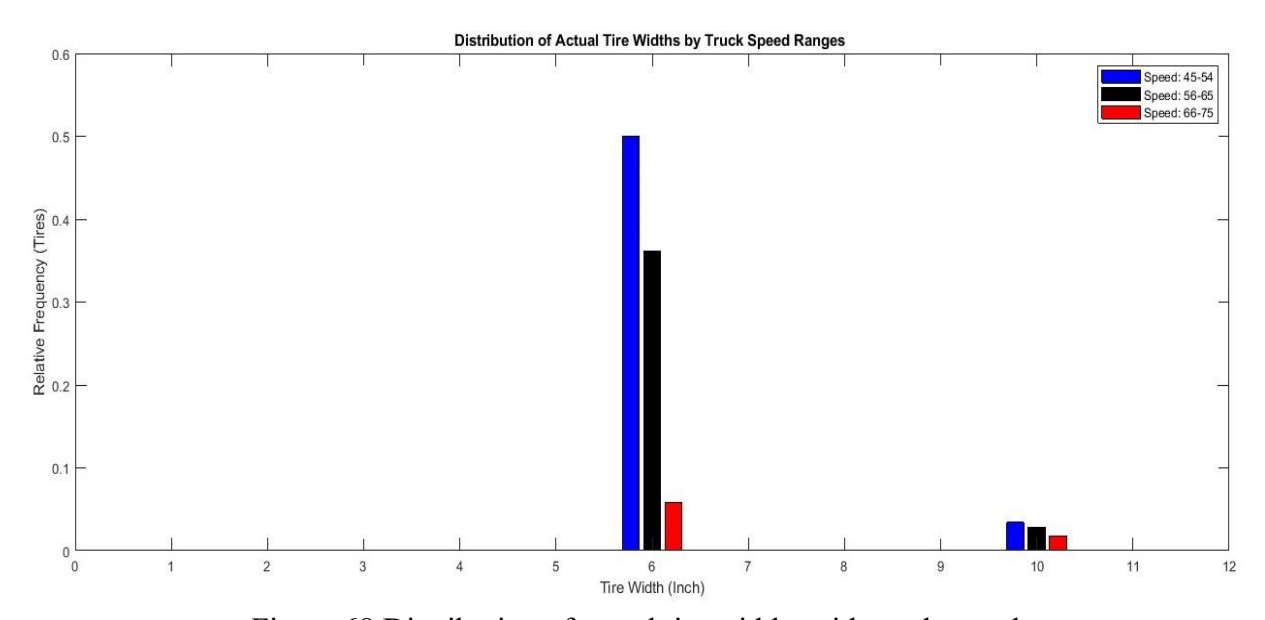


Figure 68 Distribution of actual tire widths with truck speeds

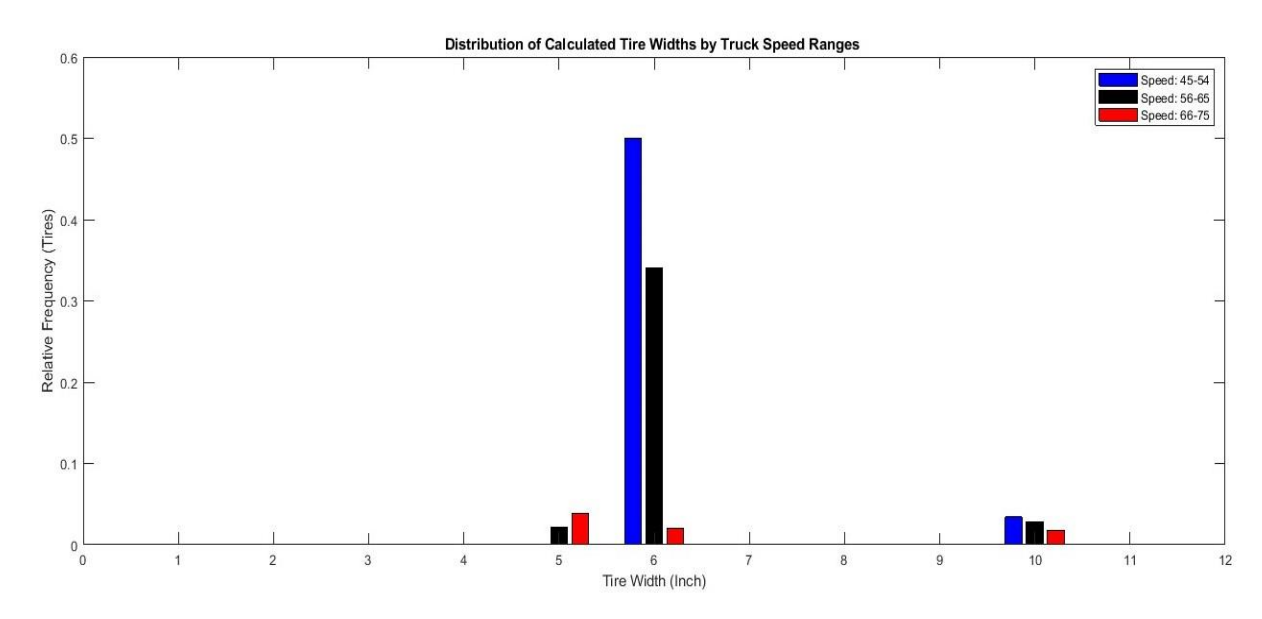


Figure 69 Distribution of calculated tire width by truck speed

The model's capacity to accurately estimate tire widths is prominently influenced by the speed at which the trucks travel. Higher speeds tend to introduce a marginally reduced accuracy in tire width calculations, primarily due to the reduced contact between the tires and sensors during these faster transits. Understanding the relationship between speed and accuracy provides valuable insights into the model's performance characteristics and informs its applicability in scenarios with varying vehicular velocities.

After tire width calculations, the model was able to classify the trucks. For trucks equipped with five axles and tire widths closely approximating 6 inches across all axles, the model consistently classified them as "Class 9 Trucks with 6" tire width." Conversely, for trucks featuring five axles, with the front tire width measuring close to 6 inches and the remaining axles having tire widths close to 10 inches, the model assigned the classification of "Wide Base Trucks". The resultant distribution of truck classifications, as depicted in Figure 70, resembles the original dataset. The similarity between the model's classifications and the actual dataset confirms the model's capacity to classify trucks based on the specified criteria accurately.

Overall, the model was able to accurately classify the trucks that resembled the original provided distribution of the trucks validating model's performance. However, a small margin of error was observed in the calculation of the computed tire widths when the trucks were operated at higher speed ranges.

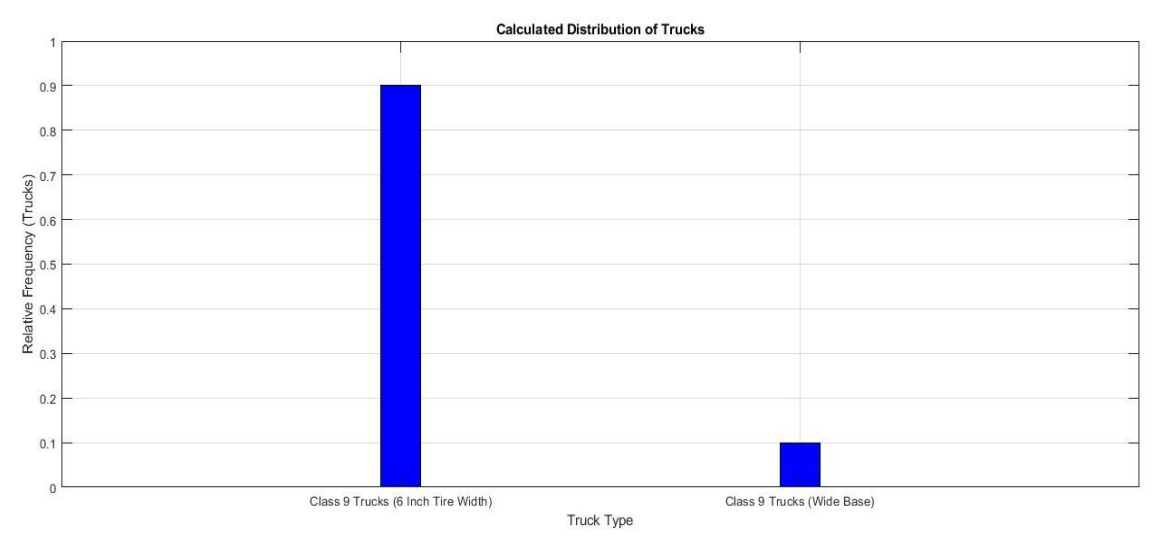


Figure 70 Computed distribution of 1000 trucks

4.2.6 Model Validation through Field Test

Following the analysis of the trucks that traversed the simulated rubber strip, the model was implemented for on-site validation. SUV and sedan vehicles were driven over the rubber strip, as shown in Figure 71. The strip was firmly fixed to the road surface to minimize the impact of thrust and jerking motions resulting from the movement of vehicle tires, which can introduce noise in the voltage outputs.



Figure 71 Rubber strip fixed to the road surface

The tire width for both SUV and sedan vehicles remained consistent with the measurements from the previous field tests, measuring 15.1 cm and 13.9 cm, respectively. Similarly, their wheelbases were 3.4 m and 2.8 m, respectively. The experimental configuration involved the SUV passing over the strip first, followed by the sedan vehicle as shown in Figure 72. The distribution of the tire width of both the vehicles is shown in Figure 73 with a mean of 14.5 cm.



Figure 72 Vehicles passing over the rubber strip

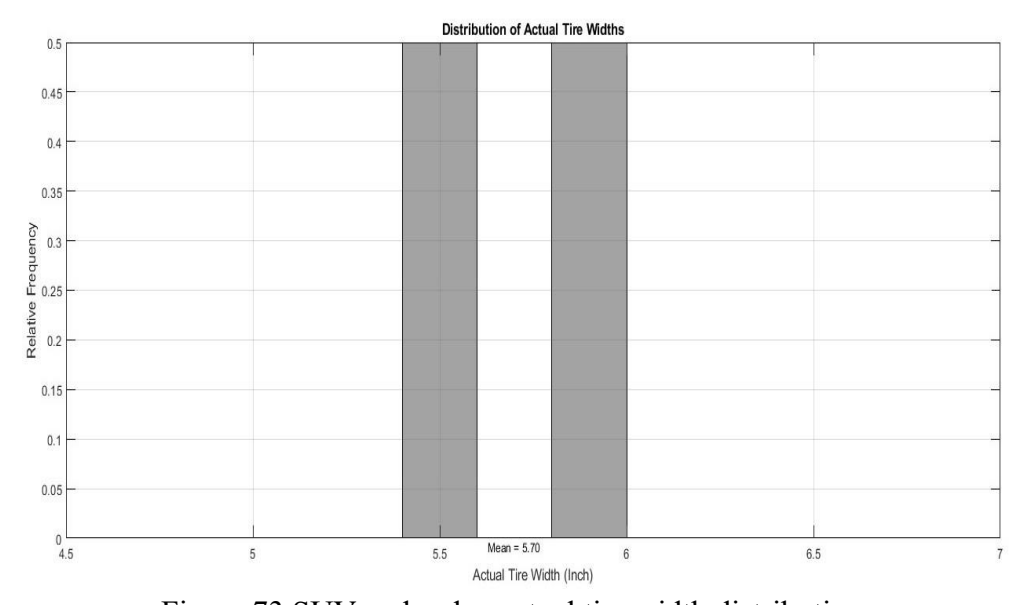


Figure 73 SUV and sedan actual tire width distribution

The vehicles were driven over the rubber strip at three distinct speeds: 35 mph, 45 mph, and 55 mph. As the vehicles tire contacted the rubber strip it induced strains that subsequently influenced the voltage output of the sensors. The voltage outputs for both vehicles at these speeds are depicted in Figures 74 to 76. The initial two peaks correspond to the passage of the SUV, while the subsequent two peaks represent the passage of the sedan.

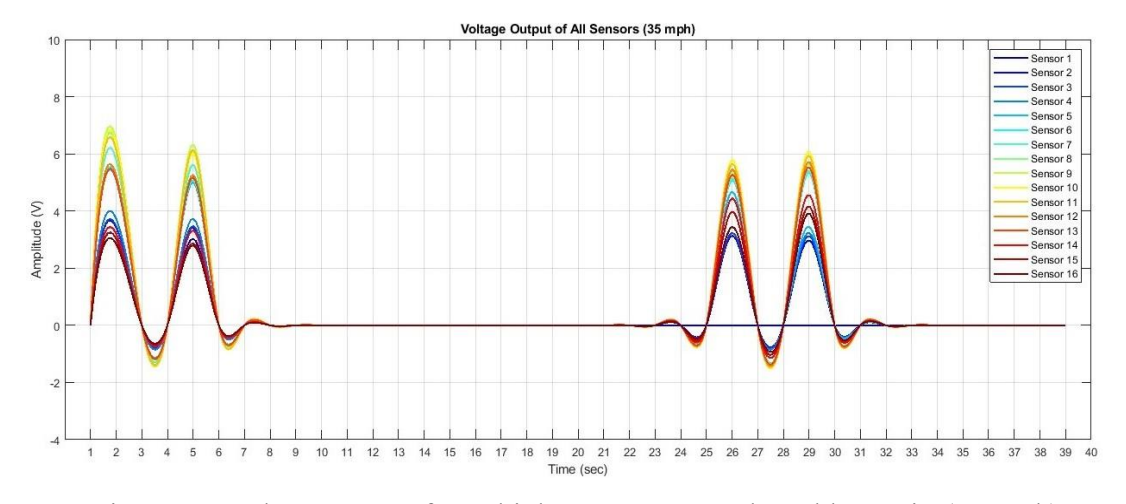


Figure 74 Voltage output for vehicle passage over the rubber strip (35 mph)

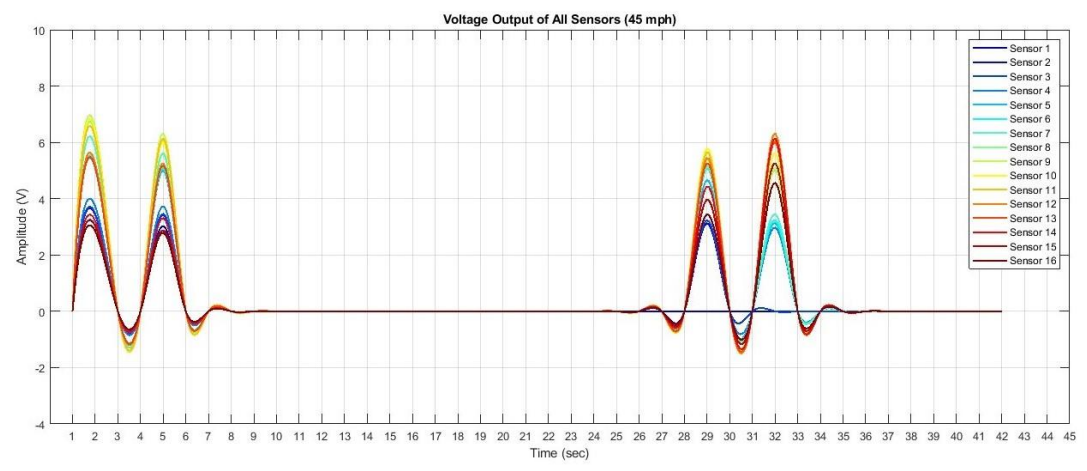


Figure 75 Voltage output for vehicle passage over the rubber strip (45 mph)

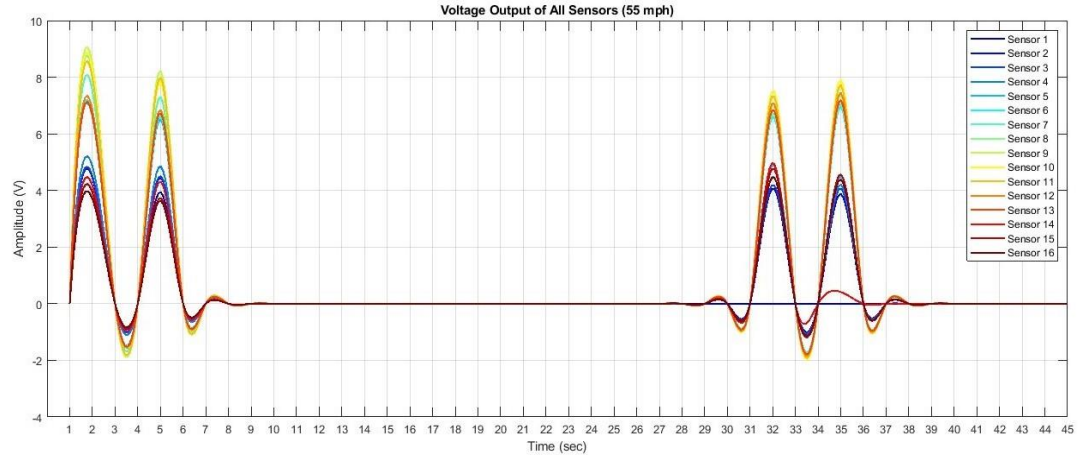


Figure 76 Voltage output for vehicle passage over the rubber strip (55 mph)

Based on the figures above, it can be deduced that voltage increases as the tires contact the sensors, reaching a peak value, and subsequently decreasing to zero as the tires pass over the

strip. Subsequently, these voltage outputs were fed into the pre-existing model to verify its capacity to accurately calculate the respective tire widths and classify the vehicles. Table 14 provides a summary of the tire widths, demonstrating a mean error of 1.471%. It's worth noting that at higher speeds, the calculated tire width was slightly less than the actual tire width.

Table 14 Summary of tire widths for SUV and sedan

Speed (mph)	Vehicle Type	Measured Tire Width (cm)	Calculated Tire Width (cm)	Error (%)
		15.1	15.03	0.46
		15.1	15.03	0.46
	SUV	15.1	15.03	0.46
		13.9	13.7	1.44
		13.9	13.7	1.44
35	Sedan	13.9	13.7	1.44
		15.1	15.03	0.46
		15.1	15.03	0.46
	SUV	15.1	15.03	0.46
		13.9	13.7	1.44
		13.9	13.7	1.44
45	Sedan	13.9	13.4	3.60
		15.1	15.03	0.46
		15.1	15.03	0.46
	SUV	15.1	14.6	3.31
		13.9	13.4	3.60
		13.9	13.9	1.44
55	Sedan	13.9	13.4	3.6
Mean				1.47%
Standard Error				1.21%
95% Confidence Interval				0.86% to 2.07%

Figure 77 displays the distribution of calculated tire widths for vehicles driven at 55 mph with a mean of 14.3 cm. Calculated tire width for sedan was slightly smaller than the measured value, which could be attributed to inadequate contact between the vehicle's tires and the rubber strip. The results presented are consistent with the outcomes derived from the model analysis using the dataset discussed in previous sections, thereby affirming the precision and reliability of the developed model.

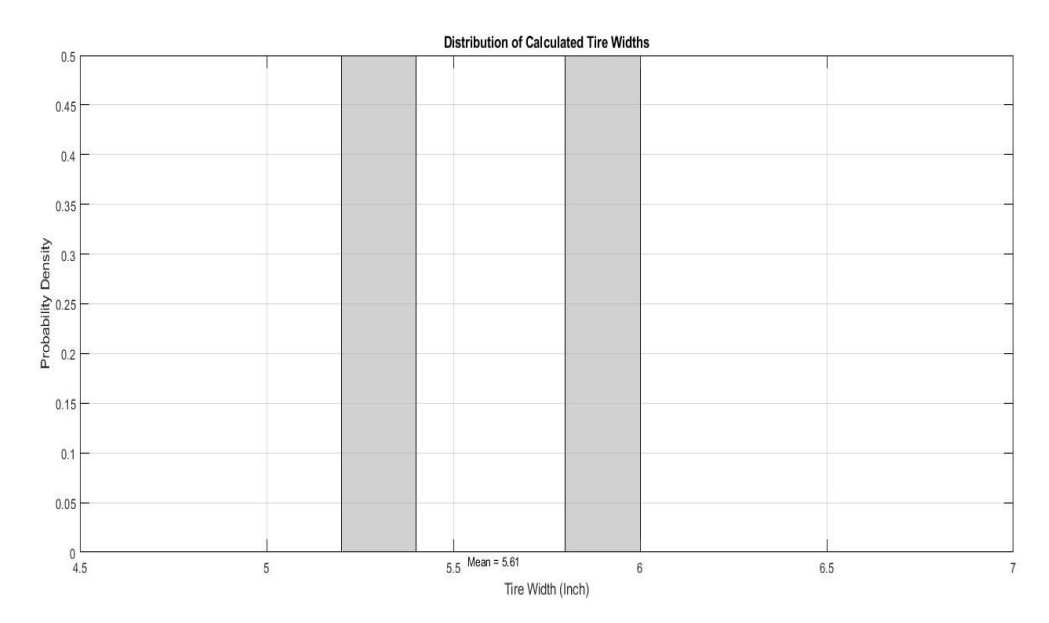


Figure 77 SUV and sedan computed tire width distribution

Similar to the wheel wander calculated for the dataset in the preceding sections, the wheel wander was also determined for both the SUV and sedan as they passed over the strip. This provided insight into the relative position of the vehicle as it moved across the rubber strip. Figure 78 illustrates the wheel wander for both the SUV and sedan.

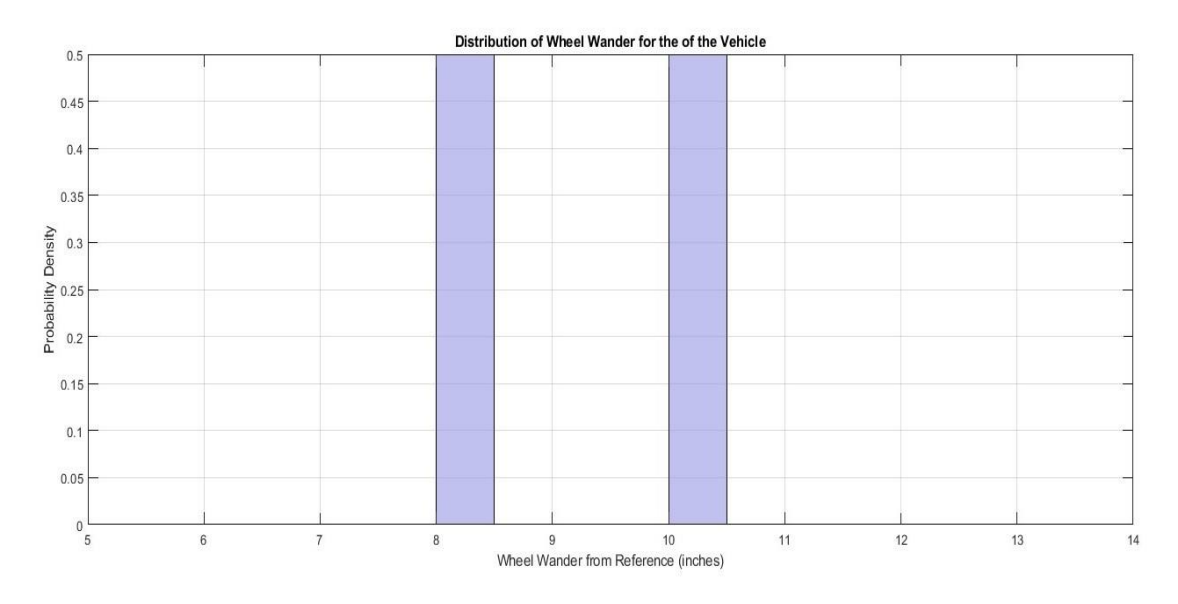


Figure 78 Wheel wander for SUV and sedan

4.3 Summary

The field test was conducted using an EPDM rubber strip integrated with 16 piezoelectric sensors and placed on a roadway to serve as an intermediary platform between the passing vehicles and the sensors. As vehicles, specifically SUVs and sedans, drove over the strip at

varying speeds between 10mph and 40mph, the longitudinal strain induced on the sensors resulted in voltage outputs due to the piezoelectric effect. These voltage signals were analyzed using two NI cards. The system effectively identified the tire's contact area on the strip, thereby accurately estimating the tire widths and the vehicles' wheelbases. Comparing these readings with actual measurements revealed only minor discrepancies. Although the sedan and the SUV exhibited distinctive response patterns, the results reinforced the efficacy of this system for realtime traffic surveillance and vehicle categorization. Furthermore, a model was developed to foster an algorithm capable of interpreting signals from the rubber strip embedded with piezoelectric sensors. Using machine learning techniques, the primary objective was to distinguish and classify trucks based on their signature signal patterns. Utilizing a finite element model, the dynamics of a rectangular EPDM rubber strip furnished with piezoelectric sensors were simulated to anticipate its response when vehicles of different weights and speeds pass over it. Upon simulating diverse truck loads, pivotal strain data was collected. Analysis of the voltage outputs from the sensors, which were directly influenced by these strains, demonstrated the system's potential in classifying trucks and approximating tire widths. The model analyzed the relationship between tire width and speed, observed lateral deviations as trucks traversed the rubber strip, and accounted for load variations and inter-truck distances. Notably, the model accurately calculated tire widths, with small margin errors for most cases. The analysis also highlighted that the accuracy of tire width calculations was influenced by truck speed, with reduced accuracy observed at higher speeds due to reduced tire-sensor contact. However, the model consistently classified trucks correctly based on tire width and other criteria. Overall, the tests demonstrate the model's effectiveness in accurately classifying trucks, offering valuable insights into its performance under varying real-world conditions, which can benefit traffic monitoring and data analysis applications.

CHAPTER 5 CONCLUSIONS AND RECOMMENDATIONS

5.1 Conclusions

In the course of this research, the field of vehicular monitoring was explored with a perspective. The approach centered around piezoelectric sensor strands encased within a resilient protective polymer to observe and record the voltage fluctuations that arise primarily from the varying tire pressures of vehicles. The aim of adopting such a technique was to devise an efficient and precise method that would be able to determine not just the exact position of a vehicle's tire but also its specific width. Understanding these parameters with precision is paramount, given that they hold significant relevance and applicability in several traffic monitoring scenarios and systems.

The foundation of this research was locating the optimal protective epoxy for the sensors because the exposure of piezoelectric sensors to environmental factors and the physical stresses from vehicular movement cause deteriorating effects on the sensors. The G-100 Ultra Impact Epoxy surfaced as the superior candidate of the three epoxy variants assessed. Its consistent performance during preliminary fatigue tests and resilience against varying conditions demonstrated its potential. The subsequent experiments, therefore, were conducted with G-100 as the shielding medium.

Integrating piezoelectric sensors with the selected epoxy showcased their effectiveness in capturing the intricate dynamics between vehicular tires and the roadway. The potential was further highlighted during direct load tests, where sensors beneath the load manifested the highest voltage outputs. This observation indicated the utility of these sensors in providing precise insights into tire dimensions and position.

An additional focus was the assessment of EPDM rubber's compatibility with these sensors. Chosen for its durability and resistance to environmental factors, EPDM rubber played a crucial role as a protective shield and a base for aligning the piezoelectric sensors. When subjected to varied load tests, the sensors' voltage outputs were contingent on force distribution and proximity to the application point. This insight, coupled with the successful implementation of resistors to accommodate larger loads, emphasized the system's adaptability and effectiveness.

The field tests, employing a sensor-integrated EPDM rubber strip, further reinforced the practicality of this system. As vehicles traversed this strip, the mechanical strain induced on the sensors yielded voltage outputs, adeptly captured and analyzed. The resultant data explained the

tire's contact area and enabled accurate estimations of tire widths and vehicles' wheelbases. The discrepancies between these findings and actual measurements were minimal, solidifying the system's precision and reliability.

A model was developed to use the data obtained from the field tests that employed machine learning techniques to discern and categorize trucks based on their distinctive signal patterns. This finite element model simulated the behavior of the EPDM rubber strip embedded with sensors under various conditions. The use of this simulation derived strain data. This strain data was important, as it played a pivotal role in determining the voltage outputs generated by the piezoelectric sensors. Through analyzing these voltage outputs, the precise position of the vehicle's tire on the strip was located, estimating the tire's width and further classifying them to the category to which the vehicle belonged. A notable observation was the system's pronounced sensitivity to the speed of load application, which could have considerable implications when implemented in practical situations.

Conclusively, piezoelectric sensors with optimal protective mediums, the practical insights derived from field tests, and the machine learning-based signal interpretation model pave a promising path forward.

5.2 Recommendations

These recommendations are based on the research conducted, encompassing the selection of epoxy material, the compatibility of EPDM rubber with piezoelectric sensors, and the development of a machine-learning model for vehicle classification based on sensor data. Implementing these recommendations can contribute to the robustness and versatility of this system. The recommendations are as follows:

- When considering piezoelectric sensors for vehicle surveillance systems, using G-100 Ultra Impact Epoxy is recommended. This is due to its ability to guard against wear and tear inflicted by vehicle tires and environmental variables. This epoxy's consistent performance and resilience have been evident under diverse conditions, ensuring the piezoelectric sensors' longevity and data precision for extended monitoring periods.
- EPDM rubber can be used for large-scale deployments of piezoelectric sensor systems.
 Whether in urban or rural environments, where sensors may be subjected to harsh weather conditions and heavy traffic, EPDM rubber can be a robust protective layer, safeguarding sensors from wear and tear.

- It is crucial to evaluate the system in extreme environmental conditions. This includes
 extreme heat, cold, and heavy rainfall scenarios. Such assessments can provide invaluable
 insights into the system's broader applicability, ensuring its reliability under various
 challenging weather conditions.
- Future designs and implementations of this technology should prioritize refining the system's sensitivity to the speed of load application. Consideration should be given to incorporating compensatory mechanisms or calibration processes that can dynamically adjust sensor responses based on the speed of the applied load.

5.3 Recommendation for Future Work

Embedding the following guidelines into future explorative and developmental pursuits will enhance the grasp of vehicular supervision and road surveillance. Implementing these suggestions can contribute to the evolution of smarter, safer, and more streamlined transportation mechanisms. The specific recommendations include:

- Extended research on the G-100 Ultra Impact Epoxy's endurance and consistent functionality
 under varying environmental conditions is required. Although initial results hint at its
 robustness, in-depth, long-term studies will shed light on the material's resilience over
 prolonged periods.
- It is recommended to gather a broader dataset to enhance the accuracy and predictive capabilities of machine learning models used for vehicle classification based on sensor data. This expanded dataset should encompass various vehicle types and sizes, including multiple makes, models, and configurations. Including a comprehensive dataset will facilitate more robust training and validation of machine learning algorithms, resulting in models that can effectively classify and differentiate between vehicles with higher precision.
- One promising direction for upcoming inquiries is the potential miniaturization of
 piezoelectric sensors without undercutting their efficacy. Minimized sensors can diminish the
 physical expanse of sensor setups, simultaneously granting versatility in application.

 Exploring innovative materials and designs that allow for downsizing while maintaining
 sensitivity can revolutionize integrating this technology into various contexts.
- To harness the full potential of this technology, it is imperative to explore how it can be seamlessly incorporated into existing smart traffic systems or future intelligent transportation solutions. The integration of this system can be efficient in optimizing traffic flow, enhancing

safety, and enabling real-time data-driven decision-making. Future work should focus on developing robust interfaces and protocols that facilitate the seamless integration of these systems into broader intelligent transportation networks.

REFERENCES

- 1. W. D. Cunagin, S. O. Majdi, and H. Y. Yeom, "Development of Low-Cost Piezoelectric Film WIM System: Research performed in cooperation with the Texas Department of Transportation Research Study Title: Development of Low-Cost Piezoelectric Film WIM System Unclassified," 1991.
- 2. C. Falconi, "Piezoelectric Nano transducers," *Nano Energy*, vol. 59, pp. 730–744, May 2019, doi: 10.1016/j.nanoen.2019.03.027.
- 3. ASTM E 1318 2009, "Standard Specification for Highway Weigh-in-Motion (WIM) Systems with User Requirements and Test Method 1, in 2007 Annual Book of ASTM Standards, ed. ASTM Committee E17-52 on Traffic Monitoring, ASTM International, USA," 2009.
- 4. B. McCall and W. Vodrazka, "States' Successful Practices Weigh-in-Motion Handbook," 1997.
- 5. B. Sivakumar, M. Ghosn, and F. Moses, "NCHRP REPORT 683—Protocols for Collecting and Using Traffic Data in Bridge Design," *Transportation Research Board*, 2011.
- 6. B. Sivakumar and F. Ibrahim, "Enhancement of bridge live loads using weigh-in-motion data" pp. 193–204, 2007.
- 7. D. Cebon, "Handbook of Vehicle–Road Interaction", *Taylor & Francis: London, UK; New York, NY, USA.* 1999.
- 8. M. Lydon and P. Callender, "Assessment of Various Sensors for Structural Health Monitoring for Bridge Weigh-In-Motion (B-WIM)," 2013. [Online]. Available: https://www.researchgate.net/publication/273044368
- 9. S. Rajab, M. O. Al Kalaa, and H. Refai, "Classification and speed estimation of vehicles via tire detection using single-element piezoelectric sensor," *J Adv Transp*, vol. 50, no. 7, pp. 1366–1385, Nov. 2016.
- 10. A. I. Dontu, L. Gaiginschi, P. D. Barsanescu, E. Rakosi, L. Andrusca, and N. A. Danila, "New concept of WIM system for urban traffic monitoring," in *IOP Conference Series: Materials Science and Engineering*, IOP Publishing Ltd, Dec. 2020. doi: 10.1088/1757-899X/997/1/012114.
- 11. I. Agape, A. I. Dontu, A. Maftei, L. Gaiginschi, and P. D. Barsanescu, "Actual types of sensors used for weighing in motion," in *IOP Conference Series: Materials Science and Engineering*, Institute of Physics Publishing, Aug. 2019. doi: 10.1088/1757-899X/572/1/012102.
- 12. Federal Highway Administration, "Weigh-In-Motion Pocket Guide Part 2 Wim Site Selection, Design, And Installation Guide," 2018.
- 13. D. J. Clark, "A comparison of bending plate and piezoelectric weigh-in-motion systems."

- 14. L. Zhang, C. Haas, and S. Tighe, "Evaluating Weigh-In-Motion Sensing Technology for Traffic Data Collection," 2007. [Online]. Available: https://www.researchgate.net/publication/228452225
- 15. L.-E. Y. Mimbela, J. Pate, S. Copeland, P. M. Kent, and J. Hamrick, "Applications of Fiber Optics Sensors in Weigh-in-Motion (WIM) Systems for Monitoring Truck Weights on Pavements and Structures,".
- 16. S. Ben Salah, "Fiber Optics for Weight-In-Motion (WIM)," 2020.
- 17. A. Batenko, A. Grakovski, I. Kabashkin, E. Petersons, and Y. Sikerzhicki, "Weight-inmotion (WIM) measurements by fiber optic sensor: Problems and solutions," 2011. [Online]. Available: https://www.researchgate.net/publication/268291161
- 18. S. Yuan, F. Ansari, X. Liu, and Y. Zhao, "Optic fiber-based dynamic pressure sensor for WIM system," *Sens Actuators A Phys*, vol. 120, no. 1, pp. 53–58, Apr. 2005, doi: 10.1016/j.sna.2004.11.008.
- 19. H. Xiong and L. Wang, "Piezoelectric energy harvester for public roadway: On-site installation and evaluation," *Appl Energy*, vol. 174, pp. 101–107, Jul. 2016, doi: 10.1016/j.apenergy.2016.04.031.
- 20. S. Z. Chen, G. Wu, and D. C. Feng, "Development of a bridge weigh-in-motion method considering the presence of multiple vehicles," *Eng Struct*, vol. 191, pp. 724–739, Jul. 2019, doi: 10.1016/j.engstruct.2019.04.095.
- 21. R. F. Mould, "Pierre Curie, 1859 1906".
- W. P. Mason, "Piezoelectricity, its history and applications," *Journal of the Acoustical Society of America*, vol. 70, no. 6, pp. 1561–1566, 1981, doi: 10.1121/1.387221.
- 23. S. H. Vaziri, "Investigation of Environmental Impacts on Piezoelectric Weigh-In-Motion Sensing System."
- 24. N. More and G. Kapusetti, "Piezoelectric material A promising approach for bone and cartilage regeneration," *Med Hypotheses*, vol. 108, pp. 10–16, Oct. 2017, doi: 10.1016/j.mehy.2017.07.021.
- 25. S. A. Mumayiz and R. M. Michaels, "Investigation of the Implementation of Weighin-Motion Operation in Illinois-Phase I," Chicago, Mar. 1989.
- 26. C. E. Lee and P. M. Ferguson, "Concepts of Weigh-in-Motion Systems," in *National Weigh in Motion Conference Proceedings*, Denver, Jul. 1983.
- 27. M. 5 Mamlouk, "Rational Look at Truck Axle Weight."
- 28. Southgate and F. Herbert, "Quality Assurance of Weigh-in-Motion Data," *Federal Highway Administration*, pp. 1-21.
- 29. S. Hashemi Vaziri, C. T. Haas, L. Rothenburg, R. C. Haas, and X. Jiang, "Investigation of the effects of air temperature and speed on performance of piezoelectric weigh-in-motion

- systems," *Canadian Journal of Civil Engineering*, vol. 40, no. 10, pp. 935–944, Jun. 2013, doi: 10.1139/cjce-2012-0227.
- 30. S. H. Alavi *et al.*, "Performance Evaluation of Piezoelectric Weigh-in-Motion Sensors Under Controlled Field-Loading Conditions," 2003.
- 31. R. Bajwa, E. Coleri, R. Rajagopal, P. Varaiya, and C. Flores, "Development of a Cost-Effective Wireless Vibration Weigh-In-Motion System to Estimate Axle Weights of Trucks," *Computer-Aided Civil and Infrastructure Engineering*, vol. 32, no. 6, pp. 443–457, Jun. 2017, doi: 10.1111/mice.12269.
- 32. L. Zhang, "An Evaluation of the Technical and Economic Performance of Weigh-In-Motion Sensing Technology."
- 33. X. Jiang *et al.*, "Improvements in Piezoelectric Sensors and WIM Data Collection Technology."
- 34. J. F. Tressler, S. Alkoy, and R. E. Newnham, "Piezoelectric Sensors and Sensor Materials," 1998.
- 35. S. Patrick and A. Maher, "Implementation of Weigh-in-Motion (WIM) Systems," 2009.
- 36. P. Ueberschlag, "PVDF piezoelectric polymer." [Online]. Available: http://www.emerald-library.com/ft
- 37. K. K. Sappati and S. Bhadra, "Piezoelectric polymer and paper substrates: A review," *Sensors (Switzerland)*, vol. 18, no. 11. MDPI AG, Nov. 01, 2018. doi: 10.3390/s18113605.
- 38. H. He, Q. Zhang, Y. Zhang, J. Chen, L. Zhang, and F. Li, "A comparative study of 85 hyperelastic constitutive models for both unfilled rubber and highly filled rubber nanocomposite material," *Nano Materials Science*, vol. 4, no. 2, pp. 64–82, Jun. 2022, doi: 10.1016/j.nanoms.2021.07.003.
- 39. N. Tahaei, J. J. Yang, M. G. Chorzepa, S. S. Kim, and S. A. Durham, "Machine learning of Truck Traffic Classification groups from Weigh-in-Motion data," *Machine Learning with Applications*, vol. 6, p. 100178, Dec. 2021, doi: 10.1016/j.mlwa.2021.100178.
- 40. ASTM C666, "Standard Test Method for Resistance of Concrete to Rapid Freezing and Thawing 1."
- 41. The Indiana LTAP Center, "Guidelines for Traffic Counts on Local Roads and Streets," Dec. 2005.

APPENDIX

FIELD VALIDATION AT DIFFERENT SPEEDS FOR SUV AND SEDAN

SUV at 10 mph

In the test, the vehicle's speed was restricted to 10 mph, and the corresponding sensor response was recorded. Among the initial set of eight piezoelectric sensors, negligible responses were observed as the passing tires did not directly traverse over these sensors, as depicted in Figure 79. However, a noticeable response was recorded when the vehicle's tire passed over them in the subsequent set of eight piezoelectric sensors. Specifically, sensor numbers 10 and 11 exhibited a maximum output of 10 volts, as illustrated in Figure 80. Moreover, the neighboring sensors in this set displayed an output of approximately 65%. This response can be further improved by increasing the spacing between the sensors, thereby reducing interference and crosstalk among adjacent sensors.

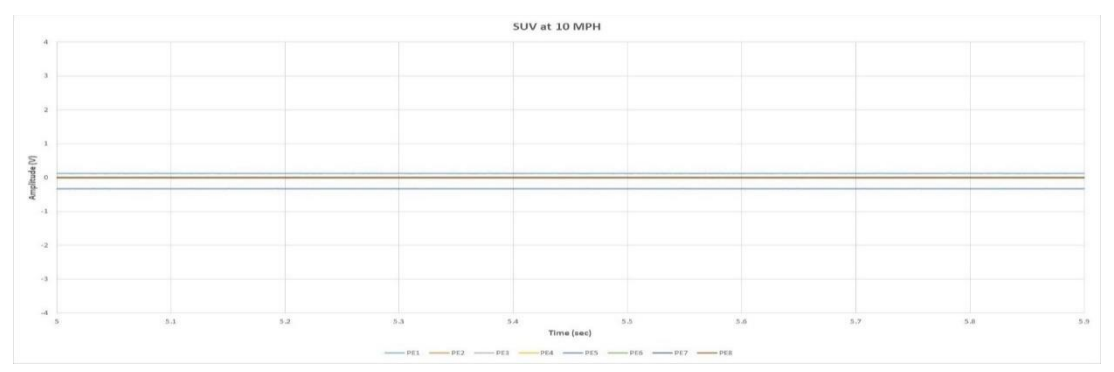


Figure 79 Voltage response of first 8 piezoelectric sensors for SUV (10 mph)



Figure 80 Voltage response of last 8 piezoelectric sensors for SUV (10 mph)

The contact patch of the tire was measured to be 15.1 cm. The tire width was determined by selectively considering the piezoelectric sensors that exhibited an output voltage exceeding 5V,

as shown in Figure 81. By measuring and summing the distances between these sensors, the tire's width was calculated as 15.4 cm.

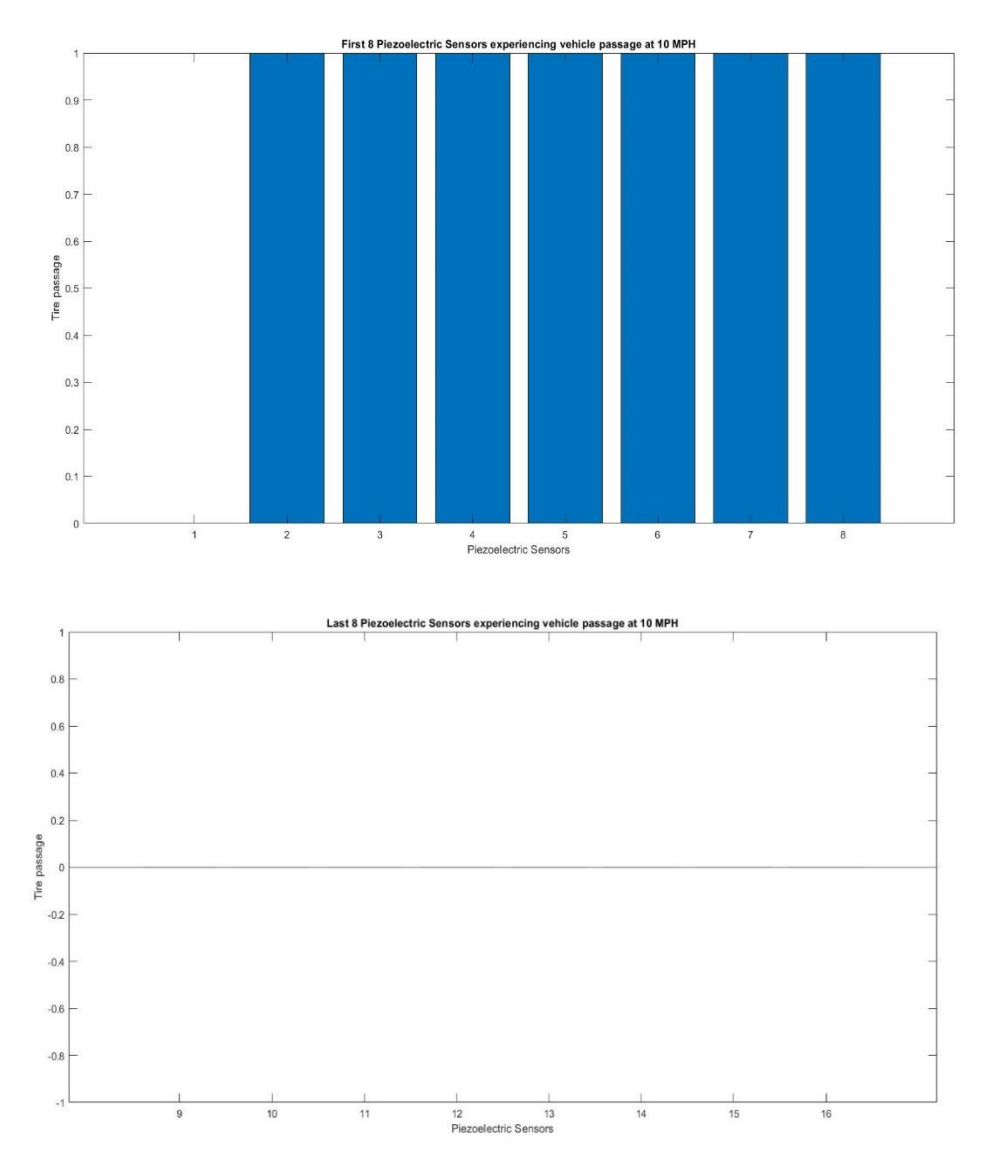


Figure 81 Sensor output at tire contact for SUV (10 mph)

SUV passing at 20 mph

The test involved the controlled passage of the vehicle at a speed of 20 mph, with the subsequent recording of sensor responses. In the initial set of eight piezoelectric sensors, sensors 7 and 8 exhibited a notable response of approximately 10V as the vehicle's tire passed over them. Similarly, in the last set of eight sensors, sensors 9 and 10 displayed a response of around 10V when the tire traversed over them. However, the remaining sensors in both sets showed a limited response, as depicted in Figures 82 and 83. Moreover, it is worth mentioning that a limited

response was also observed in the rest of the piezoelectric sensors. This diminished can be attributed to the forces of thrust and jerk exerted by the vehicle's tire on the EPDM rubber strip, given that the strip was not embedded within the pavement structure.

From the figures, it was determined that the time between the subsequent tires passing over the EPDM strip was 0.38 seconds. By utilizing the known speed of the vehicle, the calculated wheelbase was 3.39 m.

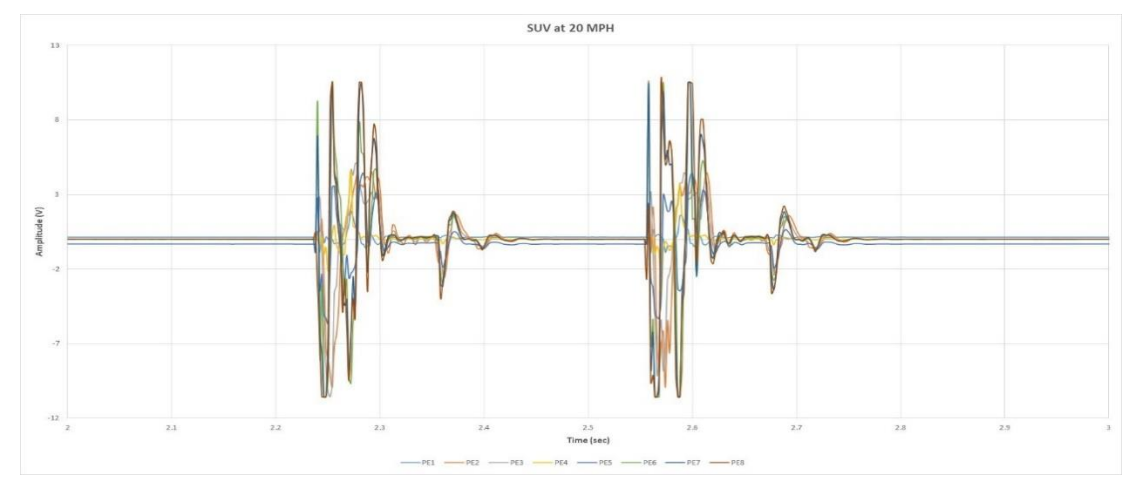


Figure 82 Voltage response of first 8 piezoelectric sensors for SUV (20 mph)

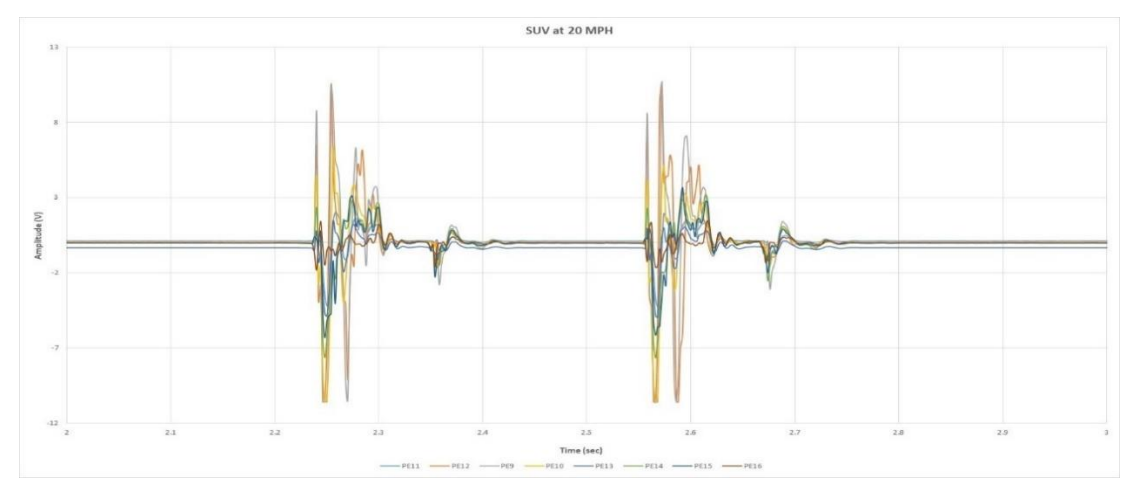


Figure 83 Voltage response of last 8 piezoelectric sensors for SUV (20 mph)

The tire width was determined by selectively considering the piezoelectric sensors that exhibited an output voltage exceeding 5V as shown in Figure 84. By measuring and summing the distances between these sensors, the tire width was calculated as 15.4 cm.

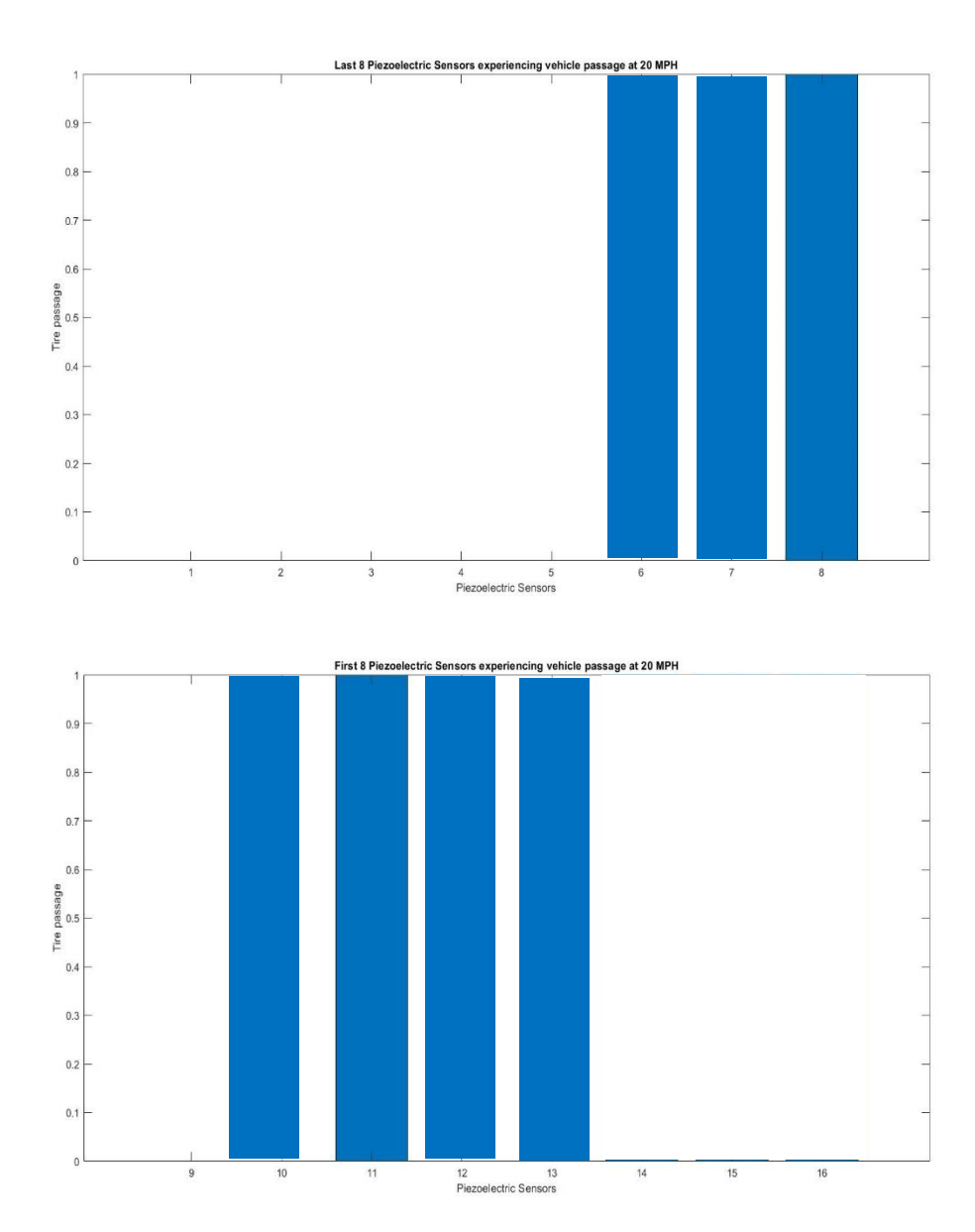


Figure 84 Sensor output at tire contact for SUV (20 mph)

SUV passing at 30 mph

During the test, precise control was exerted to limit the vehicle's speed to 30 mph, and recording of the sensor response was conducted. A response was detected in the first set of eight piezoelectric sensors, corresponding to the vehicle's traversal over those specific sensors. However, it is noteworthy that this response was limited, reaching a maximum of only 20%, as illustrated in Figure 85. This limited response can be attributed to the dynamic forces exerted by the vehicle's tire on the EPDM rubber strip. Conversely, a distinct response pattern emerged in the last set of eight piezoelectric sensors. Specifically, sensors 14, 15, and 16 displayed

approximately 8V, 10V, and 10V responses as the vehicle's tire passed over them. Remaining sensors in this set exhibited a limited response, as demonstrated in Figure 86.

From Figure 86, it was determined that the time between the subsequent tires was 0.26 seconds. By utilizing the known speed of the vehicle, the wheelbase of the vehicle was calculated as 3.48 m.

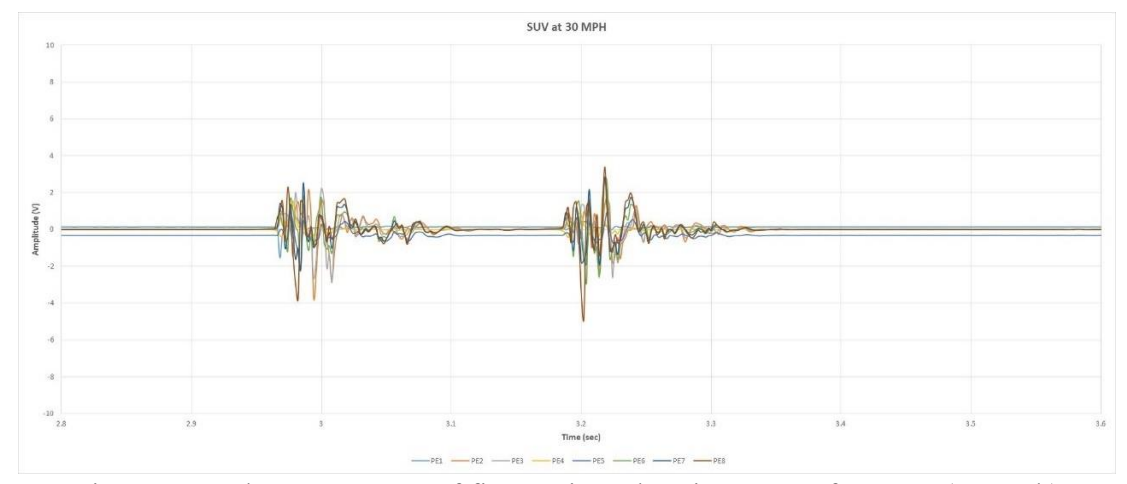


Figure 85 Voltage response of first 8 piezoelectric sensors for SUV (30 mph)

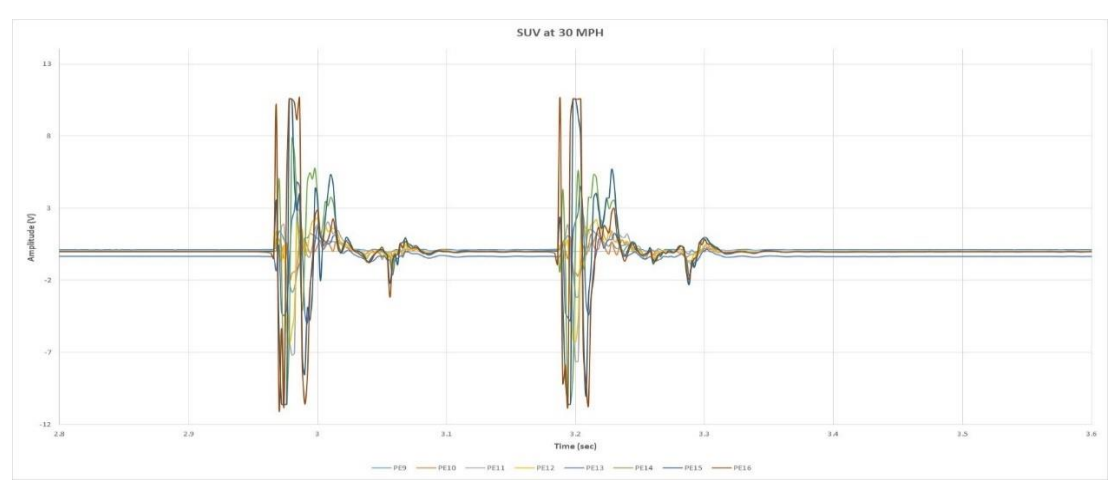


Figure 86 Voltage response of last 8 piezoelectric sensors for SUV (30 mph)

The tire width was determined by selectively considering the piezoelectric sensors that exhibited an output voltage exceeding 5V as shown in Figure 87. By measuring and summing the distances between these sensors, the tire's width was calculated as 13.1 cm.

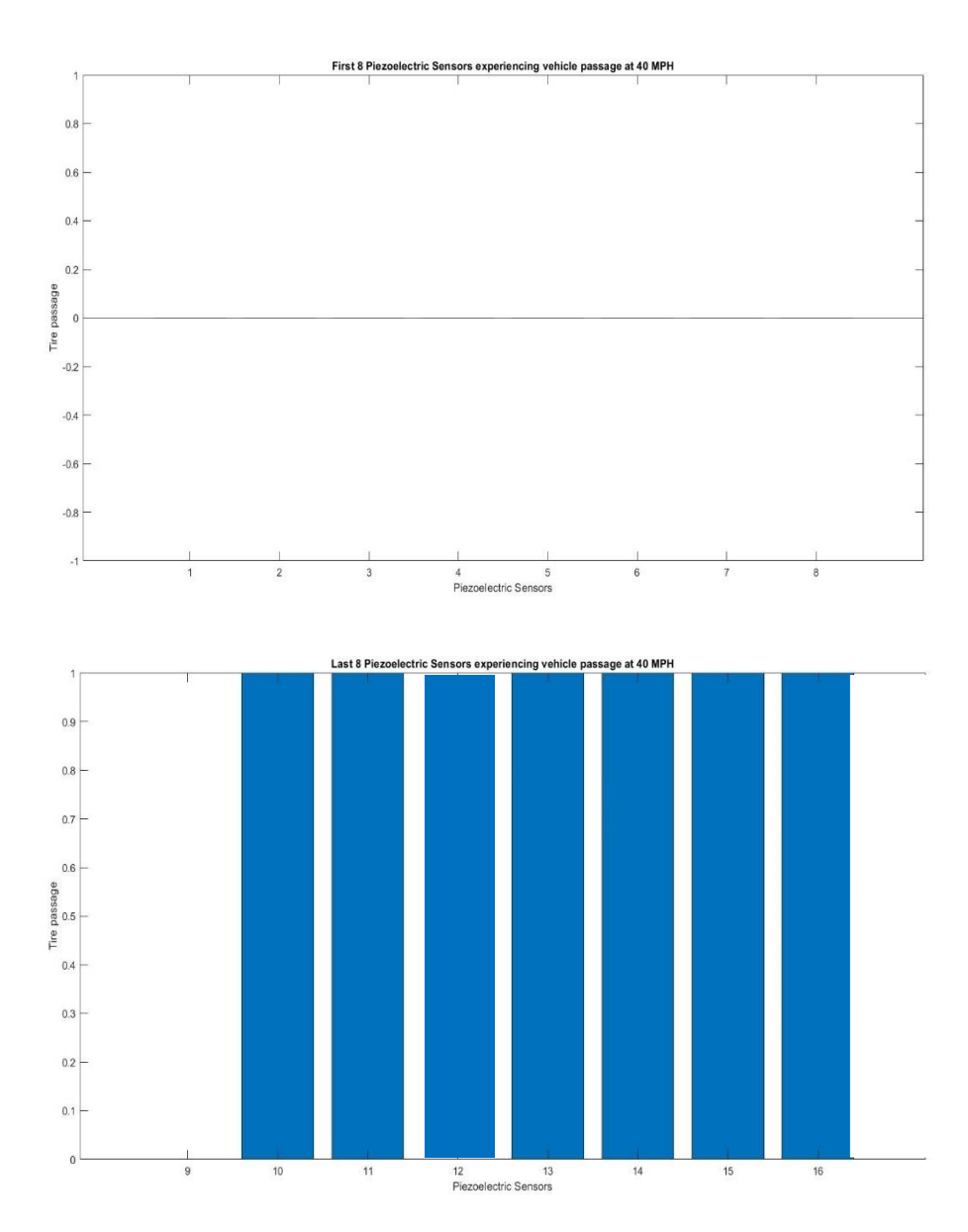


Figure 87 Sensor output at tire contact for SUV (30 mph)

SUV passing at 40 mph

During the test, the vehicle was deliberately maintained at a speed of 40 mph, and the corresponding response of the piezoelectric sensors was recorded. Notably, in the initial set of eight sensors 6, 7, and 8 sensors, an evident and robust response close to 10V was detected as the vehicle's tire traversed over these specific sensors. However, the remaining sensors in this set displayed a limited response, as demonstrated in Figure 88. Furthermore, the observed response in the final set of eight piezoelectric sensors was merely a maximum of 50%, as depicted in

Figure 89. This diminished response may potentially be attributed to the pronounced thrust and jerk exerted by the vehicle's tire on the EPDM rubber strip.

From Figure 88, it was determined that the time between the subsequent tires passing over the EPDM strip was 0.2 seconds. By utilizing the known speed of the vehicle, the wheelbase of the vehicle was calculated as 3.57 m.

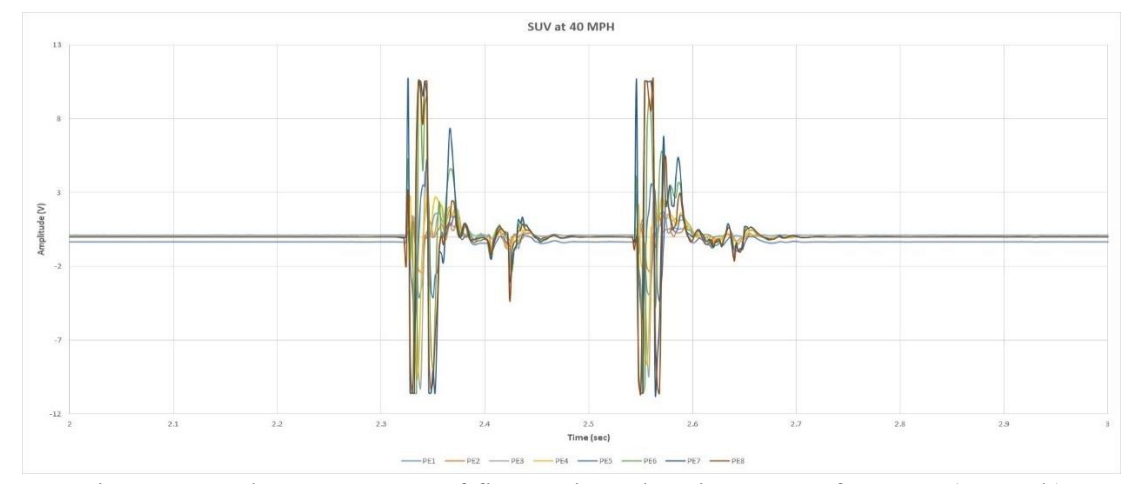


Figure 88 Voltage response of first 8 piezoelectric sensors for SUV (40 mph)

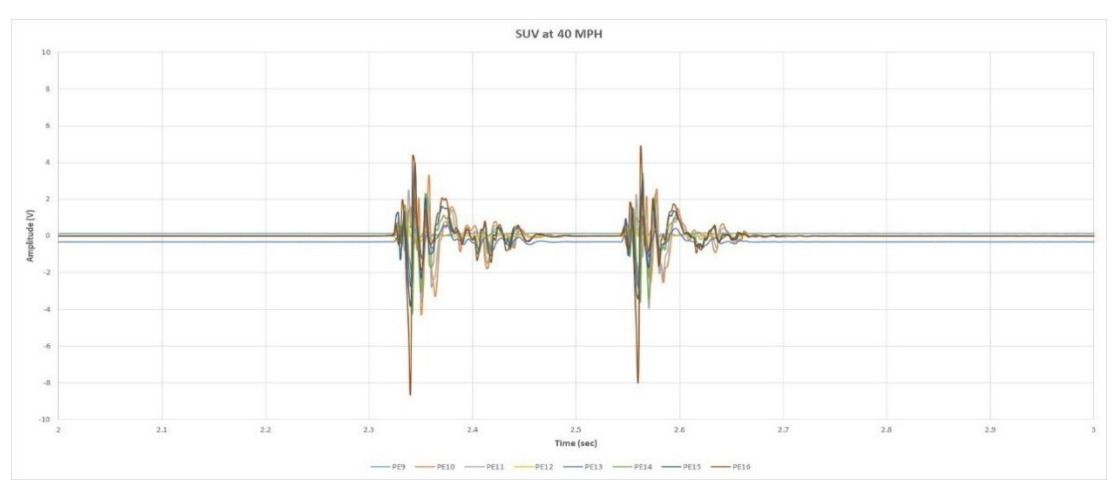


Figure 89 Voltage response of last 8 piezoelectric sensors for SUV (40 mph)

The tire width was determined by selectively considering the piezoelectric sensors that exhibited an output voltage exceeding 5V as shown in Figure 90. By measuring and summing the distances between these sensors, the tire width was calculated as 13.1 cm.

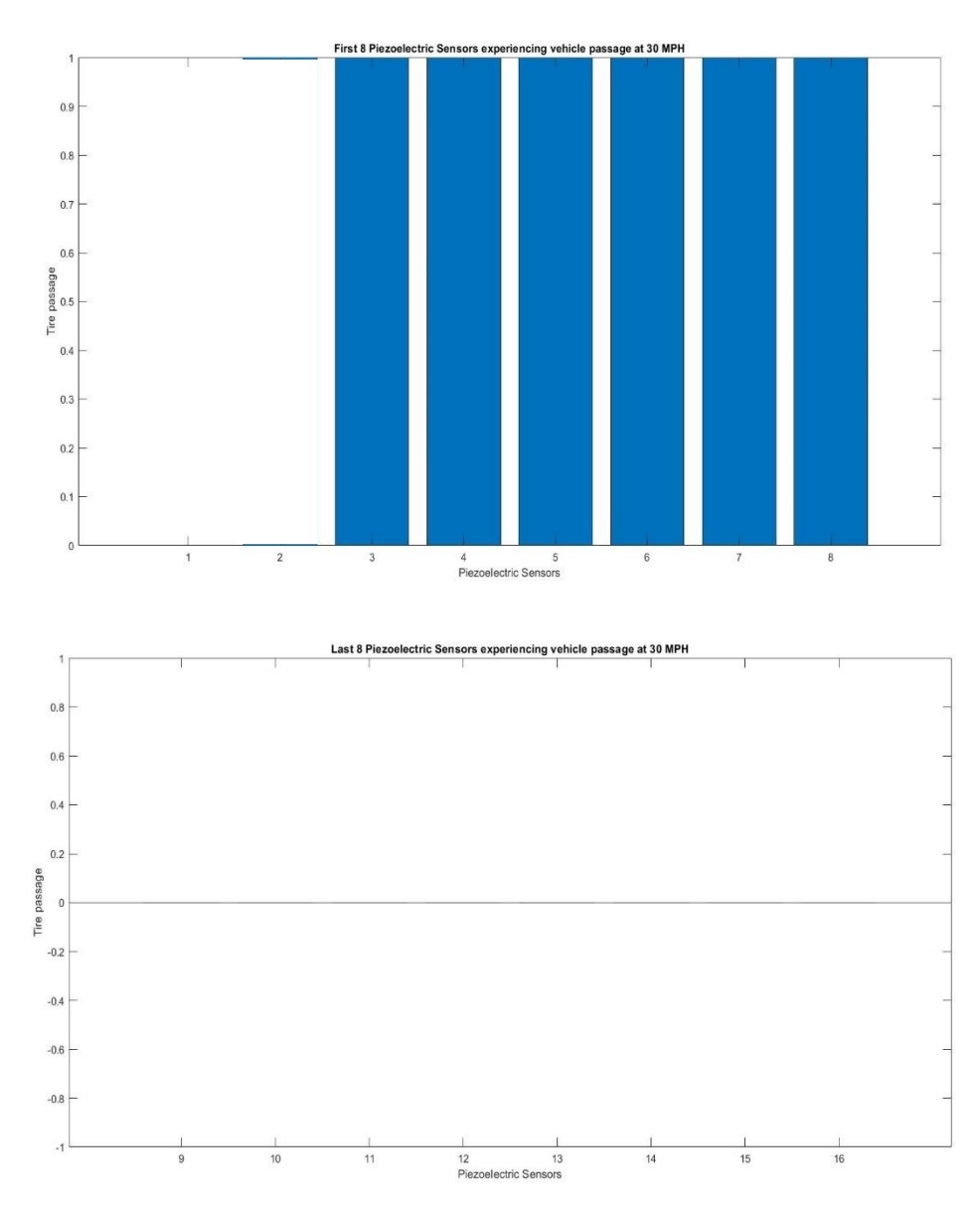


Figure 90 Sensor output at tire contact for SUV (40 mph)

Sedan passing at 10 mph

The vehicle's speed was restricted to 10 mph in the test, and the corresponding sensor response was recorded. Among the initial set of eight piezoelectric sensors, negligible responses were observed as the passing tires did not directly traverse over these sensors, as depicted in Figure 891. However, a noticeable response was recorded when the vehicle's tire passed over the subsequent set of eight piezoelectric sensors. Specifically, sensor numbers 10 and 11 exhibited an approximate output of 6V, as illustrated in Figure 92. Moreover, the neighboring sensors in this set displayed an output of approximately 20%. This response can be further improved by

increasing the spacing between the sensors, thereby reducing interference and crosstalk among adjacent sensors.

From Figure 92, it was determined that the time between the subsequent tires passing over the EPDM strip was 0.61 seconds. By utilizing the known speed of the vehicle, the wheelbase of the vehicle was calculated as 2.72 m.

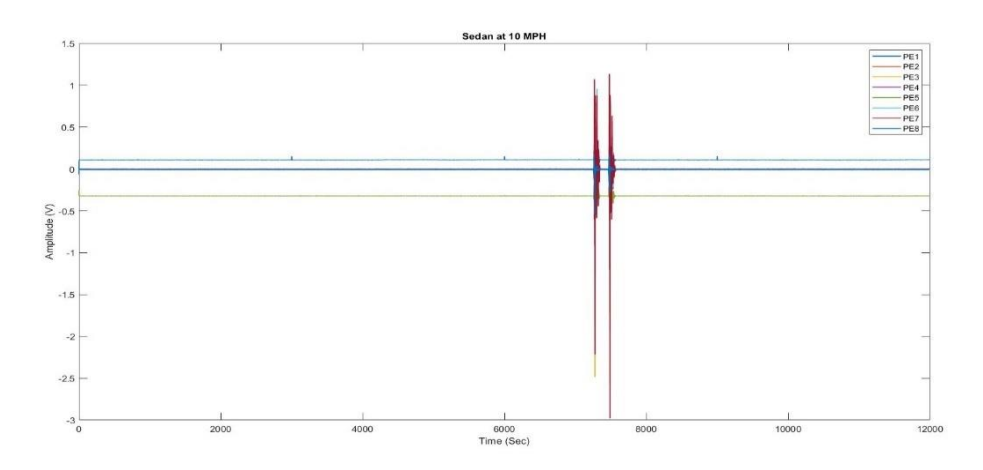


Figure 91 Voltage response of first 8 piezoelectric sensors for sedan (10 mph)

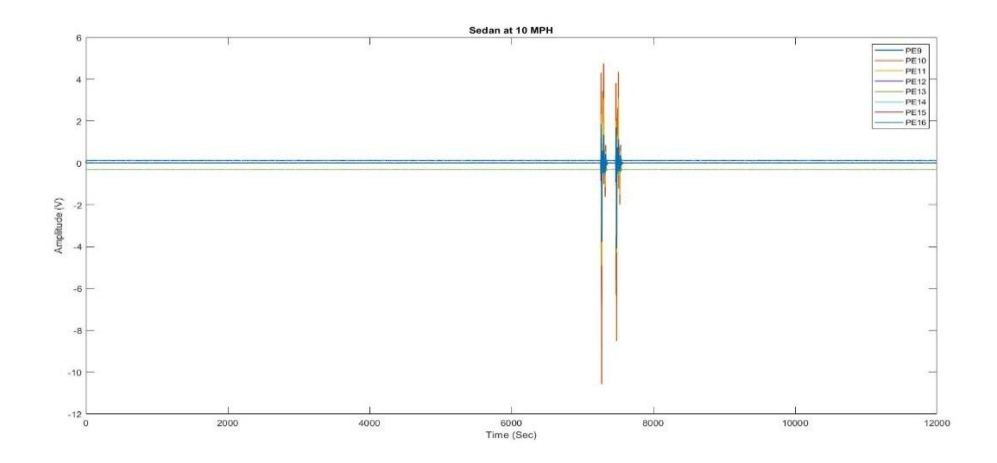


Figure 92 Voltage response of last 8 piezoelectric sensors for sedan (10 mph)

The tire width was determined by selectively considering the piezoelectric sensors that exhibited an output voltage exceeding 5V as shown in Figure 85. By measuring and summing the distances between these sensors, the tire width was calculated as 13.1 cm.

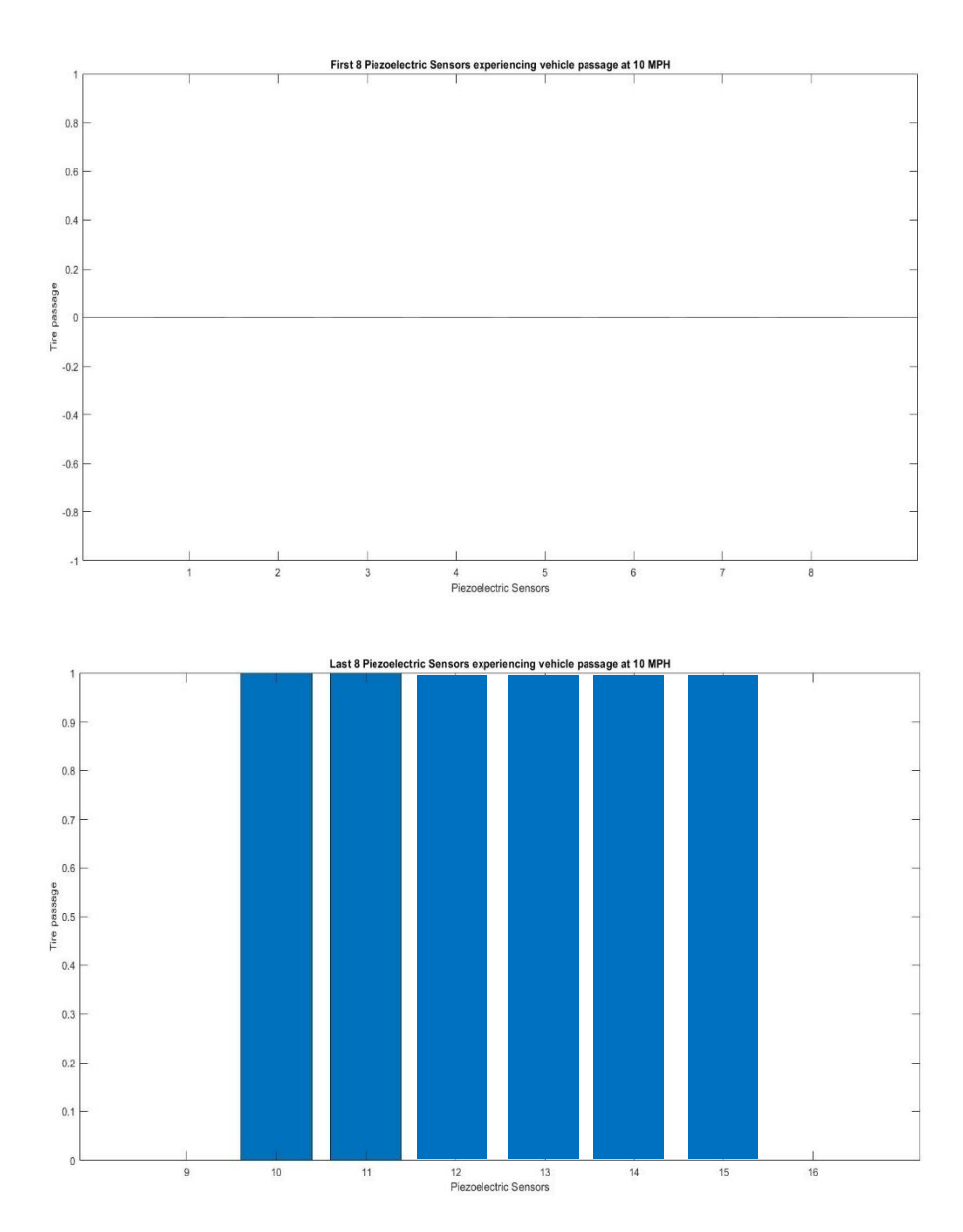


Figure 93 Sensor output at tire contact for sedan (10 mph)

Sedan passing at 20 mph

The vehicle was driven at a speed of 20 mph, with the subsequent recording of sensor responses. In the initial set of eight piezoelectric sensors, sensors 2 and 3 exhibited response of roughly 8.5V as the vehicle's tire passed over them. However, negligible response was recorded in the last set of the piezoelectric sensors as depicted in Figures 94and 95. The remaining sensors in both sets showed a limited response.

From Figure 94, it was determined that the time between the subsequent tires passing over the EPDM strip was 0.32 seconds. By utilizing the known speed of the vehicle, the wheelbase of the vehicle was calculated as 2.86 m.

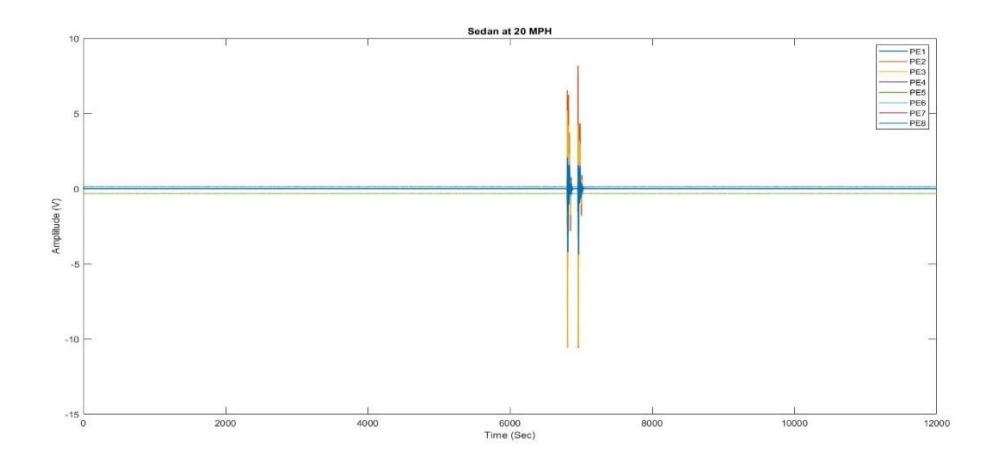


Figure 94 Voltage response of first 8 piezoelectric sensors for sedan (20 mph)

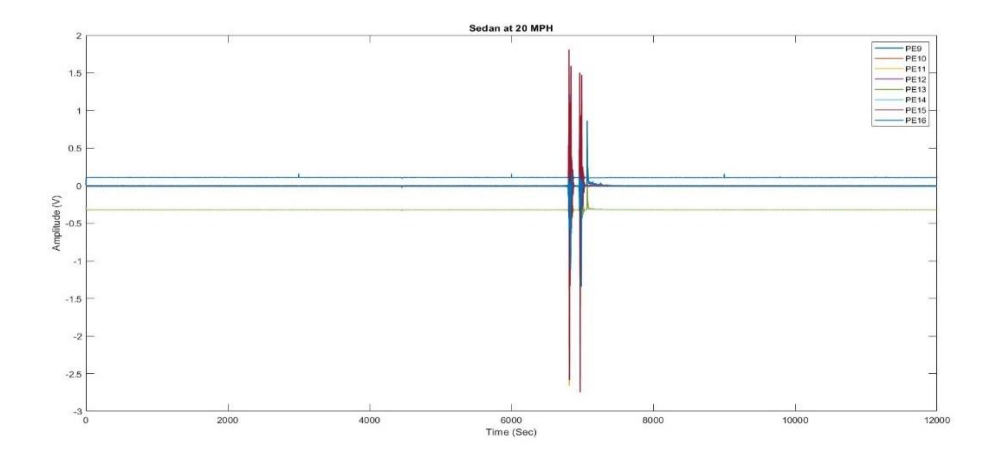


Figure 95 Voltage response of last 8 piezoelectric sensors for sedan (20 mph)

The tire width was determined by selectively considering the piezoelectric sensors that exhibited an output voltage exceeding 5V as shown in Figure 96. By measuring and summing the distances between these sensors, the tire width was calculated as 15.4 cm.

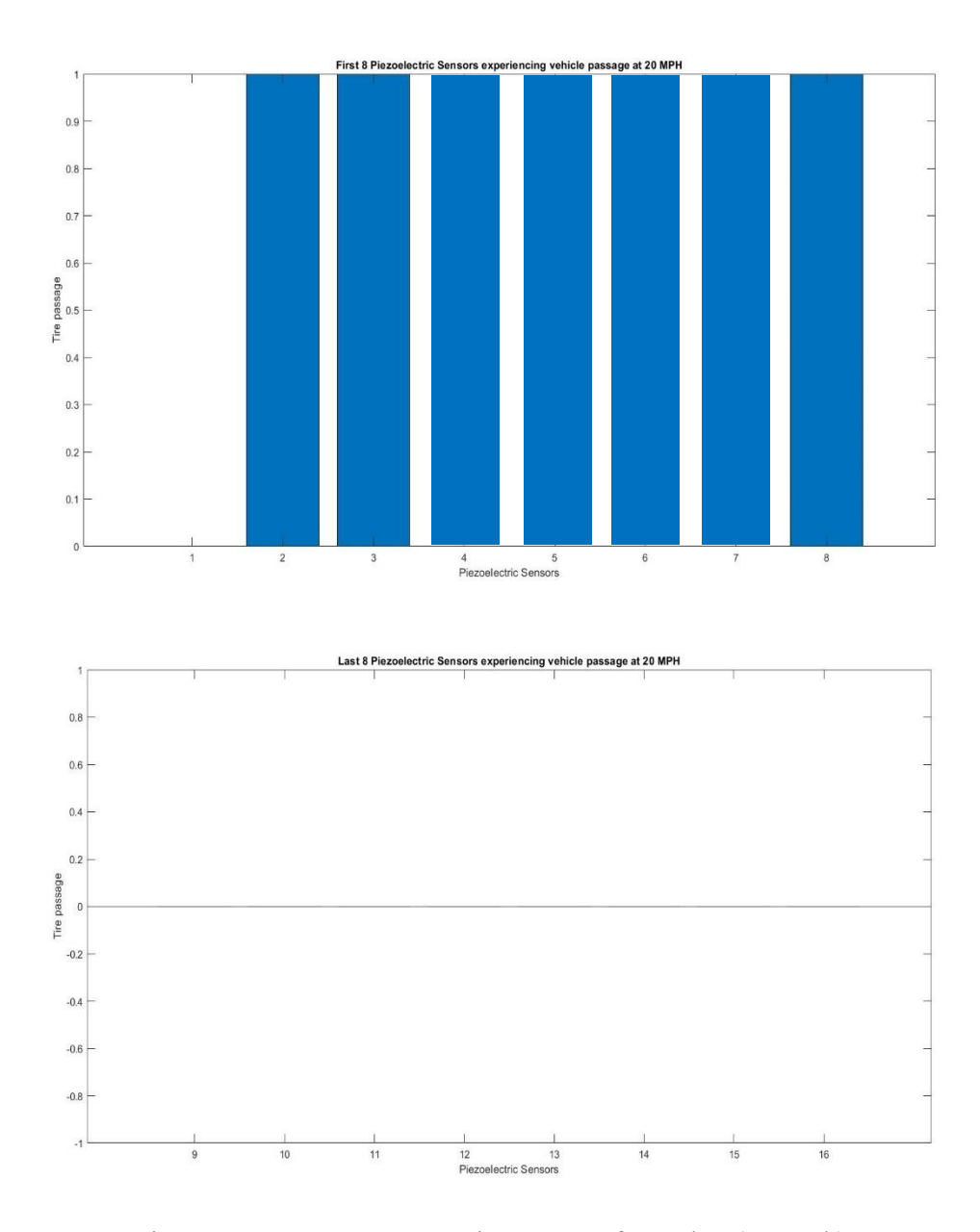


Figure 96 Sensor output at tire contact for sedan (20 mph)

Sedan passing at 30 mph

The vehicle was driven at a speed of 30 mph, with the subsequent recording of sensor responses. In the initial set of eight piezoelectric sensors, sensors 6, 7 and 8 exhibited responses of roughly 8.5V as the vehicle's tire passed over them. Similarly, in the last set of eight sensors, sensors 9, 10, 11, and 12 displayed a response of roughly 9V when the tire traversed over them. Remaining sensors in both sets showed a limited response, as depicted in Figures 97 and 98. Limited response was also observed in the rest of the piezoelectric sensors. From Figures, it was determined that the time between the subsequent tires passing over the EPDM strip was 0.22

seconds. By utilizing the known speed of the vehicle, the wheelbase of the vehicle was calculated as 2.95 m.

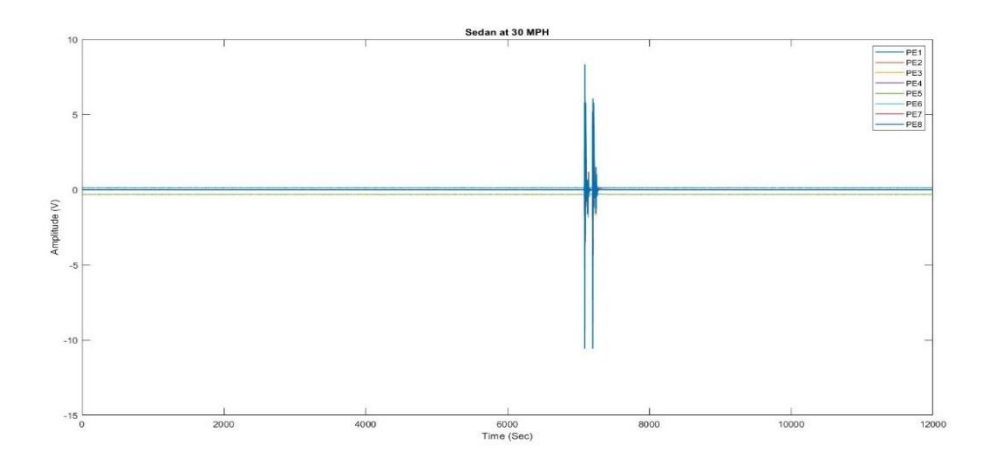


Figure 97 Voltage response of first 8 piezoelectric sensors for sedan (30 mph)

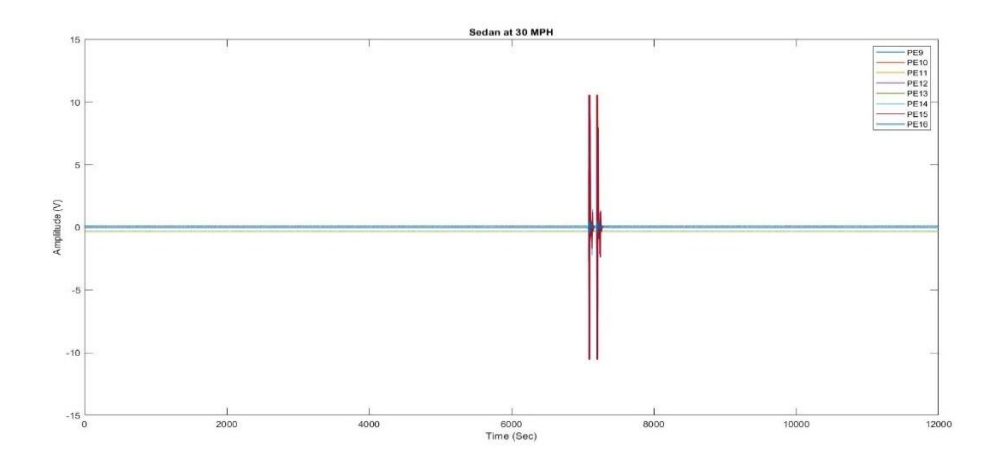


Figure 98 Voltage response of last 8 piezoelectric sensors for sedan (30 mph)

The tire width was determined by selectively considering the piezoelectric sensors that exhibited an output voltage exceeding 5V as shown in Figure 99. By measuring and summing the distances between these sensors, the tire's width was calculated as 15.4 cm.

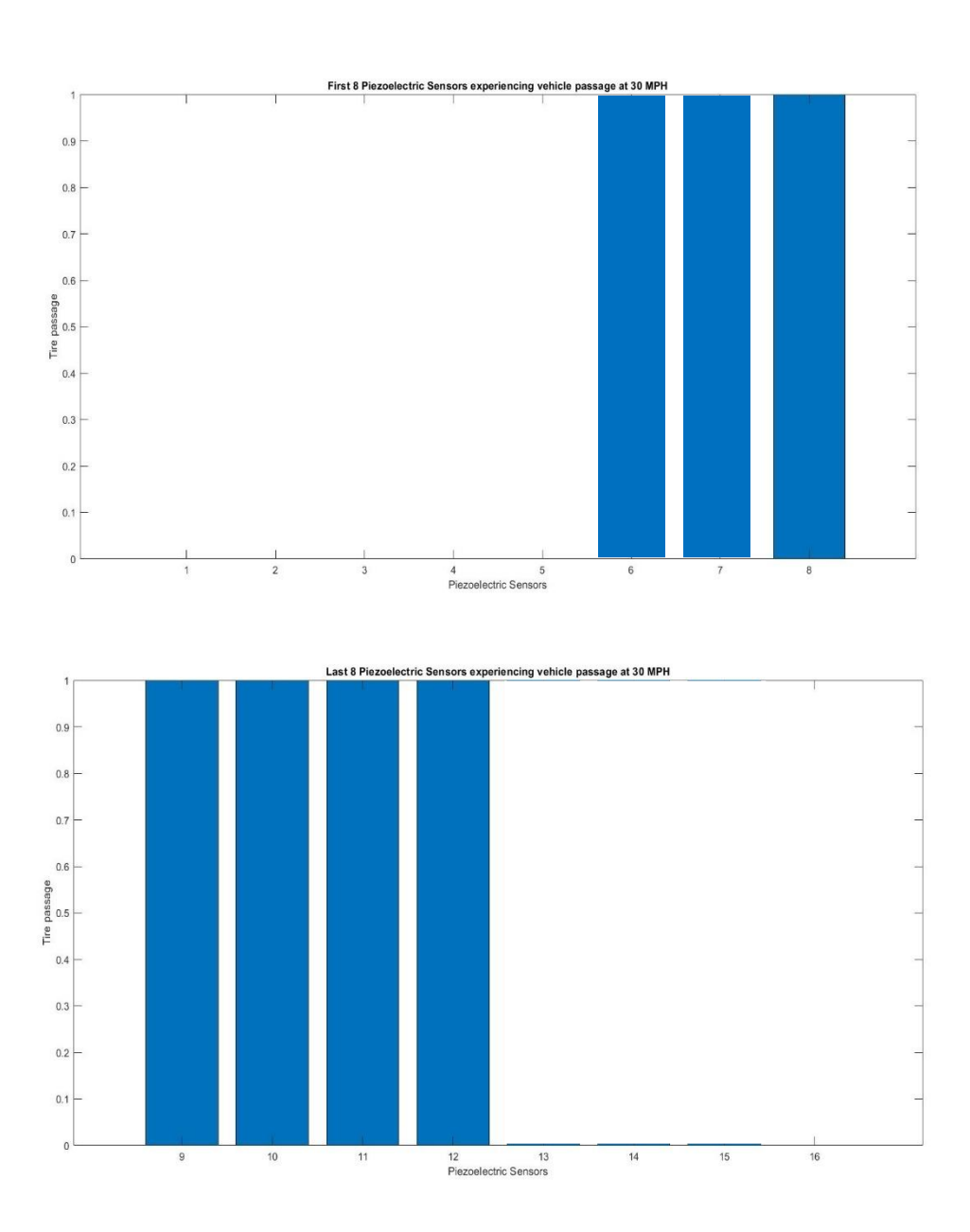


Figure 99 Sensor output at tire contact for sedan (30 mph)

Sedan passing at 40 mph

During the test, the vehicle was driven at a speed of 40 mph, and the corresponding response of the piezoelectric sensors was recorded. Notably, in the initial set of eight sensors 6, 7, and 8 sensors, an evident and robust response close to 10V was detected. Remaining sensors in this set displayed a limited response, as demonstrated in Figure 100. In the final set of eight piezoelectric 9, 10, and 11 sensors recorded a response close to 10V, as depicted in Figure 101 and the rest of the sensors recorded limited response.

From the figures, it was determined that the time between the subsequent tires passing over the EPDM strip was 0.17 seconds. By utilizing the known speed of the vehicle, the wheelbase of the vehicle was calculated as 3.04 m.

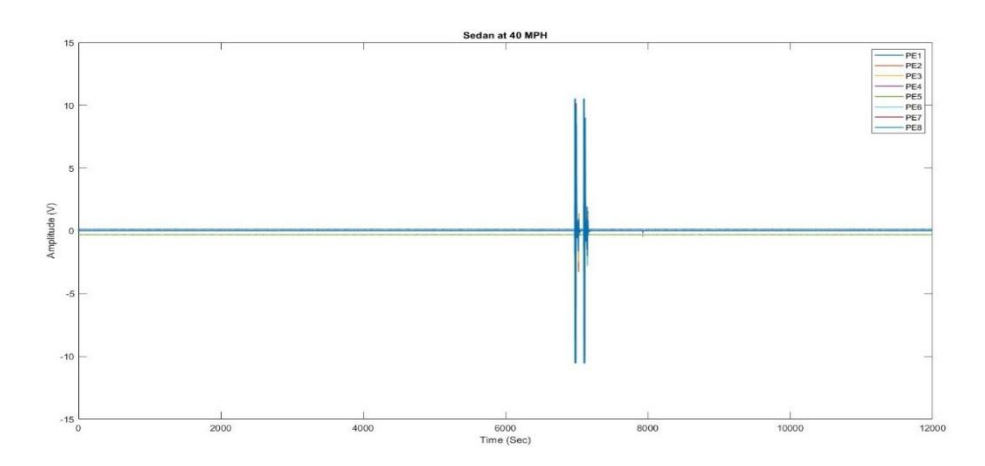


Figure 100 Voltage response of last 8 piezoelectric sensors for sedan (40 mph)

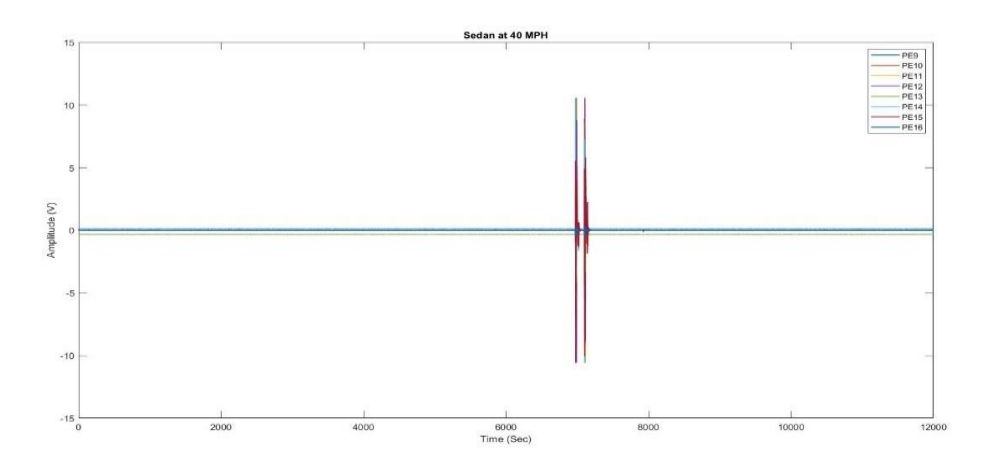


Figure 101 Voltage response of last 8 piezoelectric sensors for sedan (40 mph)

The tire width was determined by selectively considering the piezoelectric sensors that exhibited an output voltage exceeding 5V as shown in Figure 102. By measuring and summing the distances between these sensors, the tire's width was calculated as 15.4 cm.

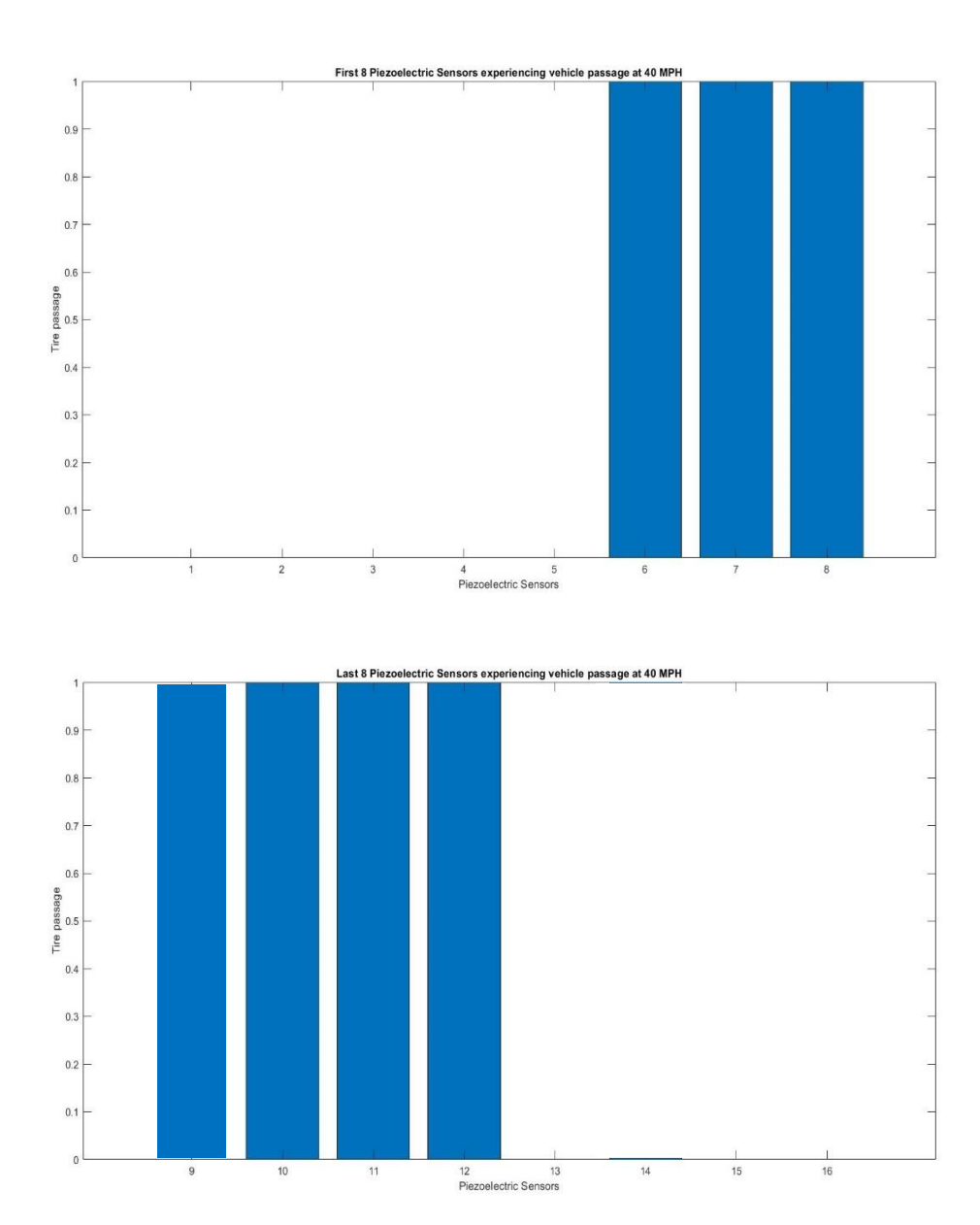


Figure 102 Sensor output at tire contact for sedan (40 mph)